FEASIBILITY STUDY ON NEAR INFRARED SPECTROSCOPY FOR EVALUATION OF COMBUSTION PERFORMANCE PARAMETERS AND MOISTURE CONTENT OF BAMBOO CHIPS

(Dendrocalamus sericeus cl. Phamon)

A THESIS SUBMITTED IN PARTIAL FULFILLMENT
OF THE REQUIREMENT FOR THE DEGREE OF
MASTER OF ENGINEERING IN AGRICULTURAL ENGINEERING
FACULTY OF ENGINEERING
KING MONGKUT'S INSTITUTE OF TECHNOLOGY LADKRABANG
2016

KMITL-2016-EN-M-100-078

FEASIBILITY STUDY ON NEAR INFRARED SPECTROSCOPY FOR EVALUATION OF COMBUSTION PERFORMANCE PARAMETERS AND MOISTURE CONTENT OF BAMBOO CHIPS (*Dendrocalamus sericeus* cl. Phamon)

AMRIT SHRESTHA

A THESIS SUBMITTED IN PARTIAL FULFILLMENT
OF THE REQUIREMENT FOR THE DEGREE OF
MASTER OF ENGINEERING IN AGRICULTURAL ENGINEERING
FACULTY OF ENGINEERING
KING MONGKUT'S INSTITUTE OF TECHNOLOGY LADKRABANG
2016

KMITL-2016-EN-M-100-078

THESIS CERTIFICATION

FACULTY OF ENGINEERING

KING MONGKUT'S INSTITUTE OF TECHNOLOGY LADKRABANG

Thesis Title Feasibility Study on Near Infrared Spectroscopy for Evaluation of Combustion Performance Parameters and Moisture Content of Bamboo Chips (*Dendrocalamus Sericeus* cl. Phamon)

Student Mr. Amrit Shrestha

Student Id. 57601309

Degree Master of Engineering

Program Agricultural of Engineering

Thesis Advisor Assoc. Prof. Dr. Panmanas Sirisomboon

Thesis Reference Number KMITL-2016-EN-M-100-078

EXAMINERS		SIGNATURES
Dr. Vasu	Udompeitaikul	
Dr. Jiraporn	Sripinyowanich Jongyingcharoen	
Assoc. Prof. Dr. Anupun	Terdwongworakul	A. Terdwongworakul
Asst. Prof. Dr. Prasan	Choomjaihan	P. Choomjaihan
Assoc. Prof. Dr. Panmanas	Sirisomboon	

Date 11th July 2016 **Time** 13:30-15:30 pm

Place Building A , Conference Room No.4

(Assc. Prof. Dr. Komsan Maleesee)

Dean, Faculty of Engineering

11th July 2016

หัวข้อวิทยานิพนธ์	การศึกษาความเป็นไปได้ในการใช้เทคนิคเนียร์อินฟราเรดสเปกโทรสโกปีในการประเมินสมรรถนะการเผาไหม้และความชื้นของไม้ไผ่สับ (*Dendrocalamus sericeus* cl. ฟ้าหม่น)
นักศึกษา	นายอมฤต เชรสธา
รหัสนักศึกษา	57601309
ปริญญา	วิศวกรรมศาสตรมหาบัณฑิต
สาขาวิชา	วิศวกรรมเกษตร
พ.ศ.	2559
อาจารย์ที่ปรึกษาวิทยานิพนธ์	รศ.ดร.ปานมนัส ศิริสมบูรณ์

บทคัดย่อ

พารามิเตอร์เกี่ยวกับสมรรถนะในการเผาไหม้ของชิ้นไม้ไผ่สับถูกเปรียบเทียบกับกระถิน ดัชนีการติดไหม้ ดัชนีการเผาไหม้ และดัชนีสมรรถนะการเผาไหม้ของชิ้นไม้ไผ่สับมีค่าเท่ากับ 88.33E-04, 0.16E-03 และ 3.95E-07 ตามลำดับ ในขณะที่ดัชนีการติดไหม้ ดัชนีการเผาไหม้ และดัชนีสมรรถนะการเผาไหม้ของกระถินเท่ากับ 6.10E-04, 8.20E-03 และ 2.19E-07 ตามลำดับ จากการวิเคราะห์ thermogravimetric สามารถสรุปได้ว่าไผ่เผาไหม้ได้ง่ายกว่ากระถินซึ่งถูกยืนยันโดยดัชนีสมรรถนะการเผาไหม้ของไผ่สูงกว่ากระถิน

ในการวัดความชื้นของชิ้นไผ่สับเครื่อง diode array near infrared 2 ชนิด ได้แก่ NIR-Gun (ช่วงคลื่นสั้น, 600-1100 nm ที่ 2 nm) และ Micro-NIR (ช่วงคลื่นยาว, 1150-2150 nm ที่ 7 nm intervals) ถูกใช้ในการสแกนชิ้นไผ่สับ ในวิทยานิพนธ์เล่มนี้ศึกษาเฉพาะสายพันธุ์ฟ้าหม่น *Dendrocalamus sericeus* cl. เท่านั้น การสแกนเพื่อวัดความชื้นถูกปฏิบัติในพื้นที่ปลูก ณ จังหวัดอุตรดิตถ์ประเทศไทยที่สภาวะบรรยากาศ จำนวนตัวอย่างทั้งหมดที่ใช้ในการสร้างแบบจำลองหลังจากกำจัดของมูลที่เป็น outlier เท่ากับ 252 ตัวอย่าง ช่วงของเส้นรอบวงของไผ่ที่ใช้ในงานวิจัยนี้อยู่ในช่วง 16-39 cm และความชื้นอยู่ในช่วง 39-86 % wb เทคนิค Partial least squares regression ถูกนำมาใช้ในการพัฒนาแบบจำลองสำหรับทำนายความชื้นของไผ่ ค่า coefficient of determination ของชุดทำนาย (R_p^2), standard error of cross validation (SECV), standard error of predication (SEP), bias และ RPD ของแบบจำลองที่สร้างจากสเปกตรัมจากเครื่อง NIR-Gun มีค่าเท่ากับ 0.924, 2.871% wb, 2.385% wb, -0.250% wb และ 3.656 ตามลำดับ ในขณะที่แบบจำลองที่สร้างจากสเปกตรัมจากเครื่อง Micro-NIR มีค่าเท่ากับ 0.743, 4.349% wb, 4.499% wb, 0.025% wb และ 1.972 ตามลำดับ สมรรถนะในการทำนายความชื้นของไผ่ของแบบจำลองจากช่วงคลื่นสั้นดีกว่าแบบจำลองจากช่วงคลื่นยาว เนื่องจากมีค่า coefficient of determination และ RPD สูงกว่า อย่างไรก็ตามผลการทดลองแสดงให้เห็นถึงองค์ประกอบทางเคมีอื่นในไผ่ส่งผลกระทบต่อแบบจำลองมากกว่าความชื้น

โดยใช้เทคนิค Partial least squares regression จำนวนตัวอย่างทั้งหมดที่ใช้ในการสร้างแบบจำลองเท่ากับ 80 ตัวอย่างสำหรับทั้ง 3 เครื่องมือวัด ตัวอย่างถูกบดเป็นชิ้นเล็กขนาด 2 มิลลิเมตร แบบจำลองจากเครื่องมือวัด NIR ของพารามิเตอร์ด้านสมรรถนะของการเผาไหม้ใช้จำนวนแฟคเตอร์เท่ากับ 13-20 แฟคเตอร์ในการสร้างแบบจำลอง อย่างไรก็ตามเครื่องมือวัด NIR ไม่สามารถ

ทำนายพารามิเตอร์ด้านสมรรถนะของการเผาไหม้ของไม้ไผ่บด สเปกตรัมได้รับผลกระทบจากสัญญาณรบกวนและความแปรปรวนของตัวอย่างในกลุ่มที่ถูกใช้ในการสร้างแบบจำลองมีค่าต่ำ (สำหรับดัชนีสมรรถนะการเผาไหม้อยู่ในช่วง 2.04-1.23E-04, ดัชนีการติดไฟอยู่ในช่วง 4.613-2.794E-07 และ ดัชนีการเผาไหม้หมดอยู่ในช่วง 11.907-6.994E-03) สิ่งนี้อาจเป็นสาเหตุให้เครื่องมือวัด NIR ไม่สามารถทำนายได้ ในทางตรงกันข้าม FT-NIR มีความสามารถในการทำนายดัชนีการติดไฟและดัชนีการเผาไหม้หมดด้วยความแม่นยำต่ำ โดยค่า R_p^2, Bias และ RPD ของแบบจำลองที่เหมาะสมที่สุดของค่าดัชนีการติดไฟมีค่าเท่ากับ 0.432, 3.960E-05 และ 1.33 ด้วยจำนวนของแฟคเตอร์เท่ากับ 4 สำหรับค่า R_p^2, Bias และ RPD ของค่าดัชนีการเผาไหม้หมดเท่ากับ 0.513, -2.210E-07, และ 1.43 ด้วยจำนวนของแฟคเตอร์เท่ากับ 7

Thesis title	Feasibility Study on Near Infrared Spectroscopy for Evaluation of Combustion Performance Parameters and Moisture Content of Bamboo Chips (*Dendrocalamus sericeus* cl. Phamon)
Student	Mr. Amrit Shrestha
Student ID.	57601309
Degree	Master of Engineering
Program	Agricultural Engineering
Year	2016
Thesis Advisor	Assoc. Prof. Dr. Panmanas Sirisomboon

ABSTRACT

The combustion performance parameter of the bamboo chips were compared with the *L. leucocephala* pellet. The ignition index, burnout index and combustion performance index of grounded bamboo chips were found to be 88.33E-04, 0.16E-03and 3.95E-07, whereas ignition index, burnout index and combustion performance index of grounded *Leucaena leucocephala* pellet were found to be 6.10E-04, 8.20E-03 and 2.19E-07 respectively. From the thermogravimetric analysis, it can be concluded that bamboo was easier to burn than the *L. leucocephala* pellet which is confirmed by the higher value of combustion performance index of bamboo than that of *L. leucocephala* pellet.

In order to measure the moisture content in bamboo chip, two diode array near infrared (NIR) instruments, NIR-Gun (short wave, 600-1100 nm at 2 nm intervals) and Micro-NIR (long wave, 1150-2150 nm at 7 nm intervals), were used for scanning the bamboo chips. Only the bamboo chips of *Dendrocalamus sericeus* cl. Phamon were used for this work. The scanning for the measurement of moisture content was performed in Thailand atmospheric condition in the plantation area, Uttaradit, Thailand. The total number of samples used for developing model after removing outliers was 252. The circumference and moisture content of bamboos used in this research were in the range between 16-39 cm and 39-86% wet basis (wb) respectively. Partial least squares regression technique was used to develop the models to predict the moisture content in bamboo chip. The coefficient of determination of prediction set, standard error of cross validation (SECV), standard error of predication (SEP), bias and RPD of optimum model of NIR-Gun are 0.924, 2.871% wb, 2.385% wb, -0.250% wb and 3.656.respectively, while the values for Micro-Nir model are found to be 0.743, 4.349% wb, 4.499% wb, 0.025% wb and 1.972, respectively. The performance of the short wavelength model was found better than long wavelength model for the prediction of moisture content in

bamboo due to higher value of coefficient of determination and RPD. However, in prediction of moisture content in bamboo chips, the model shows the effect of different constituents of the bamboo more than moisture.

On the other hand, the two diode array NIR-instruments (NIR-Gun and Micro-NIR) and Fourier transform near infrared (FT-NIR) instrument were used to make model of combustion performance parameter i.e. ignition index, burnout index and combustion performance index using the same partial least squares regression technique. The total number of the sample used for making the model was 80 for both types of instruments. The samples were grounded to 2 mm size. The diffuse NIR-instruments models of combustion performance parameter used 13-20 PLS factors for the making the model. However, the diffuse NIR-instruments were unable to predict the combustion performance parameter of the grounded bamboo chips with any accuracy. The spectra were suffered from the noise, and the variability of the calibration set samples used for making the models (for combustion index 4.613-2.794E-07, ignition index 11.907-6.994E-03, burnout index 2.04-1.23E-04) were low. This may be the reason why the diffuse NIR-instrument failed to predict. In contrast, the FT-NIR was able to predict the ignition index and burnout index but with very low accuracy. The coefficient of determination of prediction set, bias and RPD of optimum model of ignition index are 0.432, 3.960E-05 and 1.33, with the number of PLS factors of the model 4, and the coefficient of determination of prediction set, bias and RPD of optimum model of burnout index are 0.513, -2.210E-07, and 1.43, with the number of PLS factors of the model 7.

Acknowledgements

I would like to express my sincere gratitude to my advisor Associate Professor Dr. Panmanas Sirisomboon for her exemplary advice, support and guidance throughout this study period. She is the one who always inspired me for the excellence, and the one who believed on me that I can achieve that dream. I believe I would never be like as I am today without her.

I want to acknowledge to my father, mother and sister who has always been on my side, and inspire me to pursue higher degree of knowledge. Their love and care has always been a source to walk through any difficulties of life.

Finally, I would like to acknowledge King Mongkut's Institute of Technology Ladkrabang for providing financial support and instruments to conduct this research. At last, I cannot forget to acknowledge the plantation owner for providing samples, and all the teachers and friends who helped me to conduct this research directly or indirectly.

Amrit Shrestha

Table of contents

Table of contents (continued)

Table of contents (continued)

Table of contents (continued)

List of tables

List of tables (continued)

List of figures

List of figures (continued)

List of figures (continued)

Chapter 1

Introduction

1.1 Introduction to the research problems and its significance

Rising environmental air pollution, global warming and concern toward the dearth of fossil fuel has fostered the development of biomass resources as an alternative energy source [1, 2]. Biomass is an agricultural resource which supplies energy in two forms as energy crops and residue of crops [3, 4]. In order to mitigate the problems related to fossil fuels, fast growing energy crops are needed having less impact on environmental pollution. In such case, bamboo can be a crucial plant as it is one of the most fast growing, productive and versatile multi-purpose tree which can be grown in wide range of soil [5-9].

The total energy consumed in Thailand in 2013 A.D was 75,214 ktoe; where the highest energy, 47.79% of the total, was derived from the petroleum products. On the other hand, the consumption of renewable energy other than biomass was 5,278 ktoe which was in similar figure to coal and natural gas consumption, 5,947 and 5,339 ktoe respectively [10]. However, the consumption of biomass in forms of fuel wood, paddy husk, char coal, agricultural wastes was 8,076 ktoe which was higher than the consumption of coal and natural gas products [10]. These figures indicate that the biomass has potential to substitute the fossil fuels.

The energy plays a vital role in a country economy [11] and also one of the most essential needs for human beings. Thailand falls under tropical zone where the average temperature is 27 °C and annual rain fall of 1,200-1,600 mm/year [12]. Bamboo is found naturalized in most tropical and subtropical areas of the world [9]. Biomass is advantageous from both energy and environment point of view because it is considered as CO_2 neutral [13]. Furthermore, biomass can convert directly into bioenergy or biofuel in any forms either solid, liquid or gas by the means of thermochemical conversion such as pyrolysis, gasification, liquefaction, combustion, carbonization [14]. Therefore, Thailand government can take advantage of such economic and environmental benefit energy crops by establishing good rule and regulation toward afforestation of energy crops without altering the food chain. It is not only necessary to be leading exporter of biomass energy but also must be able to supply the demanded energy to its own markets. This activity will lead to a first zero emission country. On the other hand, it will create a new market and add job

opportunity too. Furthermore, the ash from biomass combustion can be used as an agricultural fertilizer, neutralizing agent and additives in building materials according to their composition [15].

Before selling the biomass commercially, its moisture content and combustion performance parameters i.e. combustion performance index, burnout index and ignition index must be recognized in advance because moisture content and combustion characteristics may be varied with different source and age so that it will get its actual monetary value instead of random cost per kilogram. These properties are equally important for biomass or its pellet production plant and the combustion plants. So, in order to measure its properties without consuming more time as thermogravimetric analysis (TGA) and oven drying methods a new method should be implemented. To mitigate this problem, near infrared (NIR) spectroscopy has found a scope for its application.

The thermogravimetric and oven drying procedure are time consuming process, approximately 3-24 hours for thermogravimetric analysis and more than 12 hours for oven drying method, which also requires a skilled manpower. NIR spectroscopy covers the electromagnetic radiation in the region from 780 to 2500 nm (12820-4000 cm^{-1}) [16]. The NIR spectroscopy technique can provide rapid results in seconds or continuously on-line, rather than in hours or days, with an accuracy and reproducibility equivalent to most reference methods. Other advantages of NIR include its low cost per test, low labor costs, no required chemicals to purchase or dispose of, great flexibility in sample presentation and the capability of testing many constituents simultaneously. This method is environmentally friendly because it requires no chemicals. The instrument is simple to install and operate, does not produce any emissions which need to be removed by drainage or exhaust and easy to prepare sample. Many instruments are of the stand-alone type and their durability allows them to work well for more than ten years. Instruments can be networked to use the same calibration with their performance controlled from a single control center [17].

NIR spectroscopy has been applied for the evaluation of moisture content of rice straw by Jin et al [18], solid biofuels by Jensen et al [19], *Jatropha curcas* kernels by Posom et al [20], compost by Suehara et al [21], *Miscanthus x giganteus* and short rotational coppice willow by Fagan et al. [22] and many other authors. Furthermore, NIR spectroscopy has been applied for the evaluation of lignocellulosic compound content of sugarcane biomass[23], straw content of straw-coal blends[24], heating value of straw [25], *Miscanthus* and coppice willow [26]. However, till this date there are no works that relate combustion parameters of biomass with NIR spectroscopy. Therefore, I propose a research on "Near infrared spectroscopy as an alternative for

the measurement of moisture content and combustion parameters by hot air oven drying and thermogravimetric analyzer" to solve the problem of delay in measurement.

1.2 Objectives

The objectives of this study were:

1.2.1 to compare the combustion performance parameters of grounded bamboo chips with grounded *Leucaena leucocephala* pellets.

1.2.2 to develop the model that correlates the NIR spectral characteristic of the bamboo chip (Dendrocalamus sericeus cl. Phamon) with its moisture content and combustion performance parameters i.e. ignition index, burnout index and combustion performance index

1.2.3 to prove the possibility of NIR spectroscopy as an alternative, rapid and accurate method for evaluation of those properties.

1.3 Scope of the research

In this research, bamboos of species *Dendrocalamus sericeus* cl. Phamon, which is well-known and popular in Thailand, were used and were procured only from single plantation farm, Uttaradit, Thailand. The moisture content and combustion performance parameter, i.e. ignition index, burnout index and combustion performance index, were studied. NIR-Gun (600-1100 nm), Micro-NIR (1150-2150 nm) and FT-NIR (12500-3600 cm^{-1}) NIR-instrument were used for NIR scanning propose, while thermogravimetric analyzer was used for combustion. This work focuses on the measurement of the moisture content and combustion performance parameters of the bamboo chip.

1.4 Expected results

This research will be helpful for process controlling using the moisture parameter during drying, pelletization and thermochemical conversion and determining the combustion parameters. This research will expand the scope of NIR on the energy sector. In addition, this research will be a reference for future NIR and energy research.

1.5 Experimental plan

The experiment plan of this work is divided into two parts:

1.5.1 Preliminary study for the comparison of combustion performance parameters of grounded bamboo chips and grounded *Leucaena leucocephala* pellet.

1.5.2 Feasibility study on near infrared spectroscopy as an alternative for the thermogravimetry and oven drying method in evaluation of combustion performance parameters and moisture content on bamboo chips (*Dendrocalamus sericeus* cl. Phamon)

The experimental flow chart is shown in Figure 1.1 and 1.2. The bamboo samples, *Dendrocalamus sericeus* cl. Phamon, were procured from Uttaradit, Thailand. The bamboo trees were then cut about 10 cm from the ground level and only about 1 m from the base of bamboos were selected for the study, and the bamboo samples were chopped by the chopping machine (P5508, Patipong, Thailand). After chopping, the bamboo chips were scanned immediately by the NIRS instruments for the analysis of moisture content and were subjected to reference analysis. Whereas, for the analysis of combustion performance parameters, firstly, the samples were dried under sun and were grounded before NIR-scanning. The scanned samples were then subject to reference analysis. Necessary pretreatments on the scanned spectra were performed firstly and then merged with the reference data for the regression analysis. Finally, the models were validated by test set validation.

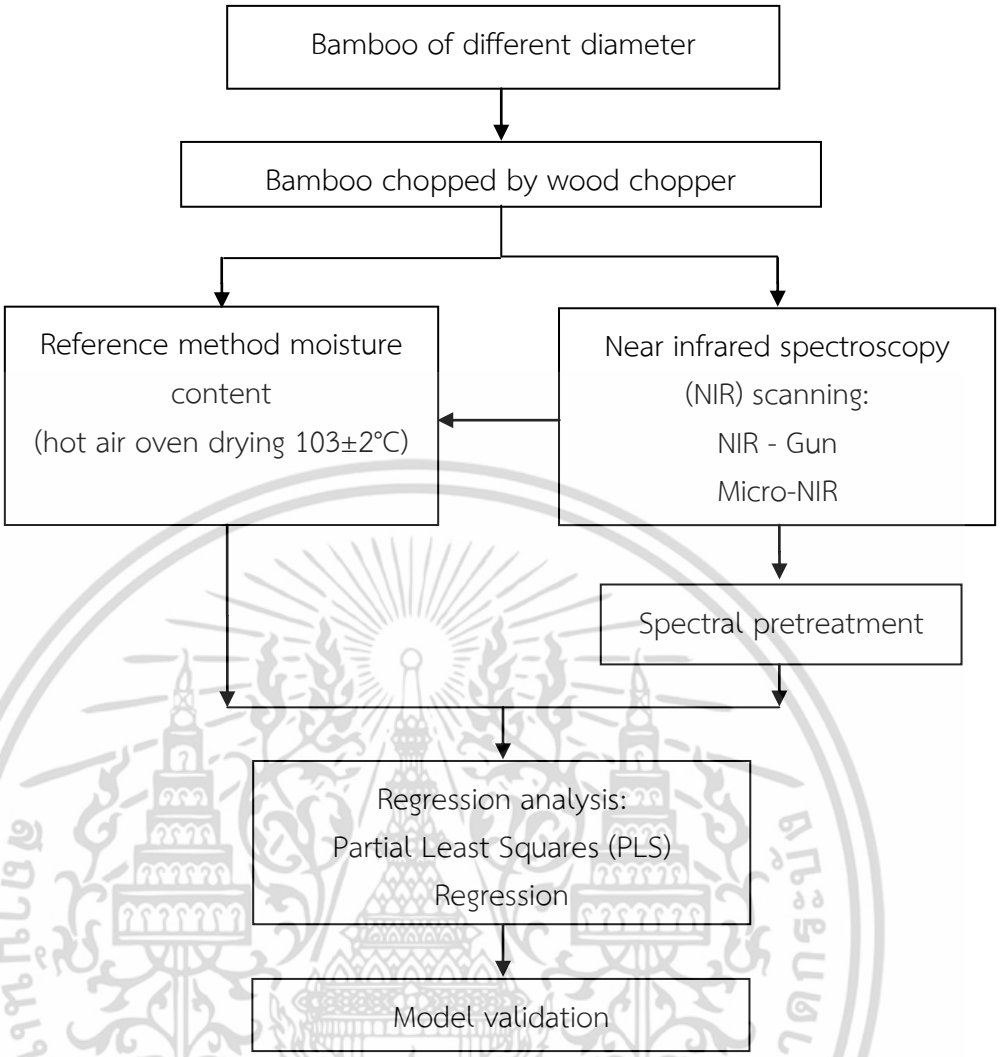

Figure 1.1 Flow chart for determination of moisture content.

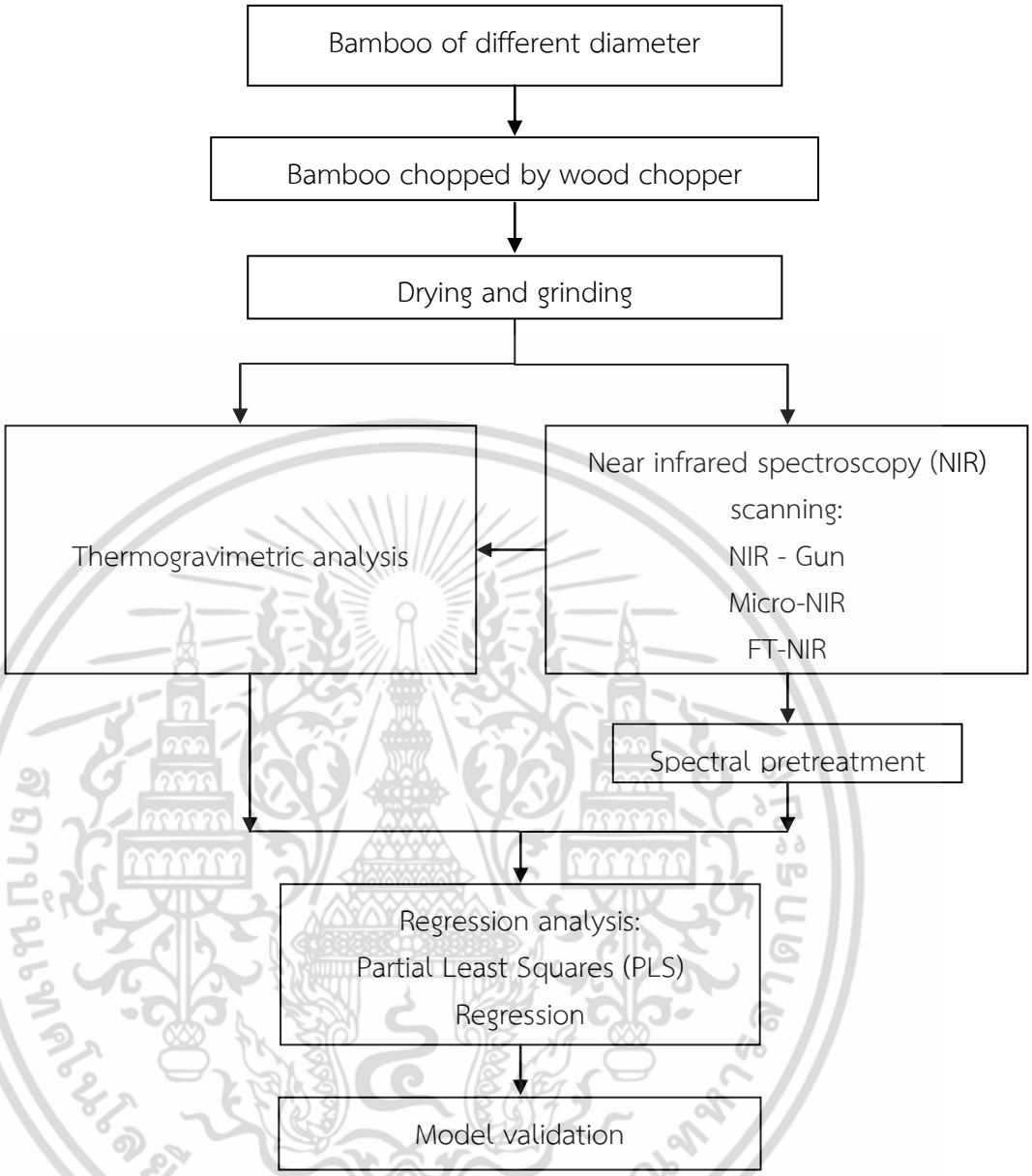

Figure 1.2 Flow chart for determination of combustion performance parameters.

Chapter 2

Theory and literature review

2.1 Near infrared spectroscopy and its basic principle

Near infrared spectroscopy is a spectroscopic technique to measure the electromagnetic radiation of near infrared region being absorbed, reflected or transmitted by the analyte. The near infrared region extends from 700 nm to nearly 3000nm [27]. The discovery of the NIR spectrum is ascribed to William Herschel. When Herschel continued his measurements of the heat energy of solar emission beyond the red portion of the visible spectrum, he found that the temperature increased markedly towards and beyond the red which is now called the near-infrared region, and the potential of this analytical technique was recognized by Karl Norris and introduced the modern NIR spectroscopy into industrial practice [28].

Organic matter mainly consist of carbon, hydrogen, oxygen, nitrogen, phosphorous and sulphur with minor amount of other elements which are combined with either covalent or electrovalent bonds to form molecules, and atoms and molecules are constantly at motion relative to each other known as the ground state. The molecules vibrate at various frequencies corresponding to wavelengths on infrared region of the electromagnetic spectrum. When the molecules are irradiated with an external source of energy they acquire the potential for energy changes [29]. These molecules will absorb photon energy only if the incident radiation is of the same frequency as one of the modes of vibration (fundamental in mid infrared, overtone and combination in near infrared) of the molecules and results on transformation to higher energy state [30].

Fundamental absorption usually occurs in mid-infrared region between 2,500-15,000nm. Other molecules absorb enough energy to reach second energy level known as first overtone. The first overtone band is weaker than the fundamental absorption and only fewer molecules reach to this state and still fewer molecules reach to the third level known as second overtone and so on. Very few molecules attain higher energy levels and the higher overtones appears as weaker bands relatives to the fundamentals. For the practical purpose, the absorbance of overtone higher than third is of little significance in quantitative NIR spectroscopy [29]. Since, most of fundamental absorptions occur in the mid-infrared region, the bands that

appear in the NIR region are all overtones or combination of fundamental absorption [27]. Combination bands occur when the absorbed photon excites two or more vibrations simultaneously. For this to happen, the energy of the photon has to equal the sum of the energies of the coupling vibration [29].

Vibrational and rotational motions are two major molecular motions. Vibrational motion is created by movements of the atoms toward and away from each other whereas rotational motion is created by rotation about the molecular axis. These motions represent the change in energy associated with atoms and molecules when they are excited to higher state level from lower level. The energy level of the molecule is the sum the rotational and vibrational energies. There are two main modes of molecular vibration, stretching and bending. Stretching is caused by the movement of atoms along the axes of bonds so that the distance between atoms changes rhythmically, while bending involves changes in bond angles between atoms [28]. Only the vibration which results in rhythmic changes in dipole moment of molecule can cause absorbance in the infrared. A pairs of atoms are said to have dipole only if they have unequal distribution of electric charge, and they possess electric field. This field will strongly couple to field of any passing light beam [29].

The most important absorption bands in the NIR region are -CH, -NH, -OH and -SH functional groups and appears as overtones and combinations bands [31]. Molecules in space possess many forms of energy such as vibrational and rotational. The energy required to cause a change in rotational states is very smaller than for vibrational state. The rotational absorption bands may only observed in cases of gases. So, for the study of IR spectra of solid and liquid, only vibrational motion is need to be considered. [28]

There are various models postulated to describe the vibrational spectroscopy. The wave model failed to account phenomena associated with the absorption or emission of energy although it explains the properties of electromagnetic radiation. So, it is necessary to view electromagnetic radiation as a stream of discrete particles called photons with and energy proportional to the frequency of the radiation. Hooke's law can be used to calculate the fundamental vibrations for diatomic molecules in IR i.e. transition from the ground state to the first excited state. However, it fails to describe the presence of overtones. Max Plank in 1900 proposed that the energy of an oscillator is discontinuous and any change in its energy content can only occur by means of a transition between two discrete energy states brought about by the absorption or emission of discrete packets of energy called quant; this idea was known as the quantum theory. The potential energy diagram of harmonic and anharmonic oscillation is shown in Figure 2.1. The quantum mechanical model for harmonic oscillator is given as:

$$E = (\upsilon + 0.5)h\nu \quad (2.1)$$

where, E is the energy, υ is vibrational quantum number, h is plank constant 6.626×10^{-34} m^2kgs^{-1} and ν is vibrational frequency.

The model allows vibrational transitions changes by one ($\Delta\upsilon = \pm1$) i.e. υ =0 to υ =1; $\Delta E = h\nu = (h/ 2\pi)\times\sqrt{(k/\mu)}$, and explains the observed IR absorption bands are due to the fundamental modes of molecular vibration but fails to explain the presence of overtone bands in the NIR which arise from the transition when $\Delta\upsilon$ is ±2, ±3... and is well explained by quantum mechanical model using Morse function for anharmonic oscillator and given as:

$$E = h\nu[1 - \chi(\upsilon + 0.5)](\upsilon + 0.5) \quad (2.2)$$

where, χ, is an anharmonicity constant. If the term $\nu[1 - \chi(\upsilon + 0.5)]$ is replace by ν'

$$E = (\upsilon + 0.5)h\nu' \quad (2.3)$$

Thus, anharmonic oscillator behaves like harmonic oscillator but with an oscillating frequency which decreases steadily with increasing ν. The energy associated with a transition from ν to $\Delta\nu$ is:

$$\Delta E = h\nu[1-(2\upsilon + \Delta\upsilon + 1)\chi] \quad (2.4)$$

And the selection rules are $\Delta\upsilon$ = ±1, ±2, ±3... thus, they are the same as for harmonic oscillator but with the additional possibility of larger jumps [28].

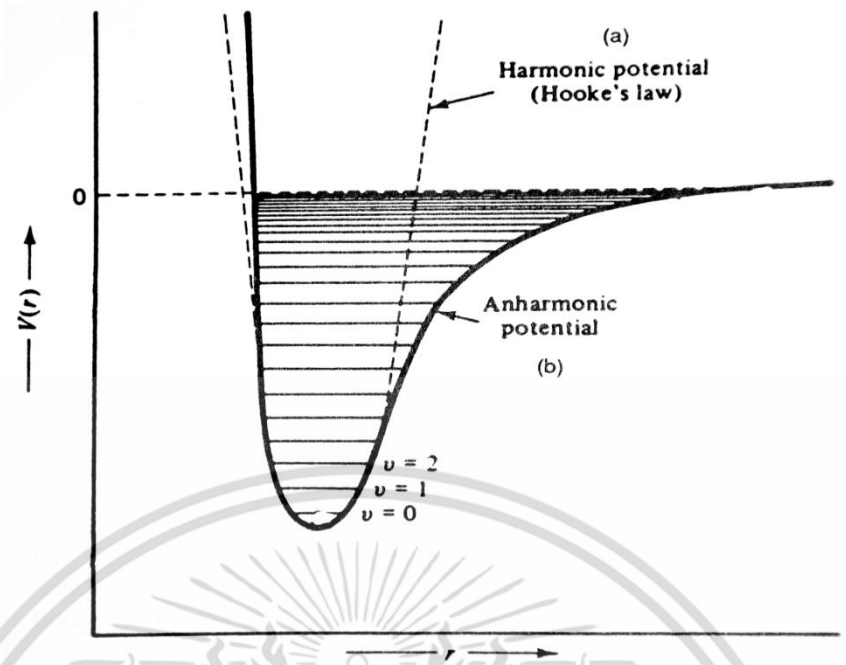

Figure 2.1 Potential energy diagram of harmonic oscillation and anharmonic oscillation [30].

2.2 Sample presentation

When the radiation fall on the sample, it will either transmit, absorbed or reflected depending on the nature of the sample. However, the total radiation incident on the sample must be equal to the sum of the radiant power transmitted, absorbed and reflected by the sample according to the law of conservation of energy [28]. The physical principles of the near infrared spectroscopy are discussed below.

2.2.1 Absorption and transmission of radiation

The attenuation of the transmitted radiation by an absorbing sample is described by the Beer-Lambert law. According to Lambert, the decrease of radiation intensity (I), Figure 2.2, with its path through material is proportional to the respective intensity (I_o) [32].

$$-\frac{dI}{dx} = a'I \qquad (2.5)$$

Where, a' is the proportionality factor so called absorption coefficient.

Integrating through the sample, x=0⟶l, gives

$$\ln I - \ln I_o = -a'l \tag{2.6}$$

which is express as,

$$I = I_o e^{-a'l} \tag{2.7}$$

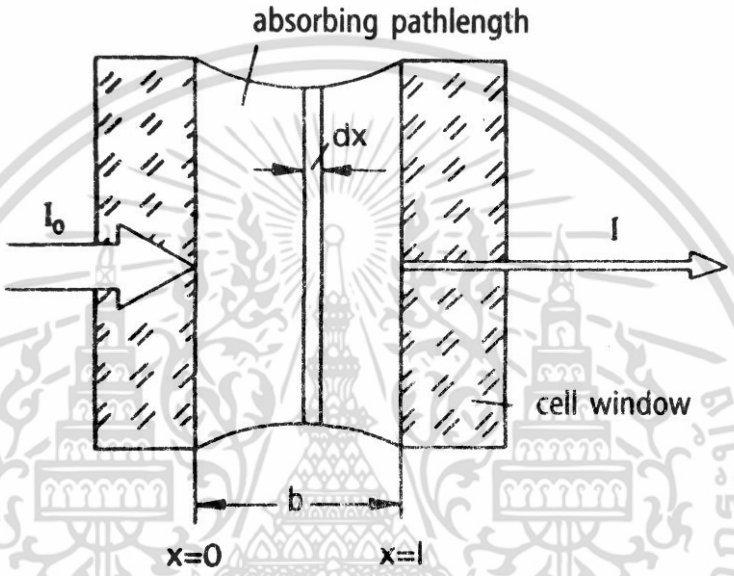

Figure 2.2 Regarding the derivation of Beer's law [32].

Beer found the uniform influence of the concentration, c, on the radiation attenuation as that of the cell thickness, b. Therefore,

$$\ln I - \ln I_o = -a'bc \tag{2.8}$$

Conversion of the Eq. 2.8 from natural logarithm to the logarithm base 10 follows:

$$\log I - \log I_o = -0.434a'bc \tag{2.9}$$

With $a = -0.434a'$ the Eq. 2.9 can be written as:

$$\log I - \log I_o = abc \tag{2.10}$$

The parameter "a" is called the absorptivity to the base 10.

$$I = I_o 10^{-abc} \quad (2.11)$$

The absorption coefficient is dependent on the concentration and is consider being constant for the specific substance at a particular wavelength. The absorbance is defined as:

$$A \equiv -\log \frac{I}{I_o} = abc \quad (2.12)$$

The transmittance of an absorbing medium is define through the Beer-Lambard law as the intensity transmitted by the sample (I_t) to the intensity of the radiation incident on the sample (I_o) [33], and mathematically define as:-

$$T = \frac{I_t}{I_o} = 10^{-A} \quad (2.13)$$

The absorbance and transmittance (T) is related as,

$$A = \log \frac{1}{T} = abc \quad (2.14)$$

The absorbance (A) is directly proportional to the concentration of the sample. When logarithm of a number is taken, it results in a small number which makes the bands with low intensity, but these bands may be significance for qualitative spectral interpretation and might not be seen clearly in spectra presented as absorbance. Therefore, absorbance must be used for quantitative spectral analysis, and transmittance, T, for qualitative interpretation of spectra [32].

2.2.2 Reflection of radiation

The different modes of reflection are specular, diffuse and internal reflection. Specular reflection is defined as reflection in which the angle of incidence on the sample is exactly same as to the angle of reflection and is difficult technique since, usually only few percentage of light is reflected. In the diffuse reflection, the angle of the reflection is different from angle of incidence. Internal reflection is the surface phenomenon and only the surface of the sample interacts with the internal

reflected beam [34].

Surface reflectance does not carry any information about the object, and the diffuse reflectance comes from within an object and carries information concerning its composition and other characteristics [27], which makes the diffuse reflection technique the most popular sampling technique among other reflection techniques. The different pathways that light energy can take through or from a sample are illustrated in Figure 2.3.

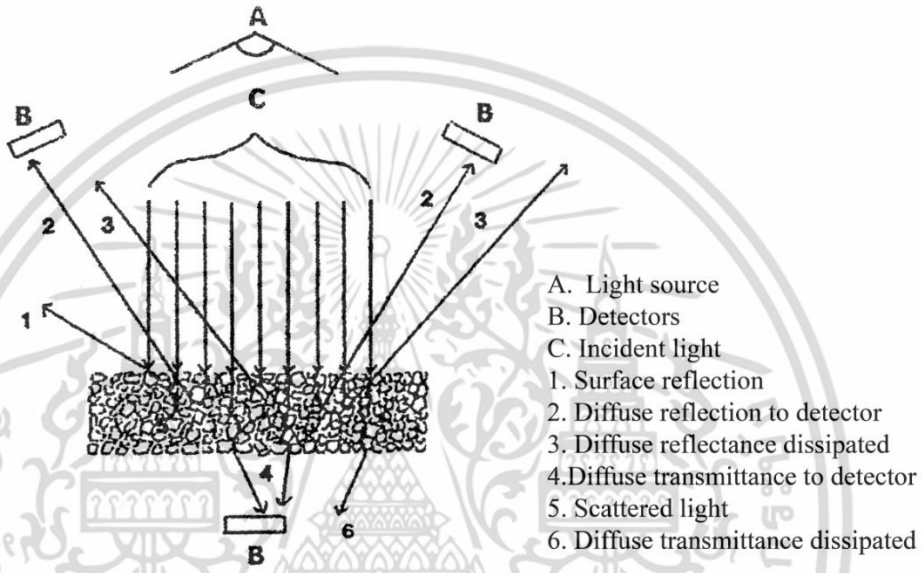

Figure 2.3 Pathways of light through a sample [27].

The diffusely reflected radiation is collected and detected by the detector which is converted into a spectrum that is similar to absorbance spectrum in transmittance spectrometry. The model put forward by Kubelka and Munk in 1931 to describe diffusely reflected radiation of paint layers is widely used and accepted in diffuse reflectance infrared spectrometry. The Kubelka-Munk theory defines the reflectance spectrum as the ratio of the sample concentration to the scattering intensity of the sample [35]:

$$f(R_\infty) = \frac{(1 - R_\infty)^2}{2R_\infty} = \frac{k}{s} \qquad (2.15)$$

where, $f(R_\infty)$ = Kubelka-Munk function, R = reflectance, R_∞ = reflectance of infinite thickness material, k = co-efficient of absorption, s = co-efficient of scattering

The absorption coefficient (k) is equal to the concentration (c) multiplied by the

absorption (a) as defined by the Beer-Lambert law

$$k = a \times c \tag{2.16}$$

For the constant scattering coefficient, the theory predicts a linear relationship between molar absorption coefficient and maximum value of Kubelka-Munk function, $f(R_\infty)$, for each peak. Since the scattering depends on the size of particle size, it must be made constant for the quantitative analysis [35]. For practical purpose the diffuse reflectance is measured with respect to a non-absorbing standard and converted to the common logarithm to produce a nearly linear relationship with concentration which is given as [28]:

$$\log\frac{R'}{R} = \log\left(\frac{1}{R}\right) + \log(R') \sim \frac{a \times c}{s} \tag{2.17}$$

where, R'=reflectance of reference material (R'>R), R = reflectance of sample

For the monochromatic radiation log(R') is constant and may be ignored since the absorption of the reference material is approximately zero i.e R'=1. Then the Eq. 2.17 can be written as:

$$\log\left(\frac{1}{R}\right) \sim \frac{a \times c}{s} \tag{2.18}$$

2.3 Near infrared instrumentation

NIR instruments have been widely utilized in agriculture, food processing, medical and pharmaceutical applications along with polymer and plastics processing, environmental analysis, material recycling and in satellites or aircraft for remote sensing, which record the overtone and combination bands, and the embedded information is extracted by the mean of chemometric technique. There are various criteria for the selection of NIR instrument. Wavelength precision, resolution, signals to noise ratio and cost are some of the most important criteria for NIR instrument [36]. The basic elements of the NIR instruments are radiation source, wavelength selection device and a detector. The basic configuration of the NIR instrument is shown in Figure 2.4. The various parts of the NIR instrument is briefly describe below:

2.3.1 Light source

The light source for NIR instrument can be categorized into two groups, broad waveband and narrow waveband. A tungsten halogen lamp is an example of broad waveband, and light emitting diodes (LEDs) and laser diodes are the example of narrow waveband. The most common light source for the NIR instrument is tungsten filament bulbs. The typical wavelength of this light source is between 400 to 5000 nm. The narrow waveband light source is used when full NIR region spectra are not necessary. LED is a semiconductor diode which emits discrete, incoherent and narrow spectral bands, while Lasers emits monochromatic radiation with high intensity [37].

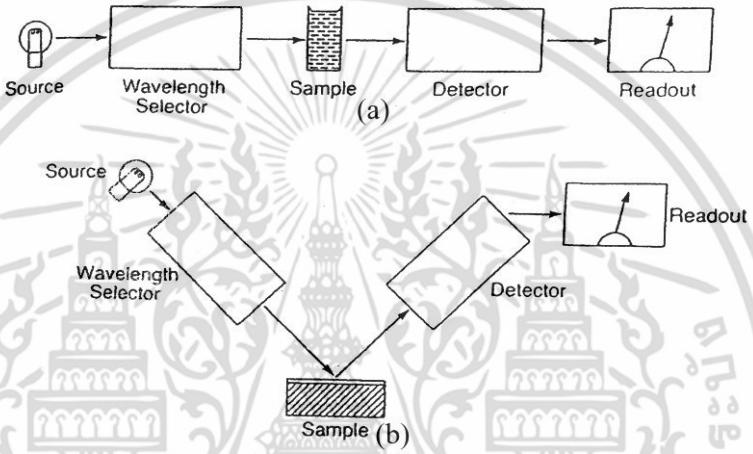

Figure 2.4 Basic configuration of the NIR instrument: (a) transmission mode and (b) reflection mode [37].

2.3.2 Wave length selector

2.3.2.1 Filters

Optical interference filter and electronically tunable filters (ETF) are two major types of filters used for selecting the wavelength in NIR. Interference filters consist of multiple thin layers of dielectric material with different refractive properties which reflects some wavelength and transmits other. It may be circular or wedge shape [37].

Electronically tunable filters are a group of devices whose spectral transmission can be electronically controlled by adjusting voltage, acoustic signal and other parameters. Liquid crystal tunable filter (LCTF) and acousto-optical tunable filter (AOTF) are two prevailing electronically tunable filters. The principle of the AOTFis based on the diffraction of light on the crystal. When radio frequency signal is applied to $LiNbO_3$ piezoelectric transducer which is embedded upon transparent anisotropic TeO_2 crystal, acoustic wave is produce which propagates through TeO_2

crystal and act as a periodic moving grating. Thus, when the light is incident, it will be diffracted [38, 39] as shown in Figure 2.5. The LCTF is a lyot filter based on the principle of polarization dispersion which uses the retardation to pass a single wavelength of light. Lyot filter is constructed by placing a series of quartz or calcite birefringent retarder with a liquid-crystal variable wave plate which can be varied electrically [40, 41].

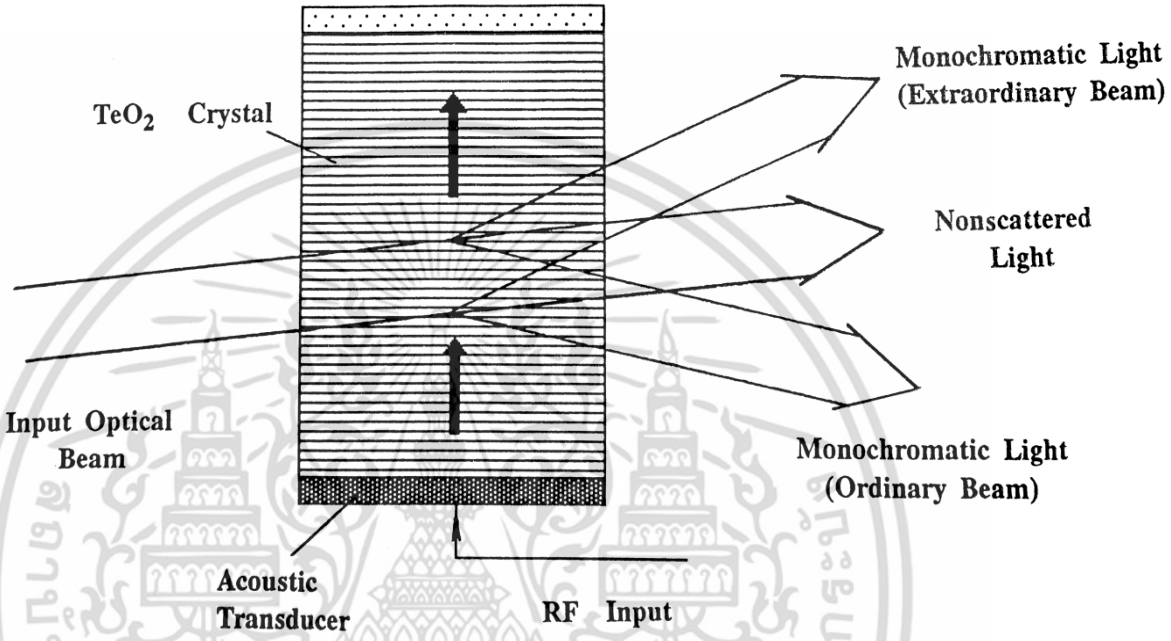

Figure 2.5 Working principle of the AOTF [38].

2.3.2.2 Prism

A prism is used to disperse incident light into a spectrum of different wavelength. The dispersion of prism depends on the refractive index of the prism material and the wavelength of the line studied: dispersion is high in UV-region but decreases rapidly with increasing wavelength, and also the resolution depend on the size of prism [42].

2.3.2.3 Diffraction grating

A diffraction grating is an optical element that separates polychromatic light into its constituent wavelengths of lights. It is a piece of substrate made of glass, metallic or ceramic material whose surface has been etched into closely spaced and replicated parallel grooves and coated with a reflecting material such as aluminum. The polychromatic light that hits the grating is dispersed, and each constituent light of different wavelength is reflected from the grating at a specific angle shown in

Figure 2.6. It performs better and more precise and efficient than prisms because grating provides the linear dispersion of wavelengths [37].

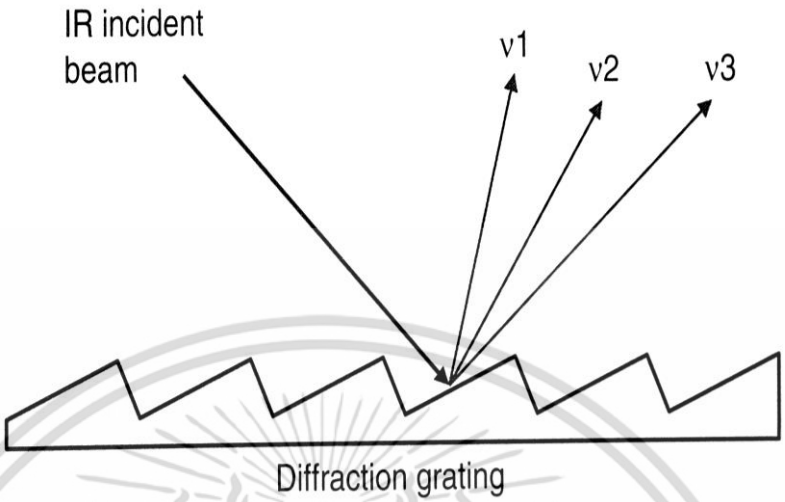

Figure 2.6 Dispersion of single beam by a diffraction grating [37].

2.3.2.4 The interferometer

Interferometer is an optical device that allows the controlled generation of interference patterns between two light beams. The light from the source when enter into the interferometer splits into two light beams and makes to travel different path length which are again recombine into single beam either constructively or destructively and leaves the interferometer [43].

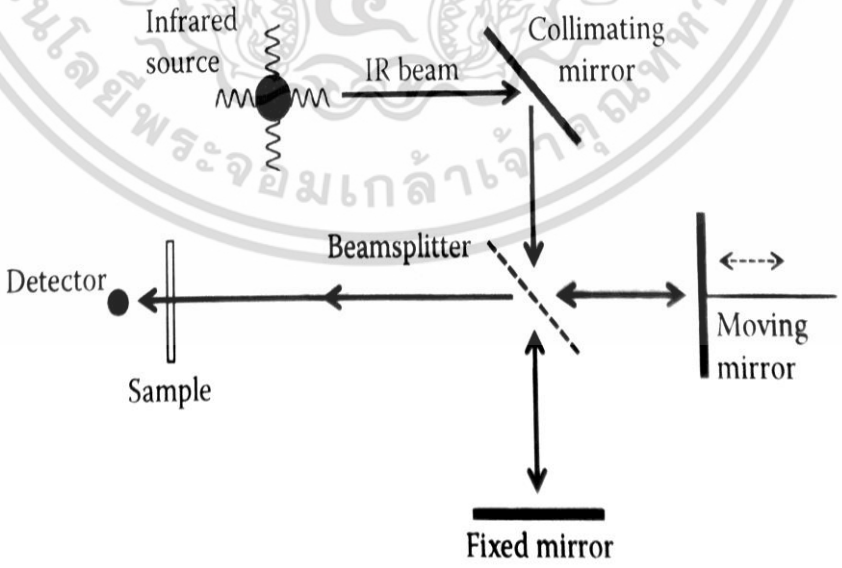

Figure 2.7 The optical diagram of Michelson interferometer [43].

A systematic diagram of the most common type of the interferometer, Michelson interferometer, is shown in Figure 2.7. It consists of source, beam splitter, a moving and fixed mirror. For NIR Spectroscopy, the source emits light in NIR region for near infrared spectroscopy. The beam splitter splits the light equally into two beams and also serves to recombine into single beam after they are reflected back by the two mirrors. Two mirrors are mounted perpendicularly and beam splitter is fixed at an angle 45°. The moveable mirror moves back and forth along the axis parallel to light source. One half of the light passes through the beam splitter to the fixed mirror is reflected back to the beam splitter while other half is reflected on to the moving mirror is also reflected back to the beam splitter. When two mirrors are in equidistance, the reflected beams are in phase which interferes constructively and the intensity of beam is highest during constructive interference. The highest intensity occur when the optical path difference (δ) between the mirror is an integer (n) multiple of wavelength (λ) and given by Eq. 2.19. In contrast, the beams interfere destructively when the two light beams from the mirrors are out of phase with each other and given by Eq. 2.20 [43]

$$\delta = n\lambda \tag{2.19}$$

$$\delta = (n+1/2)\lambda \tag{2.20}$$

2.3.3 Detector

Detectors are optical devices to measure the intensity of radiation that strikes on them by converting radiation energy into electric signals. On the basis of operation principle, detectors can be classified into two types: thermal detector and photon detector. Bolometer is an example of thermal detector. The principle of operation involves the absorption of infrared energy by a temperature-sensitive surface. The advantage of thermal detector is their uniform sensitivity at all wavelengths, but it has low response time. The principle behind photon detector is when the radiation strikes on the light detector a current is produced in the external circuit proportional to the intensity of the incident light. Silicon photodiode, indium gallium arsenide, lead selenide, mercury cadmium telluride are examples of photosensitive diode [44].

2.4 Partial least squares

There are various methods for the regression analysis. Among them PLS is one of the superior techniques for handling spectroscopic data. The multicollinearity problems that are normally associated with spectroscopic data are unable to handle

by multivariate linear regression (MLR). This collinearity problem were solved by the principal component regression (PCR) by converting independent variable (X-data) into score and loading and representing data matrix as score matrix, removing less significant score and also ensure the matrix inversion. However, during regression it does not consider the dependent variable (Y-data or concentration) and may not be highly correlated with the property of interest (X-data or spectral value). Hence, the solution may not be yielded satisfactorily. The PLS solved these problems associated with PCR by relating the spectral data and the property of interest with the outer relation called latent variables or loading weights and also ensure the maximum correlation between them during calibration and compress data on such a way that the most variance in both X and Y is explained [45-47]. The graphical representation is shown in Figure 2.8. The PLS NIPALS algorithm:-

in X-block

$$\text{Let, } u_1 = \text{any y \{y is reference data\}} \tag{2.21}$$

Calculating the weight of X-block using score of Y-block

$$w_1^T = \frac{u_1^T X}{u_1^T u_1} \tag{2.22}$$

$$w_1^T = \frac{w_1^T}{\|w_1\|} \text{(normalizing)} \tag{2.23}$$

defining the X-scores using original X-data

$$t_1 = Xw_1 \tag{2.24}$$

in Y-block

using X-score to calculate Y-loading

$$q_1^T = \frac{t_1^T Y}{t_1^T t_1} \tag{2.25}$$

calculating Y-score

$$u_{1,new} = \frac{Yq_1}{q_1^T q_1} \tag{2.26}$$

the inner relation is given as

$$\hat{u}_1 = b_1 t_1 \tag{2.27}$$

the inner regression coefficient is

$$b = \frac{u_1^T t_1}{t_1^T t_1} \tag{2.28}$$

calculating X-block loading

$$p_1^T = \frac{t_1^T X}{t_1^T t_1} \tag{2.29}$$

calculation of residual

$$E = X - t_1 p_1^T \tag{2.30}$$

$$F = Y - b\, t_1 q_1^T \tag{2.31}$$

Finally, the regression coefficient vector is

$$b = W(P^T W)^{-1} q \tag{2.32}$$

$$q = (T^T T)^{-1} T^T y \tag{2.33}$$

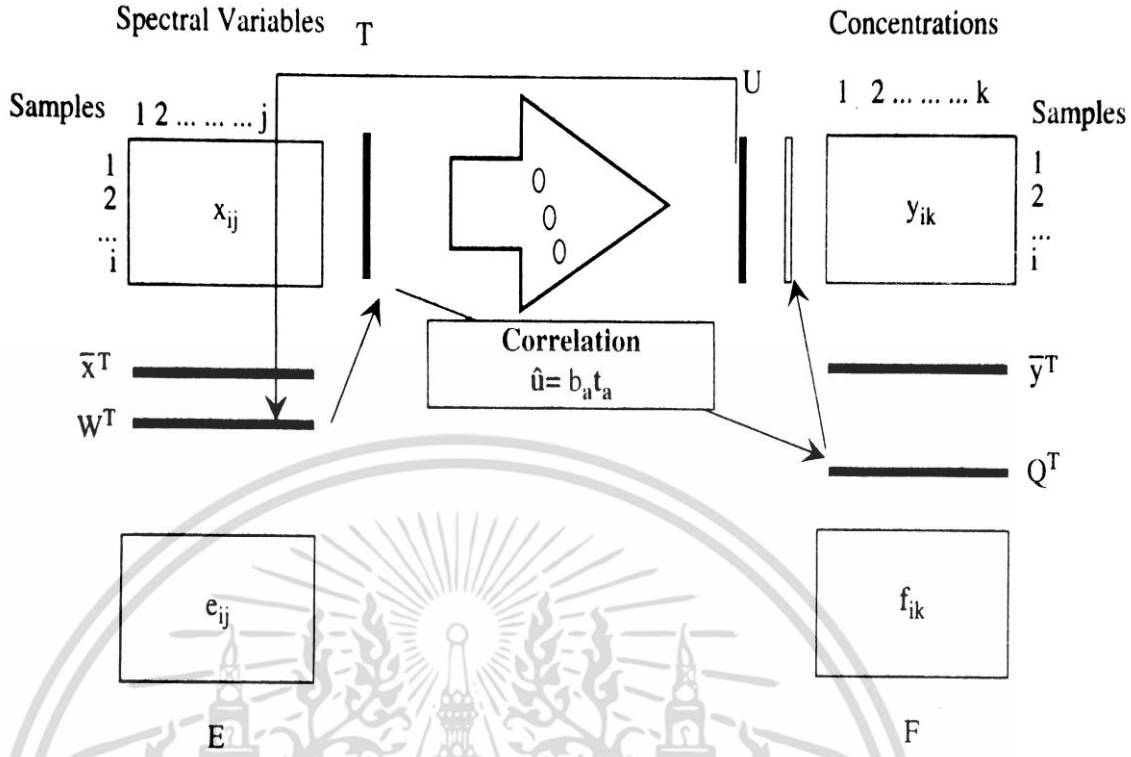

Figure 2.8 Calculation processes for the regression coefficients between t and u of PLS model [45].

Some of the properties of the PLS factors are listed below [46]:

1. p_h^T and q_h^T have unit length for each factor, h: $\| p_h^T \| = \| q_h^T \| = 1$, or $\sum p_{hj}^2 = \sum q_{hj}^2 = 1$ for j= 1 to m.
2. t and u are centered around zero for each factor, h: $\sum t_{hi} = 0$ and $\sum u_{hi} = 0$ for i= 1 to n.
3. w and t are orthogonal.

2.5 Data pretreatment

The purpose of the data pre-treatment is to reduce noise, light scattering effects to the spectra, and then to improve spectral resolution [48] so that signals will better adhere to Beer's law which states that absorbance and concentration are linearly correlated [49]

$$A = \varepsilon lc \qquad (2.34)$$

where, "ε" is the molar absorbtivity, "l" is the effective path length and "c" is the concentration of the constituent of interest. The collective term $\varepsilon \times l$ is constant for

the data set, thus making a linear relationship between A and c.

The spectra can be significantly influenced by non-linearity introduced by light scattering and differences in the effective path length. Moreover, baseline shifting, tilting overlapping, noise are the common problems seen in NIR spectra which can be eliminate by applying suitable pre-processing. Selection of suitable pre-processing depends on the successive modeling stage.

2.5.1 Savitzky-Golay (S-G) smoothing

This method fits the data points with a polynomial by least square methods. It consists of three parameters, polynomials degree, number of smoothing points and derivative order of polynomials. S-G smoothing is zero order derivatives. If m be the number of smoothing points then 2m+1 consecutive values are used to determine the best mean square fit through the value of a polynomial of degree n (n less than 2m+1) which is optimized by least square method [50]. The polynomial Eq. is given as:

$$f_x = \sum_{k=0}^{n} b_{nk} X^k = b_{no} + b_{n1} X^1 + b_{n2} X^2 + \ldots + b_{nn} X^n \qquad (2.35)$$

2.5.2 Derivatives

Derivatives are useful tool for separating overlapping peaks and baseline variation. The first derivative is useful for removing the baseline variation, while second derivative removes both baseline and linear trend. First, the data are fitted by S-G method with a polynomial and then the derivative of that polynomial is done. The first derivative is estimated as the difference between two subsequent spectral measurement points, and the second order derivative is then estimated by calculating the difference between two successive points of first-order derivative spectra [51, 52]:

$$X'_i = X_i - X_{i-1} \qquad (2.36)$$

$$X''_i = X'_i - X'_{i-1} = X_{i-1} - 2X_i + X_{i+1} \qquad (2.37)$$

where, X'_i denotes the first derivative and X''_i the second derivative at point (wavelength) i.

2.5.3 Normalization

Normalization of spectra is the process of scaling the spectra so that the unwanted sources of variabilities are minimized [53]. Normalization does not involve

a least squares fitting in their parameter estimation, so they can be sensitive to noisy entries in the spectrum [51]. The various normalization processes are:

2.5.3.1 Mean normalization

It is the process of dividing each row (each observation; ($X_{i,k}$) of a data matrix by its average value ($\overline{X}_i$). Mathematically which is given as [53, 54]:

$$X_{i,k} = \frac{X_{i,k}}{\left|\overline{X}\right|} \tag{2.38}$$

2.5.3.2 Maximum normalization

In this process, each row ($X_{i,k}$) is divided by its maximum absolute value ($\max\left|X_i\right|$) which is mathematically defined as [53, 54]:

$$X_{i,k} = \frac{X_{i,k}}{\max\left|X_i\right|} \tag{2.39}$$

2.5.3.3 Range normalization

In this process, each row ($X_{i,k}$) is divided by its range (max value – min value). Mathematically, it is defined as [53, 54]:

$$X_{i,k} = \frac{X_{i,k}}{\max(X_i) - \min(X_i)} \tag{2.40}$$

2.5.4 De-trending

Detrend correction helps to remove curvilinearity and baseline shifts of spectra [55, 56]. To correct for this effect, the baseline is fitted by a second degree polynomial and subsequently subtracted from the spectra:

$$Y_j = b_o + b_1 \times X_j + b_2 \times X_j^2 \tag{2.41}$$

$$Y_j^* = Y_j - \hat{Y}_j \tag{2.42}$$

where, Y_j* is the de-trended spectrum of the j^{th} object, $\hat{Y}_j$ is the predicted value of the absorbance using Eq. 2.41 for the j^{th} spectrum, X_j is a vector of all wavelengths, b_o, b_1, b_2 are the coefficients of the regression.

2.5.5 Standard normal variate (SNV)

SNV remove scatter effects by centering and scaling each individual spectrum. It is also used in combination with de-trending to reduce multicollinearity, baseline shift and curvilinearity in spectroscopic data [56]. To remove the multiplicative interferences of scatter and particle size a mathematical transformation of spectra, known as SNV transformation is applied. Each spectrum is transformed separately according to the following formula: [55, 56]

$$SNV_j = \frac{y_j - \bar{y}}{SD_y} \tag{2.43}$$

where, y_j is the vector representing the absorbance constituting the jth spectrum, $\bar{y}$ is the mean value of y_j, and SDy,, is the standard deviation of y_j.

2.5.6 Multiplicative scatter correction (MSC)

MSC removes artifacts or imperfections (undesirable scatter effect) from the data matrix prior to data modeling which involves two steps: Firstly, The standard spectrum is generated which is the average of whole spectra and each individual spectrum is fitted to standard by least square method [51]:

Step 1. Calculating the average spectrum of the measured spectra:

$$X_{ref} = \frac{\sum_{j=1}^{N} A_j}{N} \tag{2.44}$$

where, A_j (j=1, 2, 3,..N) is the measured spectrum of sample j.

Step 2.

a) estimation of the correction coefficients (additive and multiplicative contributions)

$$X_{org} = b_o + b_{ref,1} \times X_{ref} + e \tag{2.45}$$

b) correcting the recorded spectrum

$$X_{corr} = \frac{X_{org} - b_o}{b_{ref,1}} = X_{ref} + \frac{e}{b_{ref,1}} \quad (2.46)$$

where X_{corr} is the corrected spectra, X_{org} is one original sample spectra measured by the NIR instrument, X_{ref} is a reference spectrum used for preprocessing of the entire dataset, e is the un-modeled part of X_{org}, and b_0 and $b_{ref,1}$ are scalar parameters, which differ for each sample.

2.6 Model performance

The performance of the model is check statistically by the following statistical parameters:

2.6.1 Coefficient of determination

The coefficient of determination indicates the closeness of fit between the predicted (y) and reference (x) data over the range of composition [27]. Mathematically, it is define as [57]:

$$R^2 = 1 - \frac{SSE}{SST} \quad (2.47)$$

where, SSE = Sum of square error $\sum (X - Y)^2$; SST = Sum of square total $\sum (X - \overline{X})^2$

X is reference value, Y is predicted value, and $\overline{X}$ is mean of X

Table 2.1 Guideline for the interpretation of R^2 [27].

R^2	Interpretation
Up to 0.25	Not usable in NIRS calibration
0.26-0.49	Poor calibration, reasons should be researched
0.50-0.64	Ok for rough screening
0.66-0.81	Ok for rough screening and some other approximate calibrations
0.83-0.90	Usable with caution for most applications, including research
0.92-0.96	Usable in most applications, including quality assurance
0.98+	Excellent, usable in any application

2.6.2 Standard error of cross validation (SECV) and Standard error of prediction (SEP)

SECV is the standard deviation of difference between NIR spectroscopy prediction values and reference values in the calibration samples set whereas SEP is the standard deviation of difference between NIR spectroscopy prediction values and reference values in the prediction set of samples that have not been used in development of calibration set. SEP measure how well a calibration predicts the parameter of interest for a set of unknown samples that are different from the calibration set [27]. Mathematically,

$$SEP = \sqrt{\frac{\sum(X - Y)^2 - \frac{\sum(X - Y)^2}{N}}{(N - 1)}} \tag{2.48}$$

where, X is reference value, Y is predicted value and N is the number of samples

2.6.3 Ratio of SEP to SD (RPD)

It enables the relative evaluation of a SEP in terms of standard deviation of the reference data. Higher value of RPD indicates the efficient NIRS prediction [27]. Mathematically,

$$RPD = \frac{SD_{validation samples}}{SEP} \tag{2.49}$$

Table 2.2 Guideline for the interpretation of RPD [27].

RPD value	Classification	Application
0.0-2.3	Very poor	Not recommended
2.4-3.0	Poor	Very rough screening
3.1-4.9	Fair	Screening
5.0-6.4	Good	Quality control
6.5-8.0	Very good	Process control
8.1+	Excellent	Any application

2.6.4 Bias

Bias is the mean difference between reference and NIRS data. It measures the overall accuracy of the calibration [27]. Mathematically,

$$\text{Bias} = \frac{\sum X}{N} - \frac{\sum Y}{N} \qquad (2.50)$$

where, X is reference value and Y is predicted value, and N is the number of samples

2.7 Model validation

2.7.1 Cross validation

Cross validation uses the same samples as it used for developing the calibration model. Cross-validation is extensively used in chemometrics for visualizing model stability and finding significant variables. In full cross validation, one sample is left out from the calibration data set and the model is developed from the remaining data set. Then the left-out sample is predicted by the model and the prediction residual is computed. The process is repeated until all samples has been left out once. At last, prediction residual are calculated and combined to compute the root mean square error of cross validation (RMSECV) [58].

$$\text{RMSECV} = \sqrt{\sum_{i=1}^{N_V} \frac{(\hat{Y}_i - Y_i)^2}{N_V}} \qquad (2.51)$$

where, $\hat{Y}_i$ and Y_i are predicted and reference values of calibration set samples, and N_v is the number of sample in validation set

2.7.2 Test set validation

In the test set validation, the data set is divided into calibration set samples and test-set samples. Then the model is developed using the calibration set. Finally, the model is evaluated using the test-set samples, samples that are not used for making model, and checked by the mean error of prediction RMSEP from the respective analysis errors [57].

$$\text{RMSEP} = \sqrt{\sum_{i=1}^{N_p} \frac{(\hat{Y}_i - Y_i)^2}{N_p}} \qquad (2.52)$$

Where, $\hat{Y}_i$ and Y_i are predicted and reference values of test set samples, and N_p is the number of sample in test set

2.8 Thermogravimetric analysis

The present definition of thermal analysis formulated by the International Confederation for Thermal Analysis and Calorimetry (ICTAC) reads as follows: Thermal Analysis (TA): A group of techniques in which a property of the sample is monitored against time or temperature while the temperature of the sample in a specified atmosphere is programmed [59].

Thermogravimetric analyzer measures mass change as a function of time and or temperature, thereby subjecting the sample to a defined and controlled environment (heating rate, gas atmosphere, flow rate, crucible type, etc.). A thermo-balance is employed for measuring the quantitative composition. The exact sample temperature is detected by a thermocouple which is in direct contact with the sample crucible. Water cooling system is deployed to cool and carry the unnecessary heat with in the furnace.

The various combustion performance parameters are defined below:

2.8.1 Ignition index (D_i)

As shown in Figure 2.9, the ignition temperature (T_i) was defined as following [60-62]:

Firstly, through the DGT peak point A, vertical line was made upward to meet the TG oblique line at point B; secondly a tangent line to TG curve was made at point B, which met the extended TG initial level line at point C; thirdly another vertical line was made downwards through point C, which met the cross axle at point D. The corresponding temperature of point D is defined as ignition temperature and the corresponding time to reach that temperature is defined as ignition time.

The ignition index (D_i) is determined by the Eq. as follows:

$$D_i = \frac{(dw/dt)_{max}}{t_p t_i} \tag{2.53}$$

where, $(dw/dt)_{max}$ = maximum combustion rate, t_p = corresponding time of $(dw/dt)_{max}$ and t_i = ignition time.

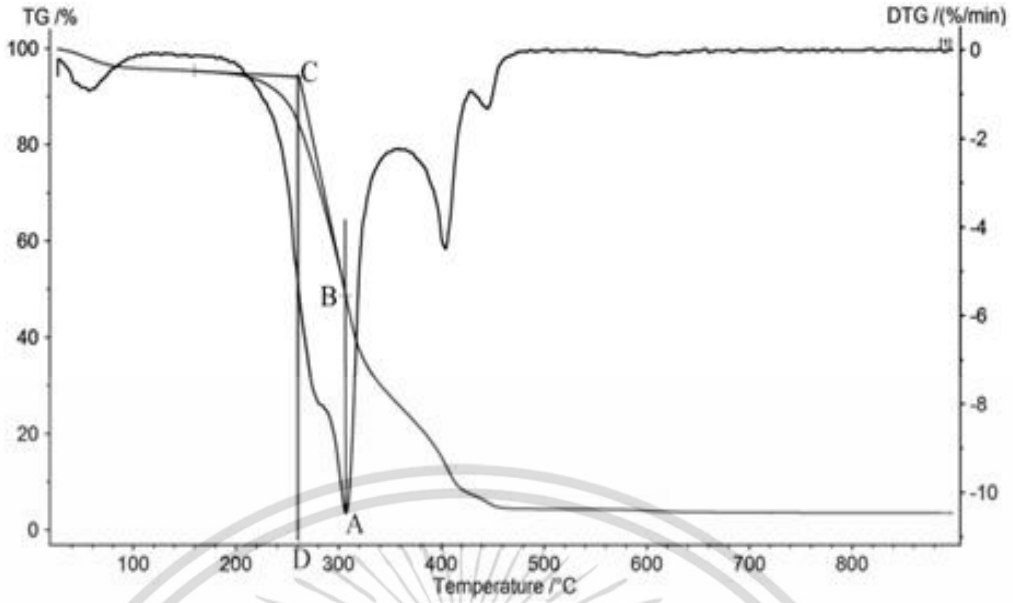

Figure 2.9 Determination of ignition temperature.

2.8.2 Burnout index (D_f)

Burnout temperature was identified as the corresponding temperature of no further weight loss in TG and DTG curves i.e. corresponding temperature at which combustion rate reduce to zero after the after the combustion process. Burnout temperature is the temperature on TG and DTG curves that shows the constant mass after the char combustion during the process and the correspondent time is known as burnout time [60, 63, 64]. The burnout index (D_f) is defined as:

$$D_f = \frac{(dw/dt)_{max}}{\Delta t_{1/2} t_p t_f} \tag{2.54}$$

where, $\Delta t_{1/2}$ = time zone of $(dw/dt)/(dw/dt)_{max} = ½$ and t_f = burnout time.

2.8.3 Combustion performance index (S)

A higher combustion index represents better combustion reactivity of the fuel which was calculated as [61, 65-67]:

$$S = \frac{(dw/dt)_{max}(dw/dt)_{mean}}{T_i^2 T_{fi}} \tag{2.55}$$

where, $(dw/dt)_{mean}$ = average combustion rate, T_i = ignition temperature and T_f = burnout temperature.

2.9 Theory of the instrument used

2.9.1 NIR instrument

The NIR-Gun (FQA, Fantec, Japan) consists tungsten halogen lamp as a light source which emits visible and NIR light over the rage 600-1100 nm. Firstly, the instrument is calibrated with the standard material, polystyrene, which is assumed to be pure reflectance and the spectrum thus generated is subtracted with the sample spectrum in order to achieve relative absorbance. The NIR-Gun uses interaction mode as a measurement method. The reflected light after interaction with sample is separated by grating and sends to silicon detector [68].

The Micro-NIR (JDSU, USA) consists of two integrated tungsten halogen lamp as a light source which emits light in the NIR region from 1150-2150 nm. The light is then subjected to the sample. The diffusely reflected light is received by InGaAs photodiode array detector through the linear variable filter dispersive element. In order to achieve relative absorbance, firstly, the instrument is calibrated with the standard material, Spectralon, which is assumed to be pure reflectance and the spectrum thus generated is subtracted from the sample spectrum [69].

The Fourier transform near-infrared (FT-NIR) instrument consist different mode for measurement. For this study, the integrating sphere measuring mode was selected. The schematic diagram of the FT-NIR instrument for the integrating sphere measuring mode is shown in Figure 2.10. It consists of interferometer which is used to create interference pattern. The light source, tungsten halogen lamp, emits the light in NIR region from 700-2500 nm (12500-4000 cm^{-1}) which is then travelled to interferometer. The light from interferometer leave either constructively or destructively which is then subjected to the sample. The diffusely reflected light from the sample is then received by PbS detector, and plot the interferogram, plot of response versus mirror displacement. This time domain signal is converted into frequency domain by applying Fourier-transform [70]. Firstly, the instrument is calibrated with the reference material, gold, which is assumed to be pure reflectance, and the spectrum thus generated is subtracted from the sample spectrum in order to achieve relative absorbance.

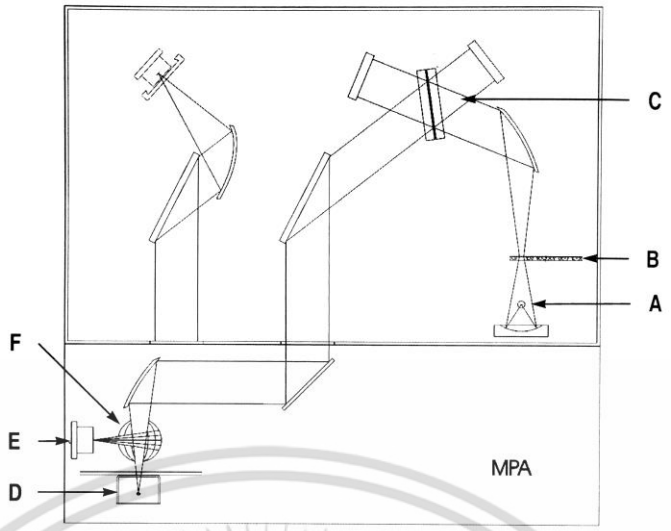

	Component		Component
A	NIR Source	B	Filter Wheel (IVU)
C	Interferometer	D	Sample
E	Detector	F	Integrating Sphere

Figure 2.10 Optical path for MPA with integrating sphere [70].

Table 2.3 Comparison of NIR instruments.

	Micro-NIR	NIR-Gun	FT-NIR
Light source	Tungsten Halogen	Tungsten Halogen	Tungsten Halogen
Detector	InGaAs	Silicon	PbS
Dispersion method	Linear variable filter	Grating	Interferogram
Measurement mode	Diffuse reflection	Interaction mode	Diffuse reflection
Standard reference material	Spectralon	Polystyrene	Gold

2.9.2 Thermogravimetric analyzer

The properties of the material change when it is subjected to the increasing temperature. This is the principle behind the thermogravimetric analyzer which measures mass change as a function of time and or temperature in a defined and controlled environment (heating rate, gas atmosphere, flow rate, crucible type, etc.). The instrument used for this research was TG 209 F3 Tarsus, Netzsch, Germany thermogravimetric analyzer. Its section view is shown in Figure 2.11.

This instrument operates between room temperature to 1000°C with heating rates from 0.001 K/min up to 50 K/min. The temperature of the sample is measured

by the thermocouple which is in direct contact with the crucible, and thermobalance is deployed to measure the instantaneous mass of the sample precisely. A shielded heating element, resistance heater based on nickel and stainless steel, is use as the heating source and the circulating water is used to cool the furnace. The resolution of the microbalance is 0.1µg. The instrument uses nitrogen gas as protective gas, and either oxygen or nitrogen as controlled atmosphere for oxidizing or inert atmosphere respectively [71].

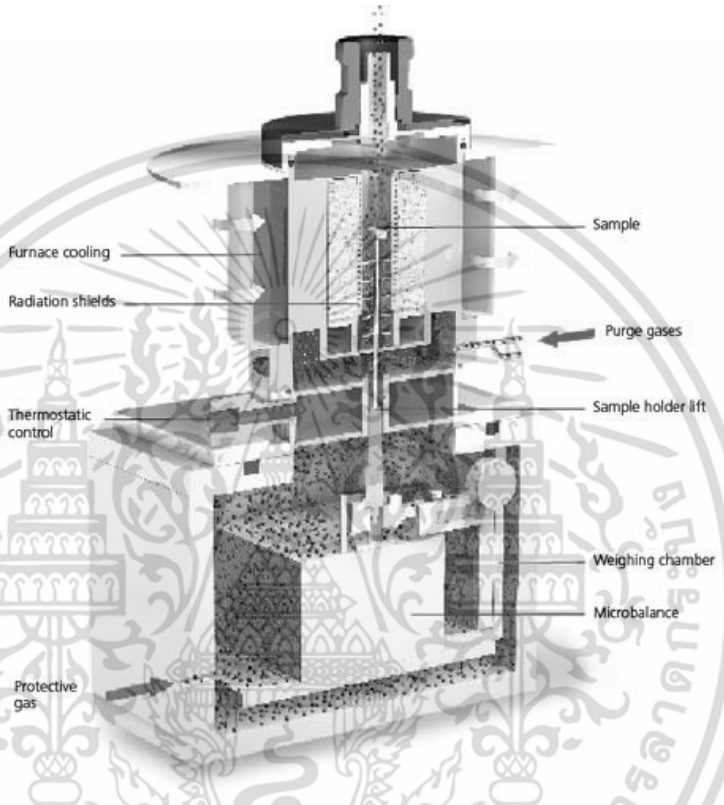

Figure 2.11 Cross section of thermogravimetric analyzer TG 209 F3 Tarsus [71].

2.10 Literature review

2.10.1 Biomass

The energy resources have been split into three categories: fossil fuels, renewable resources and nuclear resources [72, 73]. Renewable energy sources, often named as alternative energy resources, are those resources which can be used to produce energy again and again: e.g. solar energy, wind energy, biomass energy, geothermal energy, etc. [74]. Energy crops and residue of crops are the two major sources of energy that is supplied by agricultural product. Bioenergy production can replace fossil fuels contributing to the reduction of greenhouse gas (GHG) emissions by direct burning of biomass to generate electricity [3, 4]. Combustion of biomass does not contribute to net increase in CO_2 during its combustion because biomass consumes the same amount of CO_2 from the atmosphere during its growth as it release during combustion [13,75,76]. Biomass, also, plays the great role in the world economy. Although, much of the rural population in developing countries, which represents about 50% of the world's population, relies on biomass as energy but in industrialized country biomass represent only 3% of primary energy consumption [11]. The components of biomass include hemicelluloses, cellulose, lignin, extractives, lipids, proteins, simple sugars, starches, water, hydrocarbon, ash, and other compounds where cellulose, hemicelluloses and lignin plays a vital role during biomass combustion [13].

2.10.2 Bamboo

Bamboo is the vernacular woody grass (subfamily Bambusoideae, family Andropogonea/Poaceae). Bamboos are distributed mostly in tropic, occur naturally in subtropical and temperate zones of all continents except Europe, at latitudes from 46°N to 47°S and from sea level to 4000m elevation. Bamboos are use as construction and reinforcing fibers, paper, textile, food, combustion and other bioenergy applications [9]. The salient features of *Dendrocalamus sericeus* cl. Phamon commonly name as phai sang mon in Thailand [77]:-

1. height >15 m.
2. culm diameter:- 10 cm.
3. dark green culms and foliage, thick-wall culms.
4. Easy growing, moisture-retentive soil, full sun, somewhat drought-resistant.
5. Culms use for house construction and furniture, mainly planted in Thailand for producing chop-sticks and tooth-picks.

2.10.3 *Leucaena leucocephala*

The genus *Leucaena* belongs to family Fabaceae and sub-family Mimosoideae [78, 79]. This species is native to Central America and the Yucatan Peninsula of Mexico, now found naturalized in most tropical and subtropical areas. It is a thornless, evergreen, branched shrub or small tree up to 8 m high with deep roots [80]. It is very drought tolerant plant which can tolerate up to 7 months of dry season; however, growth is retarded in dry environments and poorly adapted to highly acidic soils although it is well adapted to a wide range of soils [81]. *L. leucocephala* is one of the most fast growing, productive and versatile multi-purpose tree which can be utilized in many ways such as forage for ruminants, fuel wood, charcoal, timber and pulpwood, environmental protection to soil, improver of the soil fertility and the physical conditions, controlling soil erosion and reforestation [82-85]. In addition, different parts of the *L. leucocephala* plants are used in traditional medicine; mature seeds as a substitute for coffee; young leaves, seeds, flower buds, young pods and shots are used in cooking many dishes in Indonesia, India and Thailand [80]. Generally, wood of *Leucaena* is labeled as strong and light weight [86]. *L. leucocephala* has high holocellulose and α-cellulose and low lignin content with xylan type hemicellulose [87].

2.10.4 Near infrared spectroscopy

Fagan et al.[22] predicted moisture content of *Miscanthus x giganteus* and short rotational coppice willow with a root mean square error of cross validation of 0.90% (R^2=0.99). Jin et al. [18] predicted moisture content of rice straw with standard error of prediction 1.01 % (R^2=0.8871). In addition, NIR spectroscopy has been investigated for determination of chemical content in biomass. Via et al. [88] characterized the changes in biomass (sweet gum, loblolly pine, and switch grass) with torrefaction for near infrared reflectance (NIR) and attenuated total reflectance Fourier transform infrared (ATR-FTIR) spectroscopy. Calibration models were built for the prediction of proximate analysis after torrefaction. It was concluded that both systems could be used for rapid monitoring, NIR performed better than FTIR. He et al. [24] used NIR spectroscopy for qualitative analysis of straw, blend 1 (straw content from 70-99% and coal), blend 2 (straw content from 1-30%and coal) and coal where correct classification percentage were 89.87, 79.66, 94.92 and 100%, respectively. Sabatier et al. [23] evaluated the lignocellulosic compounds including hemicelluloses, cellulose and lignin in sugarcane biomass and obtained correlation of determination (R^2) of 0.45-0.77 and standard error of prediction (SEP) of 1.16-1.37% dry matter.

2.10.5 Moisture Content

Moisture content of biomass has significant effect on the quality of fuel. Komilis et al. [89] concluded that both higher heating value (HHV) and lower heating value (LHV) decrease with increase in moisture content, whilst the caloric value depends on the individual organic matters. Li et al. [90] suggested that necessary moisture for producing good quality logs ranges from 5 to 12% for the woody materials (oak, oak bark, pine and cottonwood) under studied and also suggested that optimum moisture content is in the neighborhood of 8%. Logs made at around 8% moisture content had both high-density and good long term performance.

2.10.6 Thermogravimetric analysis (TGA)

The present definition of thermal analysis formulated by the International Confederation for Thermal Analysis and Calorimetry (ICTAC) reads as follows: Thermal Analysis (TA): A group of techniques in which a property of the sample is monitored against time or temperature while the temperature of the sample, in a specified atmosphere, is programmed [59]. TGA helps us to study the thermal behavior of any sample under inert and reactive atmosphere. Taking the advantage of TGA, various researchers performed research on pyrolysis and combustion characteristic of biomass deploying thermogravimetric analyzer as follows:

Luo et al. [91] performed “experimental study on the oxygen-enriched combustion of biomass micro fuel” and concluded that the oxygen enriched atmosphere improves the combustion, however volatile releasing temperature, ignition temperature and burnout temperature decreases which was also proved by Qing et al. [65]. From the experiment of Yang et al. [92], it was concluded that particle size of 250μm to 2mm has insignificant influence on pyrolysis process, also, pyrolysis process can be categorized into four zones: initially, in the temperature range of below 220°C, moisture evaporation takes place around 100°C, hemicellulose decomposes around 220-300 °C, cellulose around 300-340°C and lignin decomposition manly occur above 340°C. Barneto et al., [93] studied the pyrolysis characteristic and combustion behavior of *Leucaena leucocephala* biomass and its compost with the help of TG and DTG along with the biomass component i.e. hemicellulose, cellulose and lignin. Sivasangar et al. [2] studied the thermal behavior of lignocellulosic materials under aerobic/anaerobic environments comparing raw and demineralize empty palm fruit’s bunch (EFB) and concluded that the mineral contents in raw EFB act as a catalyst which enhance the decomposition of raw biomass at lower temperature as compared to demineralize EFB. Also, hemicellulose shows the early decomposition followed by the cellulose and lignin. Furthermore, the reactive environment favors complete decomposition than inert atmosphere.

2.11 Possibility of applying NIR spectroscopy on evaluation of moisture content and combustion performance parameters

Many authors have successfully applied the NIR spectroscopy technique for the measurement of moisture content [18-22]. However, the combustion performance parameters are physical parameters and temperature dependent which have no NIR absorption bands but it should correlate with its chemical constituents which have the absorption bands. So, the combustion performance parameters may have relation with its lignocellulosic compound, i.e. hemicelluloses, cellulose and lignin [94-96] where there is NIR absorption bands at 1218, 1360, 1492, 1584, 1728, 1830, 2110, 2186, 2262, 2314 nm are for hemicelluloses [28] and at 1780, 1820, 2270, 2336, 2488 nm are for cellulose [16]. For lignin, the wavelength range at 2449-1287 nm (4083-7773 cm^{-1}) was used successfully for lignin prediction in corn stalk [97]. Jin at al. [18], Liu et al. [97] and Sabatier et al. [23] proved that NIR spectroscopy is suitable for the analysis of compounds (hemicelluloses, cellulose and lignin) in lignocellulosic material. These reviews indicated that there was a possibility to evaluate the combustion performance which was derived from the thermogravimetric analysis based on combustion. However, to apply NIR spectroscopy, due to broad band of vibration, it needs chemometric in multivariate analysis such as partial least squares regression to develop calibration model. NIR spectroscopy has been successful in determination of some physical characteristics such as rubber latex viscosity with R^2 of 0.95 [98], refractive index of vegetable oil with R^2 of 0.94 [99], wood density with R^2 of 0.96 [100] and higher heating value of torrefied biomass with R^2 of 0.92 [88].

Chapter 3

Methodology

The experiment in this study is divided into two main parts. In the first phase, preliminary studies were done for the comparison of combustion performance parameters of grounded bamboo chips and grounded pellet of *Leucaena leucocephala* pellets, whereas in second phase, feasibility studies were done to prove near infrared spectroscopy as an alternative for the measurement of moisture content and combustion performance parameters i.e. ignition index, burnout index and combustion performance index.

1. Preliminary study for comparison of combustion performance parameters of grounded bamboo chips and grounded pellet of *Leucaena leucocephala*.
2. Feasibility study on near infrared spectroscopy as an alternative for the thermogravimetry and oven drying method in evaluation of combustion performance parameters and moisture content of bamboo chips (*Dendrocalamus sericeus* cl. Phamon).

3.1 Preliminary study for the comparison of combustion performance parameters of grounded bamboo chips and grounded pellet of *Leucaena leucocephala*

3.1.1 Sample preparation

The *Leucaena leucocephala* pellet, which was pelletized for commercial purpose, was bought from Nakhonrachasima Province, Thailand, whereas bamboo samples were procured from Uttaradit, Thailand. The bamboo samples of *Dendrocalamus sericeus* cl. Phamon were only used. The bamboo trees were cut about 10 cm from the ground level and about 1 m from the base of bamboos was selected for the study. The bamboos were chopped by the chopping machine (P5508, Patipong, Thailand) and were dried. Both samples were grounded to pass through 2mm sieve.

3.1.2 Thermogravimetric experiment

The grounded *Leucaena leucocephala* pellet and grounded bamboo chips samples were subjected for thermogravimetric analysis in order to study the combustion performance parameters. The experiment was performed on the thermogravimetric analyzer (TG 209 F3 Tarsus, Netzsch, Germany, 0.1 µg resolution, heating rate ranges from 0.001 to 100 $Kmin^{-1}$, 6.8 mm diameter aluminum oxide (AL2O3) crucible) in an air conditioning room temperature of 25±2°C and the thermogravimetric (TG) profile and differential thermogravimetric (DTG) profile were analyzed using Proteus 6.0.0. (Netzsch Software, Germany). At the heating rate of 10°$Cmin^{-1}$, the temperature of furnace was increased from 33°C to 900°C in an air flux (O_2) of 20 $mLmin^{-1}$. The samples were kept isothermal at 33°C for 10 minutes. The mass loss of the sample was monitored continuously as a function of temperature and time. The sample size was kept constant at around 6 mg. And, from the thermogravimetric curve Ignition index (D_i), Burnout index (D_f), Combustion performance index (S) were calculated as discussed in section 2.9-2.11.

3.2 Feasibility study on near infrared spectroscopy as an alternative for the thermogravimetry and oven drying method in evaluation of combustion performance parameters and moisture content on bamboo chips (*Dendrocalamus sericeus* cl. Phamon)

3.2.1 Sample preparation

The bamboo samples, *Dendrocalamus sericeus* cl. Phamon, were procured from Uttaradit, Thailand. The bamboo trees were cut about 10 cm from the ground level, and about 1 m from the base of bamboos was selected for the study. The bamboos were then chopped by the chopping machine (P5508, Patipong, Thailand). The total number of bamboo trees were 90 consisting of various circumference ranging from 16-39 cm.

3.2.2 Near infrared (NIR) scanning for moisture measurement

The chopped bamboo were transferred in an aluminum cup (50 mm in diameter and 30 mm in height) and scanned by two NIR instrument: NIR-Gun (FQA, Fantec, Japan) in reflectance mode over the short wavelength range from 600-1100 nm at 2 nm intervals and Micro-NIR (JDSU, USA) in reflectance mode (operating in the long wavelength range between 1150-2150 nm) at 7 nm intervals. Each sample was divided into three sub-samples and each sub-sample was scanned two times. Hence, the total numbers of samples available for making NIR-model were 270. The samples were scanned in atmospheric condition of Thailand. The reflectance (R) spectra was

transformed into absorbance, log (1/R), spectra using CA maker software (Fantec, Japan) and The Unscrambler X 10.3 (Camo, Norway) for spectra obtained by NIR-Gun and Micro-NIR, respectively. The part of spectra that contain noise or unusual characteristics was erased and was not used for model development.

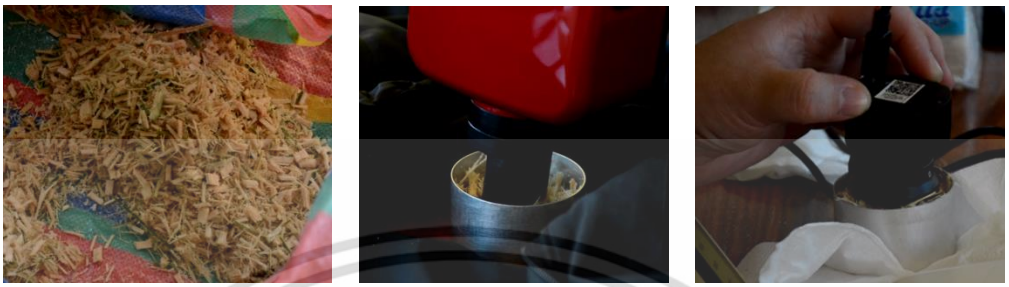

(a) (b) (b)

Figure 3.1 Chopped bamboo chips (a), Near infrared scanning performed by (b) NIR-gun and (c) Micro-NIR

3.2.3 Near infrared (NIR) scanning for combustion performance parameters

The chopped bamboo chips were dried under sun and were grounded to pass through 2 mm diameter sieve (SM100, Retsch, Germany). The grounded samples were then scanned by three NIR instruments: NIR-Gun (FQA, Fantec, Japan) in reflectance mode (over the short wavelength range from 600-1100 nm at 2 nm intervals, Micro-NIR (JDSU, USA) in reflectance mode (operating in the long wavelength range between 1150-2150 nm) at 7 nm intervals and FT-NIR (12500-3600 cm^{-1} at 8 cm^{-1} resolution). The total numbers of samples used for making NIR-model were 80. Each sample was scanned two times. The samples were scanned in air conditioning room, 25±2°C. The reflectance (R) spectrum were transformed into absorbance, log(1/R), spectra using CA maker software (Fantec, Japan) and The Unscrambler X 10.3 (Camo, Norway) for spectra obtained by NIR-Gun and Micro-NIR respectively, while, OPUS version 7.0.129 (Bruker, Germany) for making the FT-NIR model. The part of spectra that contain noise or unusual characteristics was erased and was not used for model development.

(a) (b)

Figure 3.2 Bamboo chips sample (a) dried bamboo chips (b) grounded bamboo chips

(a) (b) (c)

Figure 3.3 Near infrared scanning for combustion performance parameters performed by (a) NIR-gun and (b) Micro-NIR and (c) FT-NIR

3.2.4 Measurement of moisture content using reference method

Moisture content of raw materials was determined according to the procedure described in ASTM International D4442 - 07 — Method A—Primary Oven-Drying Method. About 3g of the chopped bamboo was taken in a dried aluminum cup and oven dried in a preheated oven for 3 hours at 103±2°C (ULM 500, Memmert, Germany) in a room relative humidity of less than 70%. The sensitivity of the balance (AR2140 Adventure, Ohauss,) was 0.1 mg. The temperature of the oven was calibrated by the thermocouple (51/52 II, Fluke, USA). The weight of the sample was measured in a 3 h drying interval until the weight was constant and moisture content, wet basis, in a sample was calculated as follows:

$$MC = \frac{W - D}{W} \times 100 \qquad (3.1)$$

where, W = wet mass (g), D= oven-dry mass (g)

3.2.5 Thermogravimetric analysis

The grounded samples after scanned by the NIR-instruments were subjected for thermogravimatric analysis for the combustion performance which was performed by the thermogravimetric analyzer (TG 209 F3 Tarsus, Netzsch, Germany, 0.1 µg resolution, heating rate ranges from 0.001 to 100 $Kmin^{-1}$, 6.8 mm diameter aluminum oxide (AL2O3) crucible) in an air conditioning room temperature of 25±2°C and the thermogravimetric (TG) profile and differential thermogravimetric (DTG) profile were analyzed using Proteus 6.0.0. (Netzsch Software, Germany). At the heating rate of 10°$Cmin^{-1}$, the temperature of furnace was increased from 33°C to 900°C in an air flux (O_2) of 20 $mLmin^{-1}$. The samples were kept isothermal at 33°C for 10 minutes. The mass of the sample was monitored continuously as a function of temperature and time. The sample size was kept constant at around 6 mg. And, from the thermogravimetric curve Ignition index (D_i), Burnout index (D_f), Combustion performance index (S) were calculated as discussed in section 2.9-2.11.

3.2.6 Spectra pretreatment and mathematical modeling

The spectrum pre-treatments and model development were performed on The Unscramble X 10.3 software (Camo, Norway) for the spectra scanned by the NIR-Gun and Micro-NIR, and OPUS version 7.0.129 (Bruker, Germany) was used for FT-NIR. After the wet-test, the reference data were merged with corresponding spectral data. The data were then arranged in descending order, and data were separated into calibration and prediction set. The highest and lowest reference values were included in calibration set. By Unscrambler X, various pre-treatments on calibration data set were performed before model development which includes no pre-treatment, Savitzky-Golay (S-G) smoothing (2^{nd} order polynomial with 11 and 21 points), mean normalization, maximum normalization, range normalization, 1^{st} derivative (2^{nd} order polynomial with 11 and 21 points), 2^{nd} derivative (2^{2n} order polynomial with 11 and 21 points), baseline offset, linear baseline correction, standard normal variate (SNV), de-trending, SNV plus de-trending and multiple scatter correction (MSC). Similarly, for OPUS, various pretreatment includes: no pretreatment, constant offset elimination, straight line subtraction, vector normalization, SNV, min-max normalization, MSC, 1^{st} derivatives, 2^{nd} derivatives, 1^{st} derivatives + straight line subtraction, 1^{st} derivatives + SNV and 1^{st} derivatives + MSC.

Partial least square regression technique was used to develop the NIR models. The models were checked by test set validation method, and the optimum model was selected for lowest number of factor, highest coefficient of determination of prediction, and low value of standard error of cross validation, standard error of prediction and bias.

Chapter 4

Result and discussion

4.1 Comparison of combustion performance parameters of grounded bamboo chips and grounded pellet of *Leucaena leucocephala*

4.1.1 Comparison of combustion characteristics

The thermogravimetric profile of grounded bamboo chip and grounded *Leucaena leucocephala* pellet is shown in the Figure 4.1 and its derivative thermogravimetric profile (DTG) curve is shown in Figure 4.2. The combustion profile of biomass can be categorized into four stages: moisture removal (<110°C); devolatilization (197-350°C); char combustion (360-600°C) and residue decomposition (>600°C). Biomass consist mainly holocellulose (hemicellusose, cellulose) and lignin [93]. When the moisture is removed from the sample, the samples started to degrade slowly. After 195°C, volatilization of volatile soared up, which leads to formation of char [1,101]. The combustion begins with the volatilization of hemicellulose, cellulose and partial decomposition of lignin [102, 103]. Hemicellulose shows the early decomposition [2, 104] followed by cellulose [2,105] and lignin, which showed the wide range of decomposition [2, 104].

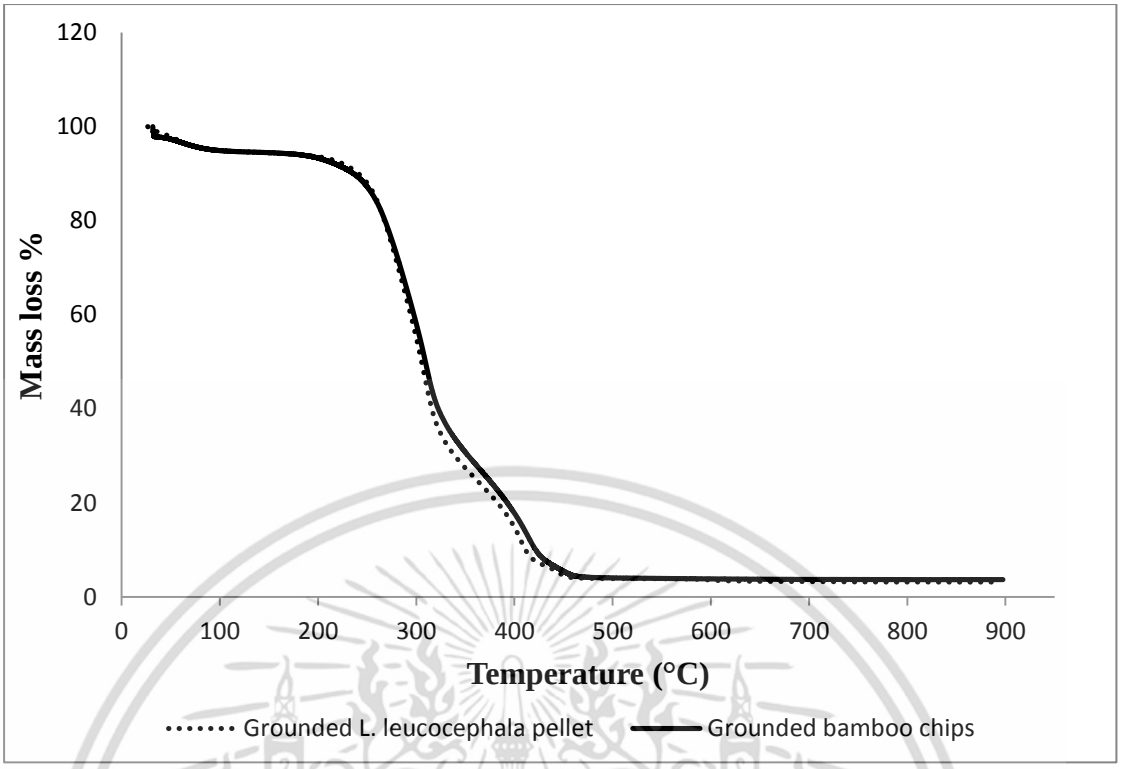

Figure 4.1 Thermogravimetric profiles of grounded bamboo chip and grounded *Leucaena leucocephala* pellet.

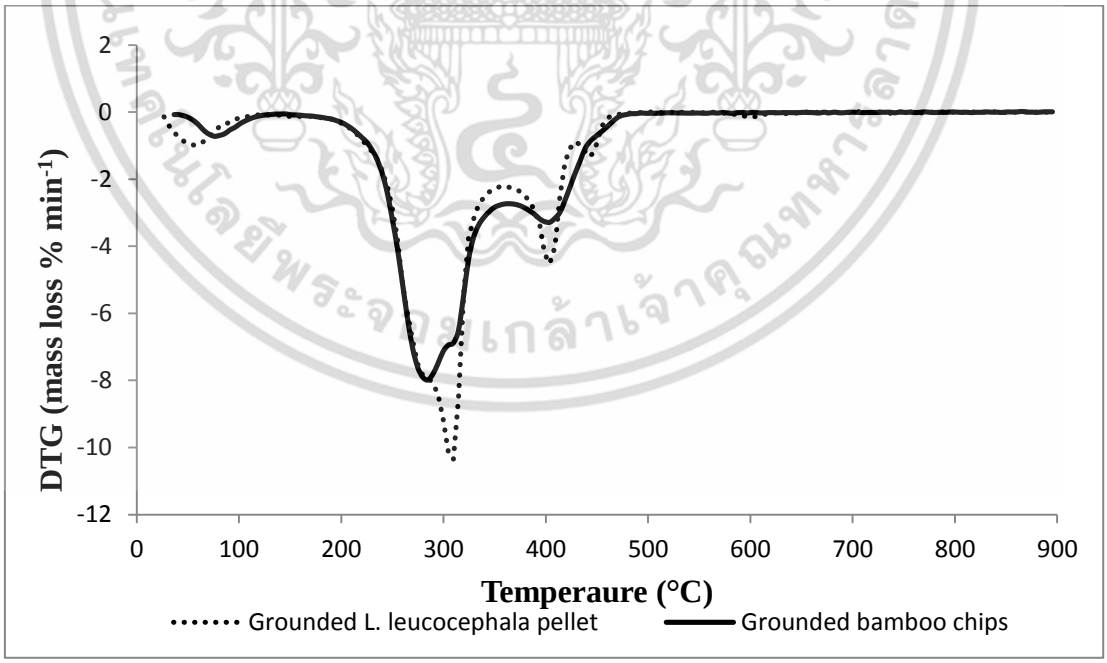

Figure 4.2 Derivative thermogravimetric profile of grounded bamboo chip and *Leucaena leucocephala* pellet.

The peak temperature associates with different stages with peak mass loss are compared in Table 4.1. The temperature range 200°C to 355°C is normally associated with decomposition of holocellulose [106, 107]. In the bamboo, hemicellulose was found to be dominant peak at 284.26°C with the cellulose peak at 319.47°C as minor peak to it right side, while for *Leucaena leucocephala* pellet, cellulose was found to be dominant peak at 307.5°C with hemicellulose shoulder peak at 284.6°C on left side. The hemicellulose seems to be major constituent for bamboo whereas cellulose for *Leucaena leucocephala* pellet.

The third stage is associated with the char oxidation which depicted two separate peaks, one with high mass loss at lower temperature and other at higher temperature with lower mass loss, which is the peak of holocellulose and lignin oxidation, respectively. The first char oxidation peak of bamboo occurred at 393.93°C with mass loss rate 3.28 $\%min^{-1}$ and for *L. leucocephala* wood pellet at 405.6°C with mass loss rate 4.57 $\%min^{-1}$ is associated with the oxidation of holocellulose [93]. However, cellulose contributes less to the char formation as most of it mass loss during the volatilization [108-113]. Therefore, this peak is mainly associated with the hemicellulose. The lignin oxidation peak of *L. leucocephala* pellet is seen at 443.7°C [1, 93], whereas no independent peak was seen for bamboo. Similarly, lignin curve was also seen during combustion of lignocellulosic biomass, pine bark, at lower heating rate [1]. The profile above 600°C was defines as the remaining char residue and inorganic compound decomposition. A very insignificant peak was observed above the temperature of 605°C which was mainly associated with the combustion of inorganic matter [1, 93].

Table 4.1 Comparison of combustion characteristics of grounded bamboo chips and *Leucaena leucocephala* pellet.

Stage	Parameters		*L. leucocephala* pellet	Bamboo
Devolatilization	T_{peak} (°C)		308.1	284.26
	$(dw/dt)_{max}$ $(\%min^{-1})$		10.44	10.085
Char oxidation	Holocellulose oxidation	T_{peak} (°C)	405.6	393.93
		$(dw/dt)_{max}$ $(\%min^{-1})$	4.57	3.37
	Lignin oxidation	T_{peak} (°C)	443.7	—
		$(dw/dt)_{max}$ $(\%min^{-1})$	1.34	—
Residue (%)			3.37	4.10

4.1.2 Comparison of combustion performance parameters

The ignition temperature (T_i), ignition index (D_i), burnout index (D_f) and combustion index (S) with the peak temperature (T_{max}) and respective mass loss $(dw/dt)_{max}$ are listed in Table 4.2. Ignition temperature determines the easiness to ignite the fuel. A fuel with high ignition temperature is more difficult to ignite and vice versa [63]. The higher value of combustion performance of fuel is desired for better combustibility, whereas higher burnout temperature defines the difficulty to burn and thus requires longer time while lower value indicates the reduced presence of unburnt [65].

The combustion performance index of bamboo was found higher than that of *L. leucocephala* pellet which implies that the bamboo is easier to burn. The higher value of the ignition index of bamboo also implies that the bamboo is easier to ignite as a fuel which is verified by the lower value of ignition temperature. The higher value of ignition temperature and burnout temperature made the *L. leucocephala* pellet to ignite difficult and last longer than bamboo. Consequently, leads to the higher burnout index.

Table 4.2 Comparison of combustion performance parameter of grounded *L. leucocephala* pellet and bamboo chips

Parameter	*L. leucocephala* pellet	Bamboo
$(dw/dt)_{max}$ ($\%min^{-1}$)	10.45	10.09
$(dw/dt)_{mean}$ ($\%min^{-1}$)	1.11	1.09
Peak temperature (T_{max}, °C)	307.5	284.26
Ignition temperature (T_i, °C)	261.7	250.65
Burnout temperature (T_f, °C)	776.25	486.94
Burnout time (t_f, min)	74.95	55.91
Ignition index (D_i)	6.10E-04	88.33E-04
Burnout index (D_f)	8.20E-03	0.16E-03
Combustion performance index (S)	2.19E-07	3.59E-07

4.2 Evaluation of moisture content in bamboo chips with diode array near infrared instruments

The average log(1/R) spectrum of bamboo chip scanned from two diode array instruments i.e. NIR-Gun and Micro-NIR of different moisture content is shown in Figure 4.3-4.4 and its optimum pretreatment is shown in Figure 4.5-4.6. On the raw spectrum of NIR-Gun, the peaks are seen in the range of 645-655 nm and 975-985 nm. The bands vibration between 613-645 nm is associated with visible spectrum which represents the chlorophyll absorption [23, 114], and 950-1040 nm represents the second overtone of O—H stretch [29]. For Micro-NIR spectrum, small rise is seen in the range of 1400-1500 nm and sharp peaks in the range of 1830-1900 nm which corresponds to first overtone of O—H bond (O—H stretch, internal OH bonds, single bridge and/or polymeric) and third overtone O—H deformation (primary and secondary alcohol) [29].

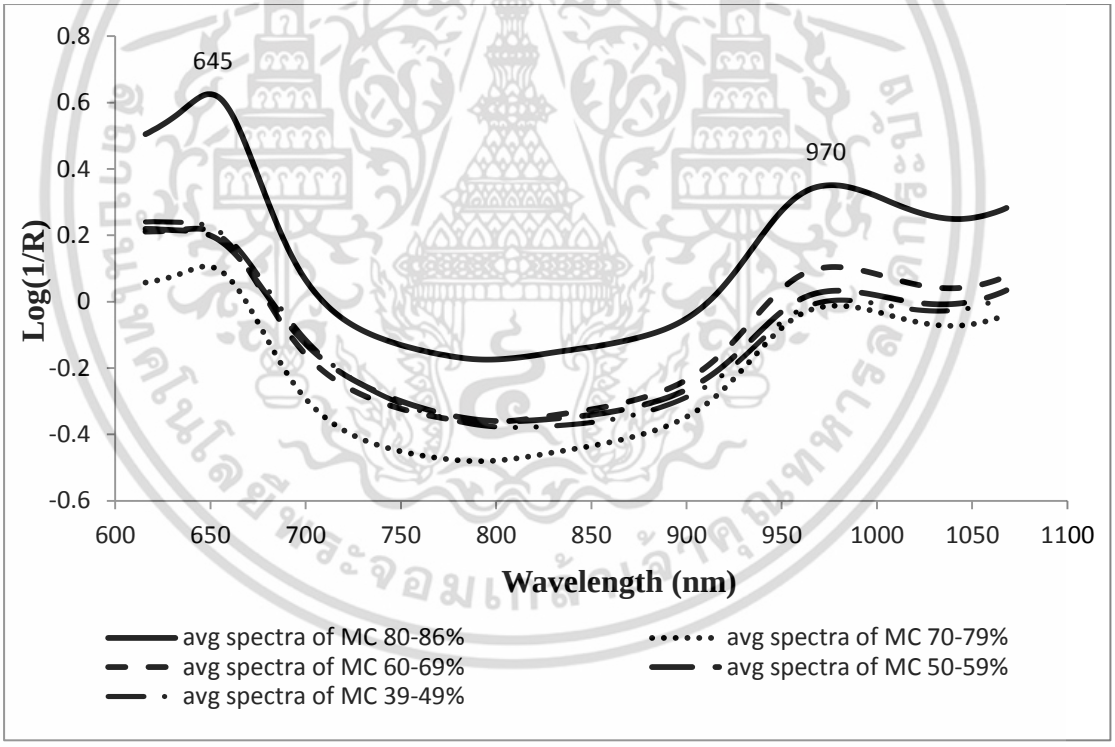

Figure 4.3 Average raw spectra of bamboo chips of different moisture content (MC) on wet basis scanned by NIR-Gun spectrometer.

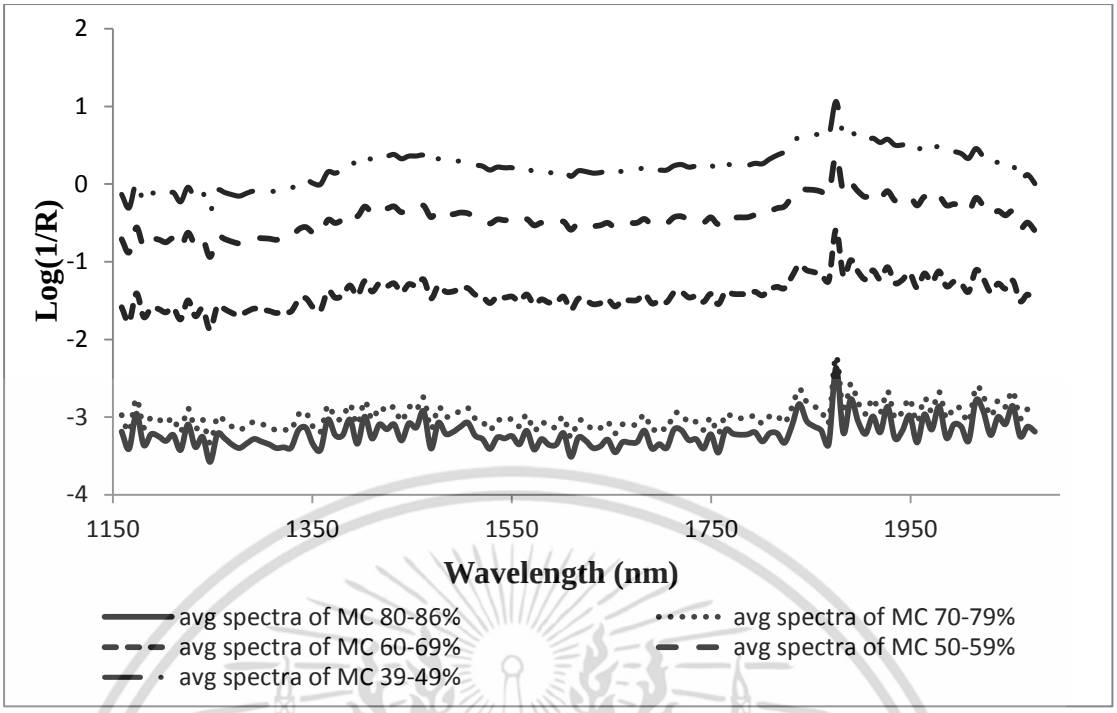

Figure 4.4 Average raw spectra of bamboo chips of different moisture content (MC) on wet basis scanned by Micro-NIR spectrometer.

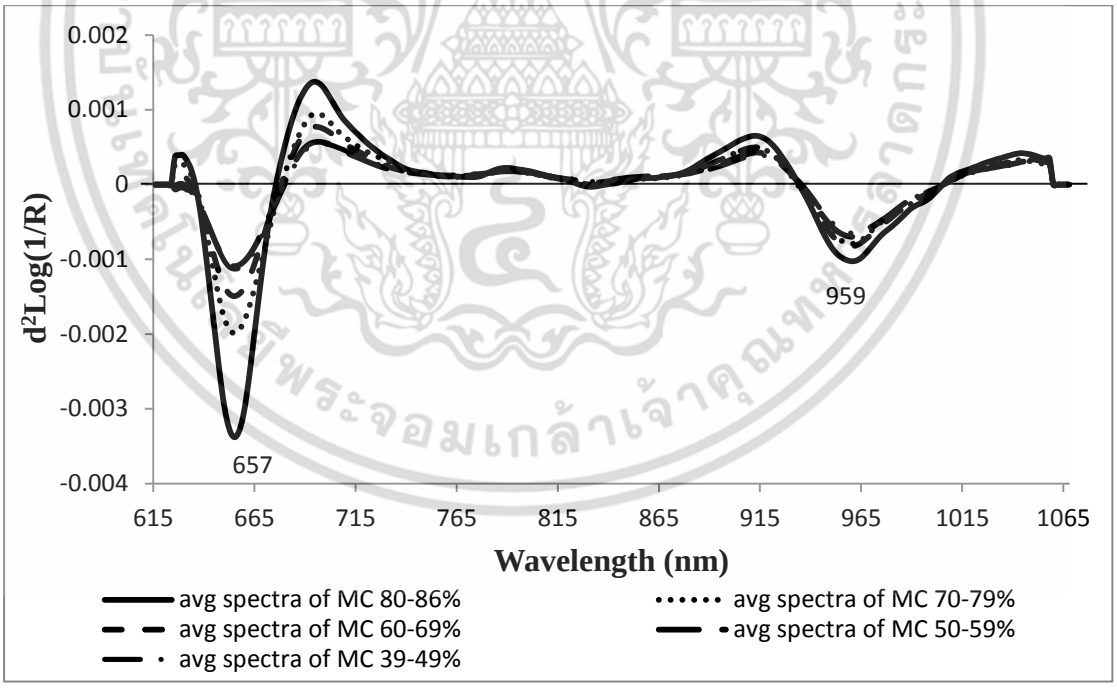

Figure 4.5 Second derivative pretreatment on the raw spectra of bamboo chips of different moisture content (MC) on wet basis scanned by NIR-Gun spectrometer.

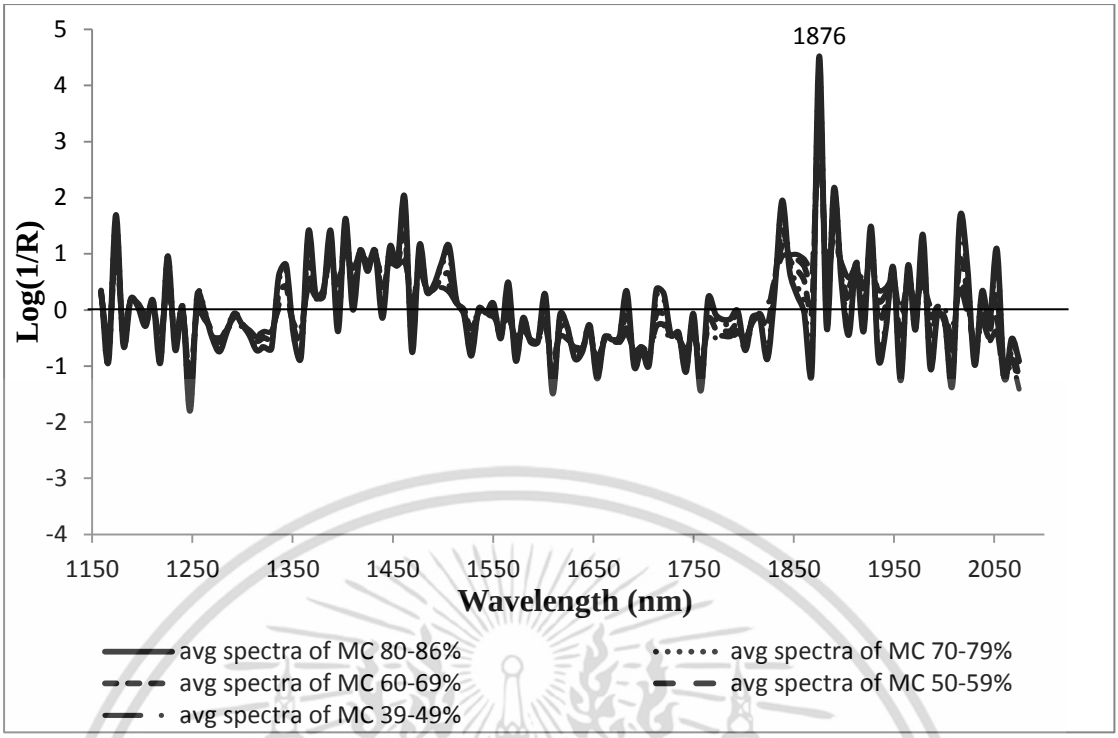

Figure 4.6 SNV + Detrending pretreatment on the raw spectra of bamboo chips of different moisture content (MC) on wet basis scanned by Micro-NIR spectrometer.

The circumference range of bamboos used in this research to measure moisture content were in between 16-39 cm and the moisture content were in range of 39-86% wet basis. The descriptive statistics of calibration and prediction set for the measurement of moisture content are shown in Table 4.3. The outliers of reference data were removed by standard normal distribution for the Z-score greater than 3, while principal component analysis (PCA) was used to find the spectral outlier using Hotelling's T-squared statistic which are isolated from the cluster. The total number of outlier was found to be eighteen, 7 from reference test and 11 from spectrum, in both cases. The model was created from remaining 252 sub-samples.

Table 4.3 Statistical data of moisture content (% wb) of bamboo sample used for developing model.

Model	Calibration					Prediction				
	N	Max	Min	Mean	SD	N	Max	Min	Mean	SD
NIR-Gun	232	85.585	39.001	56.687	9.002	20	75.942	41.382	57.628	8.719
Micro-NIR	232	85.585	39.001	58.086	9.547	20	75.942	41.382	58.867	8.873

where, N is number of sample, Max is maximum value, Min is minimum value and SD is standard deviation.

The selected wavelength range for creating the model was 615-1068 nm and 1158-2075 nm for short wavelength (NIR-Gun) and long wave length (Micro-NIR) respectively; however, the wavelength range of instruments are 600-1100 nm and 1150-2150 nm respectively. Because of noise at the beginning and end of spectra, some points were skipped. Firstly, smoothing on spectra was performed and various pre-treatment were done. The second derivative (second order polynomial with 5 points) was found to be the most optimum effective treatment for the NIR-Gun spectra, while standard normal variate (SNV) + De-trending was found to be the most optimal pretreatment for the spectra scanned by Micro-NIR. The second derivative helps to separate overlapping peaks and baseline shift on spectra caused by the light scattering and particle size into independent peaks of different concentration. After second derivative pretreatment of NIR-Gun spectra, the spectra has common baseline and are arranged in order of increasing moisture content. Higher moisture content depicts higher absorption peak and vice versa. On the other hand, the NIR diffuse reflectance spectra transposed by SNV + Detrending methods are free from multi-collinearity [56].

The PLS models statistics for the measurement of moisture content in bamboo chips by NIR-Gun and Miro-NIR are shown in Table 4.4-4.5 respectively. The R_p^2, SECV, SEP, bias and RPD of optimum model of NIR-Gun are 0.924, 2.871% wb, 2.385% wb, -0.250% wb and 3.656. In the case of Micro-Nir model, R_p^2, SECV, SEP, bias and RPD are found to be 0.743, 4.349% wb, 4.499% wb, 0.025% wb and 1.972 respectively.

Table 4.4 PLS models statistics for the measurement of moisture content in bamboo chips by NIR-Gun spectrometer.

S.No.	Method	Factors	Calibration			Prediction			
			R_c^2	SECV	BIAS	R_p^2	SEP	BIAS	RPD
1	Raw	11	0.917	2.675	0.001	0.912	2.541	-0.457	3.431
2	S-G (5 points)	11	0.917	2.677	0.002	0.912	2.548	-0.461	3.422
3	S-G (11 points)	11	0.916	2.684	0.001	0.909	2.568	-0.456	3.395
4	1st Derivative (5 points)	9	0.911	2.773	0.002	0.905	2.689	-0.144	3.242
5	1st Derivative (11 points)	8	0.902	2.886	-0.002	0.890	2.843	-0.506	3.067
6	2nd Derivative (5 points)	7	0.906	2.871	-0.001	0.924	2.385	-0.250	3.656
7	2nd Derivative (11 points)	8	0.923	2.598	0.005	0.925	2.392	-0.074	3.645
8	Mean normalization	1	0.001	16.993	0.582	-	8.719	-0.927	1.000
9	Maximum normalization	11	0.855	3.547	0.003	0.876	3.042	-0.425	2.866
10	Range normalization	11	0.890	3.085	-0.001	0.896	2.810	-0.054	3.103
11	Baseline offset	11	0.908	2.824	0.003	0.898	2.770	-0.219	3.148
12	Linear baseline offset	11	0.917	2.688	0.001	0.250	3.576	-6.590	2.438
13	SNV	9	0.893	2.983	0.002	0.903	2.716	0.038	3.210
14	Detrending	9	0.907	2.834	0.001	0.887	2.927	-0.081	2.979
15	SNV +Detrending	7	0.886	3.121	-0.004	0.885	2.944	-0.337	2.962

Table 4.5 PLS models statistics for the measurement of moisture content in bamboo chips by Micro-NIR spectrometer.

S.No.	Method	Factors	Calibration			Prediction			
			R_c^2	SECV	BIAS	R_p^2	SEP	BIAS	RPD
1	Raw	12	0.839	4.064	-0.004	0.774	4.852	-0.104	1.829
2	S-G (5 points)	10	0.807	4.398	0.006	0.706	5.797	0.975	1.531
3	S-G (11 points)	10	0.796	4.463	0.001	0.662	6.082	0.752	1.459
4	1st Derivative (5 points)	7	0.805	4.370	0.005	0.738	5.459	0.891	1.625
5	1st Derivative (11 points)	9	0.778	4.608	-0.005	0.667	6.110	0.926	1.452
6	2nd Derivative (5 points)	9	0.837	4.006	-0.003	0.824	4.607	0.970	1.926
7	2nd Derivative (11 points)	9	0.820	4.209	0.004	0.711	5.559	0.477	1.596
8	Mean normalization	15	0.752	5.154	-0.022	0.625	6.559	1.121	1.353
9	Maximum normalization	16	0.827	4.403	-0.036	0.763	4.976	-0.102	1.783
10	Range normalization	10	0.821	4.218	-0.018	0.778	4.805	-0.275	1.847
11	Baseline offset	12	0.853	3.911	-0.005	0.796	4.617	0.042	1.922
12	Linear baseline offset	12	0.853	3.923	-0.007	0.810	4.449	-0.188	1.994
13	SNV	11	0.853	3.860	-0.009	0.849	3.917	-0.668	2.265
14	Detrending	13	0.875	3.704	0.001	0.855	3.879	-0.314	2.287
15	SNV +Detrending	6	0.806	4.349	-0.008	0.743	4.499	0.025	1.972
16	MSC	7	0.808	4.325	-0.008	0.758	4.359	-0.195	2.036

The scatter plots of the optimum models are shown in Figure 4.7-4.8. Williams [27] suggested that R^2 of 0.66-0.81 is ok for screening and some approximate calibration and 0.83-0.90 is usable with caution for most applications, including research. This shows that short wavelength was better than longer wavelength for the measurement of moisture content in bamboo.

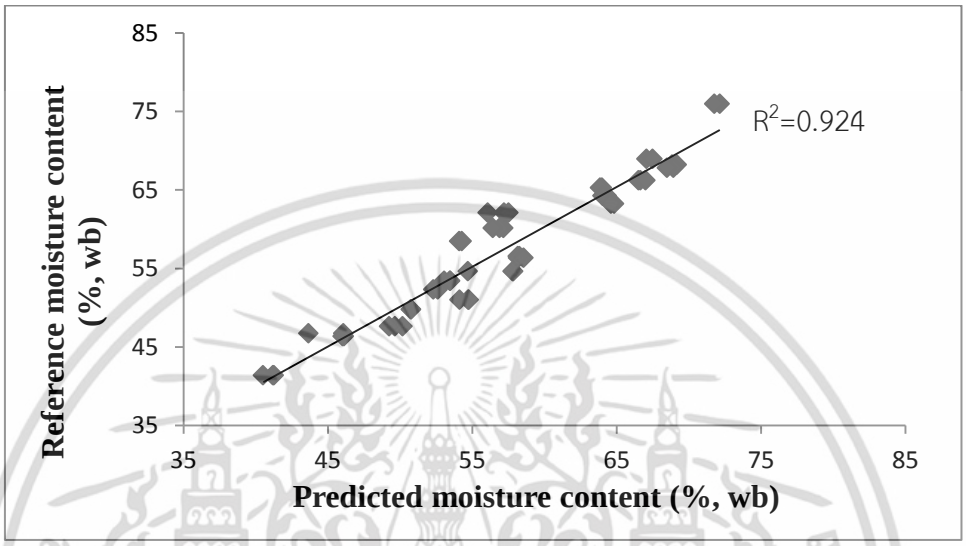

Figure 4.7 Comparison of moisture content (%, wb) in bamboo chips predicted by near infrared (NIR) spectroscopy (NIR-Gun) and measured by reference test.

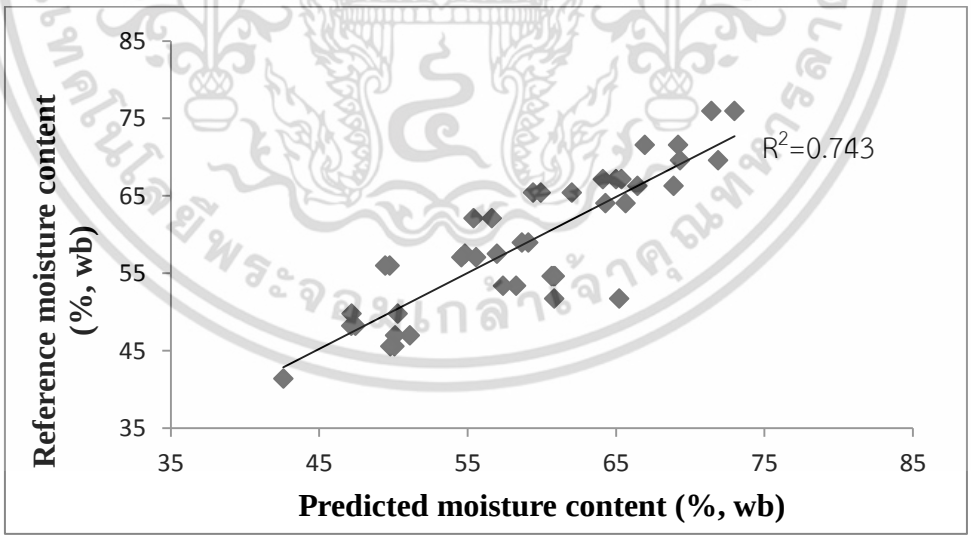

Figure 4.8 Comparison of moisture content (%, wb) in bamboo chips predicted by near infrared (NIR) spectroscopy (Micro-NIR) and measured by reference test.

Regression coefficient plot and X-loading of first three PLS-factors of NIR-Gun model is shown in Figure 4.9 and 4.10 respectively. The most important variance used in computing the final calibration model can be described by the areas of spectrum for which the regression coefficients are biggest [27]. The most important peaks seen in regression coefficient and X-loading and the corresponded vibration bonds are tabulated in Table 4.6. The highest peaks seen in regression coefficient plot were at 900, 942 and 977 nm which corresponds to the vibration of C-H str. 3rd overtone (CH_3) C—H str. third overtone (CH_2) and O—H str. second overtone (ROH and H_2O), CH_3 (C—H str. third overtone) respectively [28]. Minor peaks were also seen in the visible region between 600-700 nm which are related with chlorophylls absorption [23, 114]. In X-loading plot, the most influential region was seen between 630-700 nm and 935-1000 nm. The X-loading plot shows the higher effect of visible region, 630-700 nm, than infrared region. The effect of chlorophylls absorption seen in the region between 630-700 nm in X-loading plot is also seen in regression coefficient. In addition, the first three factors show the presences of hydrocarbon (900, 942), alkyl alcohol (959, 967 nm) and moisture (730, 977 nm).

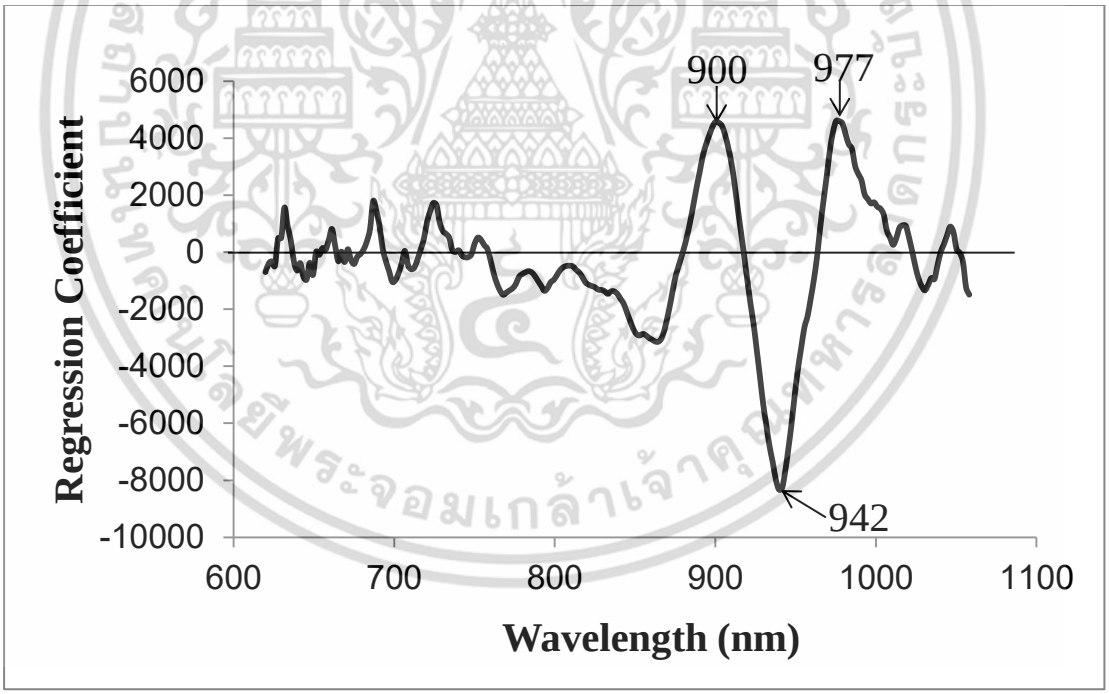

Figure 4.9 Regression coefficient plot of optimum model of moisture content in bamboo chips developed from the spectra scanned by NIR-Gun spectrometer.

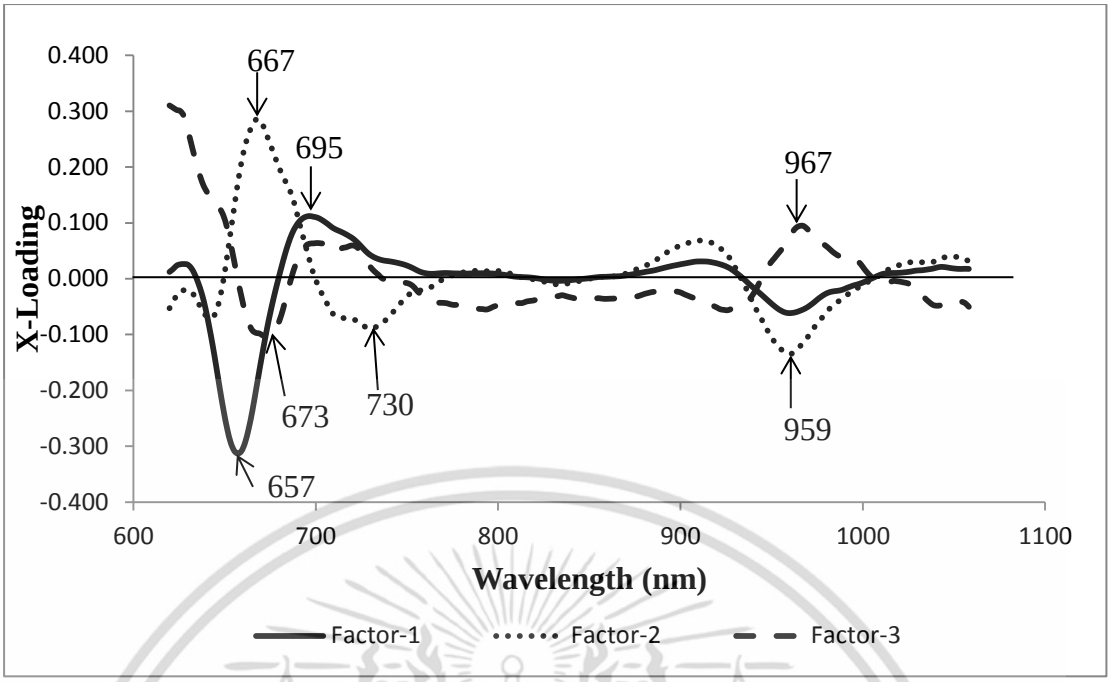

Figure 4.10 First 3 X-Loading plot of optimum model of moisture content in bamboo chips developed from the spectra scanned by NIR-Gun spectrometer.

Table 4.6 The dominant peaks on regression coefficient plot and X-loading plot of NIR-Gun model.

Peak wavelength (nm)	Nearest wavelength, (nm)	Bond vibration	Functional group	Structure	Reference
730	740	OH str. 3rd overtone		H_2O	[28]
900	900	C—H str. 3rd overtone		CH_3	[28]
942	938	C—H str. 3rd overtone		CH_2	[28]
959	962		O—H alkyl alcohols O—H with no hydrogen bonding (R—C—OH) in CCL_4	alkyl alcohols	[16]
967	970	O—H		ROH, H_2O	[28]

		str. 2nd overtone O—H		
977	970	str. 2nd overtone	ROH, H_2O	[28]

Similarly, Figure 4.11 and 4.12 depicts regression coefficient and X-loading plot of the Micro-NIR model and the vibration modes associated with main peaks on regression coefficient and X-loading plots are tabulated in Table 4.7. The highest peaks seen in regression coefficient are 1366, 1809 nm. The peak at 1366 nm is assigned as the bond vibration of 2×C—O str. + C—H def. of CH_3 [28], and the peak at 1809 nm as the bond vibration of O—H str. + 2×C—O str. of cellulose [28]. In regression coefficient plot, the original moisture peak at 1940nm appears as a small shoulder peak with small peak at 1927 nm which is assign as O—H stretching and H—OH bending combination from water molecules [16]. The most important regions seen in X-loading for determination of moisture content are 1160-1450 nm and 1865-1880 nm and 2050-2070 nm. The peaks in the region 1150-1240 nm as assign as the second overtone of C—H stretch, carbonyl compounds [29] and the peak in the region 2050-2070 nm as second overtone of NH_3 deformation [29].

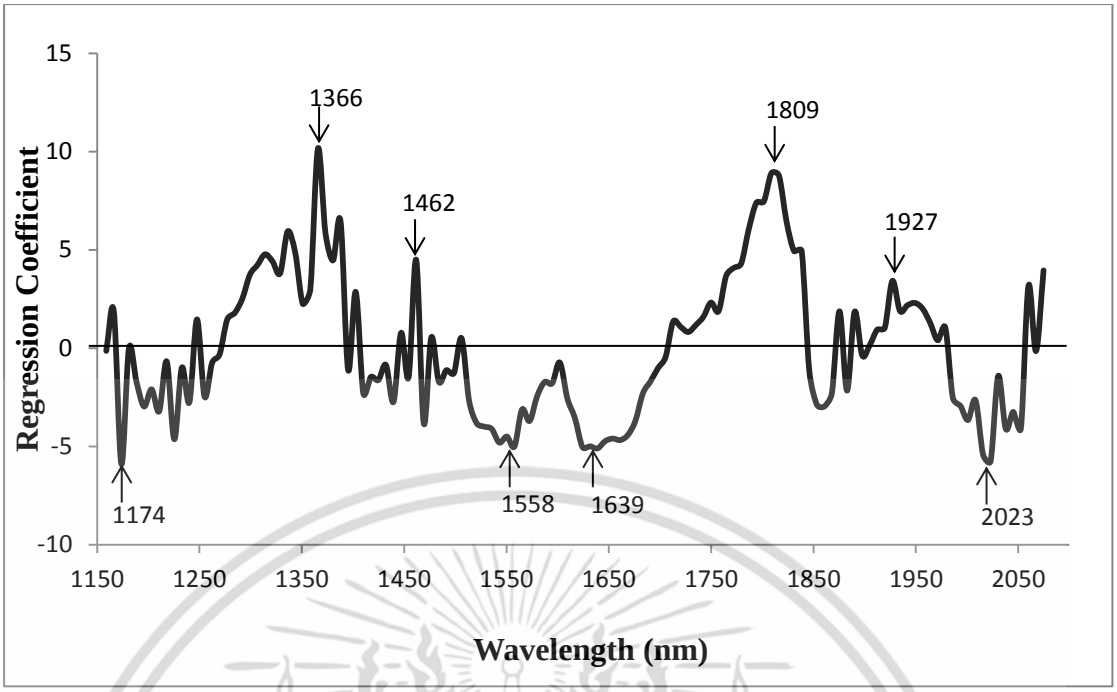

Figure 4.11 Regression coefficient plot of optimum model of moisture content in bamboo chips developed from the spectra scanned by Micro-NIR spectrometer.

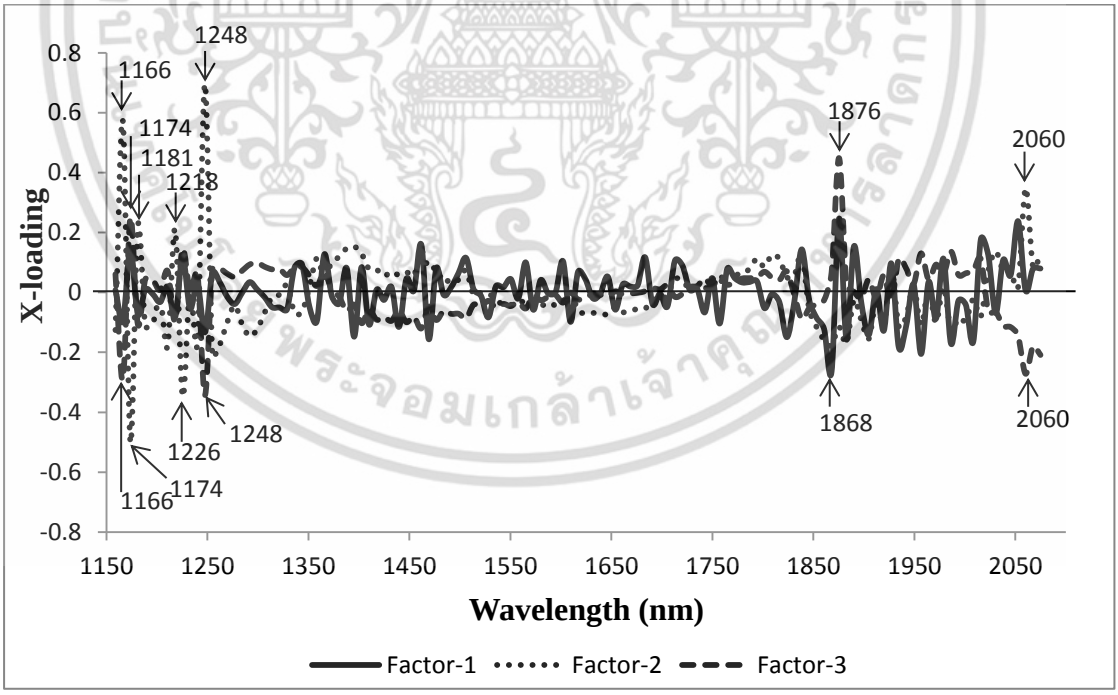

Figure 4.12 First 3 X-loading plot of optimum model of moisture content in bamboo chips developed from the spectra scanned by Micro-NIR spectrometer.

Table 4.7 The dominant peaks on regression coefficient plot and X-loading plot of Micro-NIR model.

Peak wavelength (nm)	Nearest wavelength (nm)	Bond vibration	Functional group	Structure	Reference
1166, 1174	1170	C—H str. 2nd overtone		HC═CH	[28]
1218	1215	C—H str. 2nd overtone		CH_2	[28]
1225	1225	C—H str. 2nd overtone		CH	[28]
1366	1360	2×C—H str. + C—H def		CH_3	[28]
1462	1460	N—H str. 1st overtone		$CONH_2$	[28]
1639	1637		C-H from vinyl group as (CH_2═CH—)	C-H from vinyl group	[16]
1868	1860		C—CL chlorinated organics (.C—CL group)	C—CL (7v), .C—CL	[16]
1927	1920	C═O str. 2nd overtone		CONH	[28]
2023	2024		N—H/C═O combination from of native Rnase A	Rnase A	[16]
2060			N—H as amide as (.CONH) and ($.CONH_2$)	N—(3δ) and N—H stretching combination	[16]

The models, in both cases, were seen to be mostly affected by the different constituent of bamboo. No such clear independent peaks of moisture were seen, however, strong correlations can be seen between moisture and related absorbance peak. Shifting of bands was seen more common in Micro-NIR spectra due to the fluctuating environment temperature. The peaks are likely to be shifted to higher wavelength with increasing temperature [16]. The models mostly represent the bands associated with hydrocarbon present in bamboo rather than moisture in either case. However, NIR-Gun model was most affected by moisture than Micro-NIR model.

Bamboo is a lignocellulose biomass which is mainly composes of cellulose, hemicellulose and lignin. The major constituent of cellulose is glucose units [115] while hemicellulosic is xylose [116], and lignin is a polymer of aromatic compounds [115]. Instead of independent peaks of cellulose, hemicellulose and lignin, peaks of their major constituent can be seen in X-loading plot.

4.3 Evaluation of combustion performance parameter of bamboo chips with diode array near infrared instruments Fourier-transform near infrared

4.3.1 Measurement of combustion performance parameters by diode array instruments

The raw spectra, log(1/R), of the grounded bamboo samples scanned from NIR-Gun is shown in Figure 4.13. The raw spectra obtained from the NIR-Gun scanning show unusual characteristics to each other, so the scanning that shows similar characteristics/features were selected and second derivative (second order polynomial with 5 points) was performed in order to study the spectral characteristics, Figure 4.14 and 4.15, respectively. The raw spectra show the absorption in the region 620-680 nm, 720-840 nm and in 960-1000 nm. The region 600-700 nm is associated with the visible range which is normally associated with chlorophyll absorption [23]. The region 960-1000 nm is associated with the third overtone of O—H stretching and hydrocarbon. The second derivative shows the several peaks in the region 620-680 nm, 720-840 nm, and independent peak at 973 nm is associated with the second overtone of O—H stretching, principally water, and the overlapping peaks are associated with C—H stretch third overtone [117,118]. The several peaks in 720-840 nm region are observed with the noticeable peaks at 733 nm, 760 nm (O—H str., third overtone, water) [28], 788 nm (N—H str., third overtone, $ArNH_2$) [28].

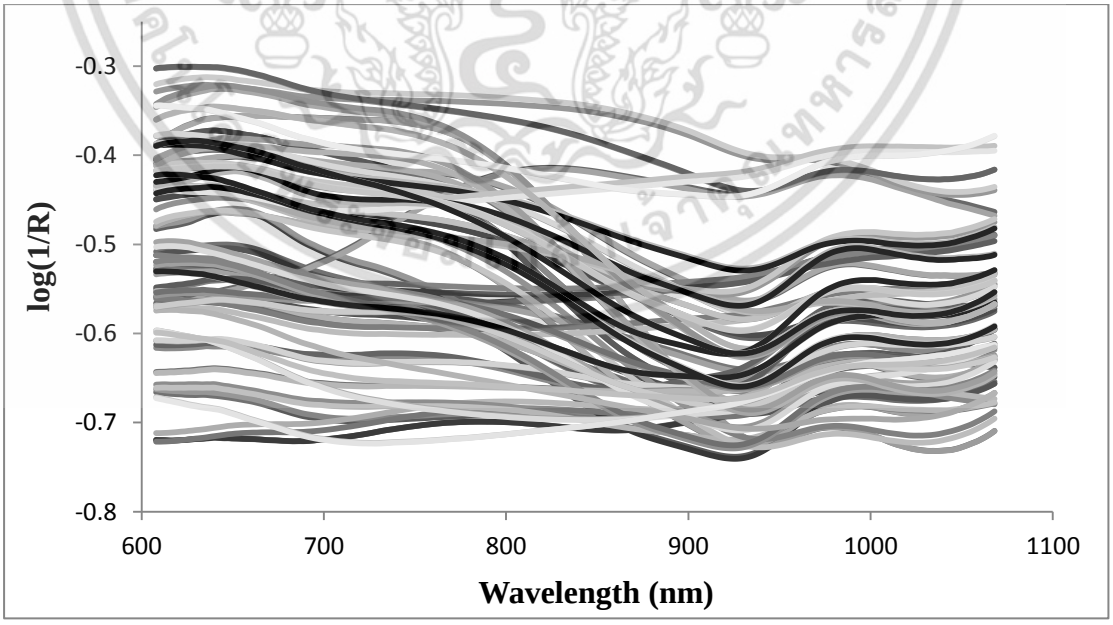

Figure 4.13 Raw spectra of the grounded bamboo chips scanned by NIR-Gun spectrometer.

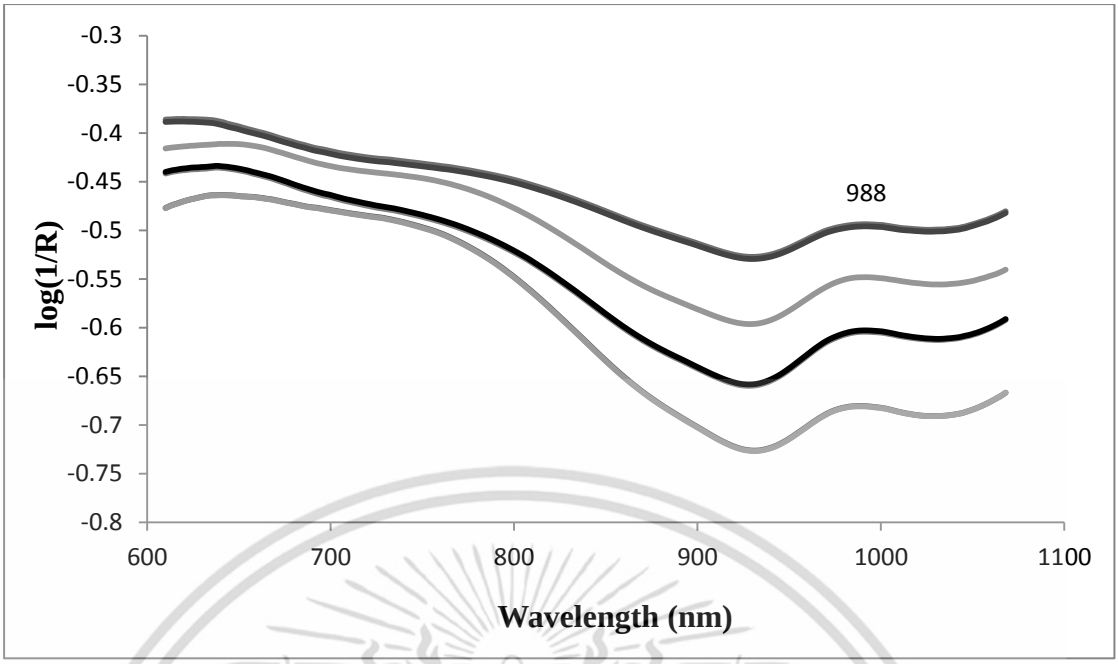

Figure 4.14 Selected raw spectra of the grounded bamboo chips scanned by NIR-Gun spectrometer.

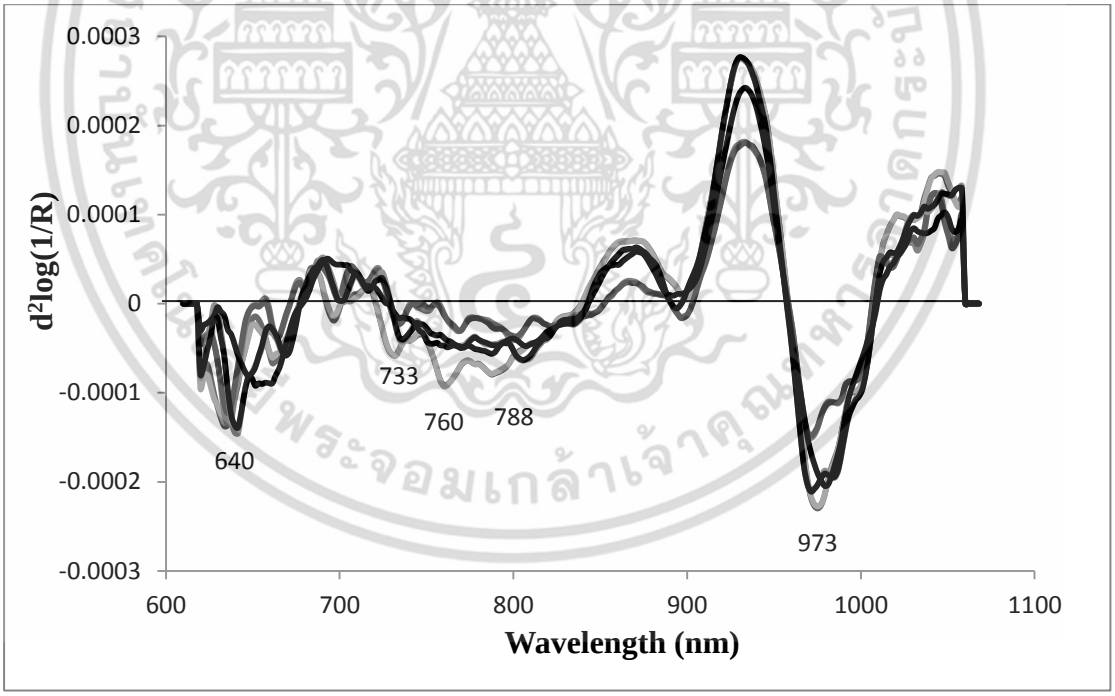

Figure 4.15 Second derivative (second order polynomial with 5 points) of the selected raw spectra of the grounded bamboo chips scanned by NIR-Gun spectrometer.

The raw spectra of the Micro-NIR, Figure 4.16, scanning show the similar characteristics unlike NIR-Gun scanning, however, the spectra seem noisy. In order to study the spectral characteristics, Savitzky-Golay (S-G) smoothing (second order polynomial with 11 points) and second derivative (second order polynomial with 5 points) of the spectra, Figure 4.17 and 4.18 respectively, were performed. Since the raw spectra contained noise, the S-G smoothing of the raw spectra was taken into consideration which shows the absorption in the region 1380-1580 nm, 1800-1900 nm and 2020-2060 nm. The region 1380-1580 nm is assigned as first overtone of O—H stretching, 1800-1900 nm third overtone of CH deformation, and 2020-2060 nm is assigned as second overtone of —C=H— stretch [29]. The second derivative shows the several peaks in the region 1180-2050 nm. The noticeable peaks are at 1285 nm, 1358 nm (2×C—H str. + C—H def., CH_3), 1440 nm (O—H str. first overtone, sucrose, starch), 1506 nm (N—H str. first overtone, protein), 1572 nm (N—H str., first overtone, -CONH-), 1669 nm (C-H aromatic C-H (aryl)), 1780 nm (C—H str., first overtone, cellulose), 1860 nm (C—Cl chlorinated organics, chlorinate hydrocarbons), 1898 nm (O—H str. + 2×C—O str., starch), 1979 nm (N—H asym. Str. + amide 2, protein), 2038 nm (N—H combination band from urea (NH_2—C=O—NH_2, urea) [16, 28]

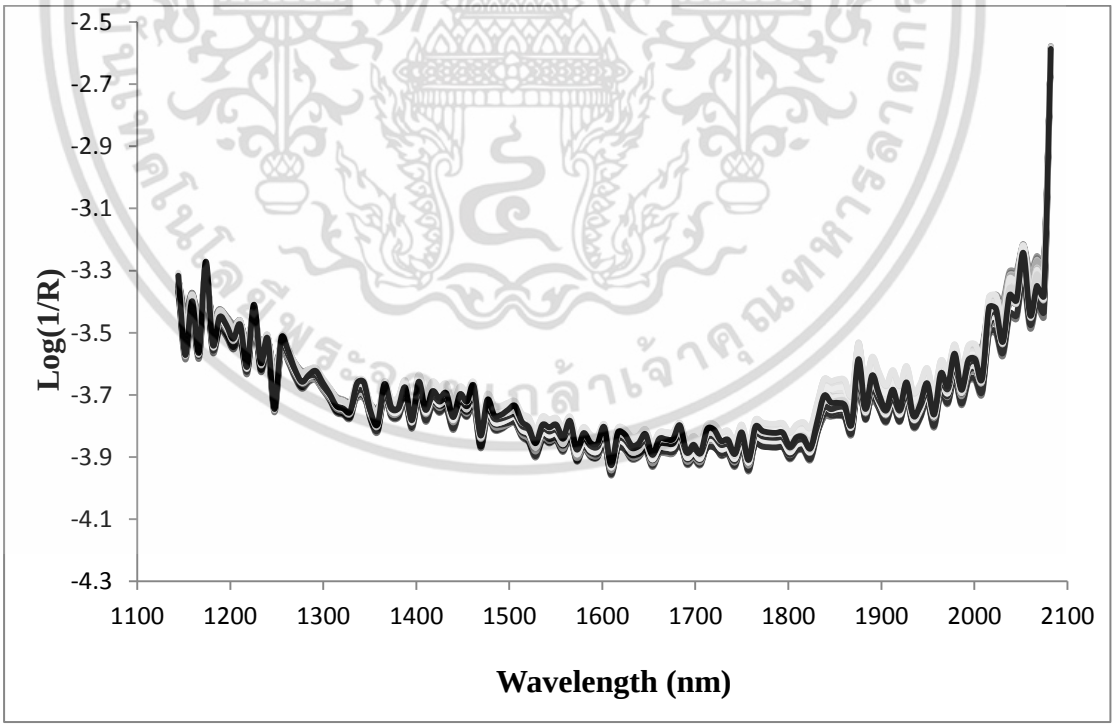

Figure 4.16 Raw spectra of the grounded bamboo chips scanned by Micro-NIR spectrometer.

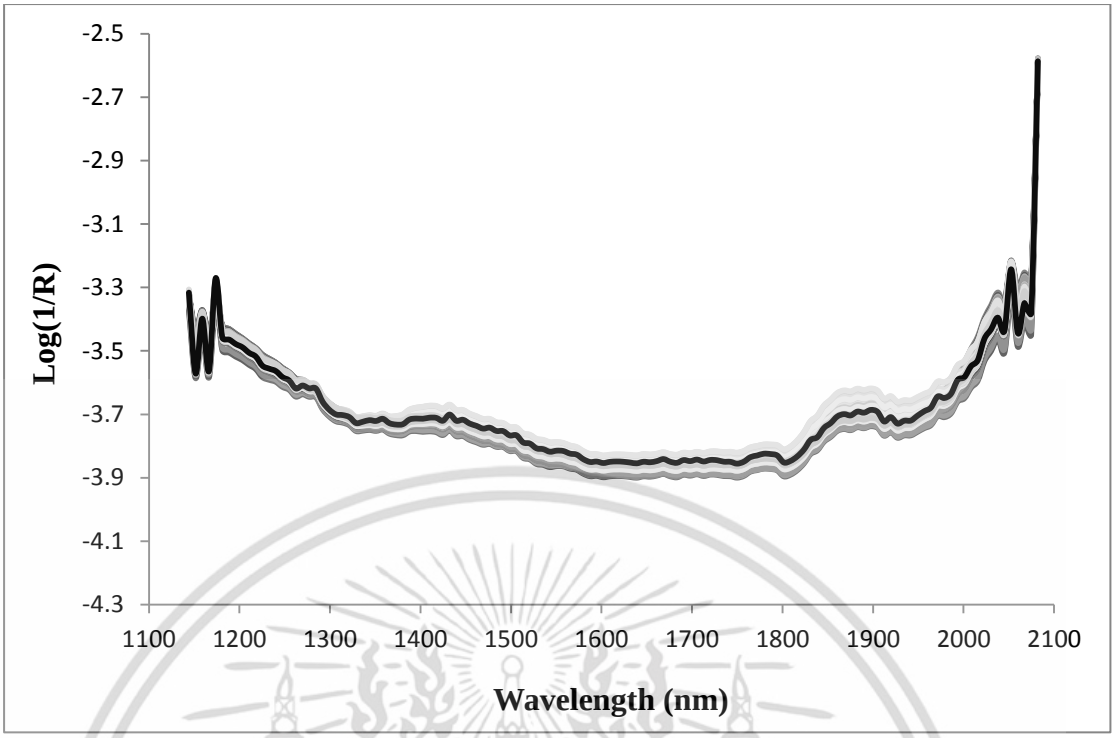

Figure 4.17 S-G smoothing (second order polynomial with 11 points) of the raw spectra of the grounded bamboo chips scanned by Micro-NIR spectrometer.

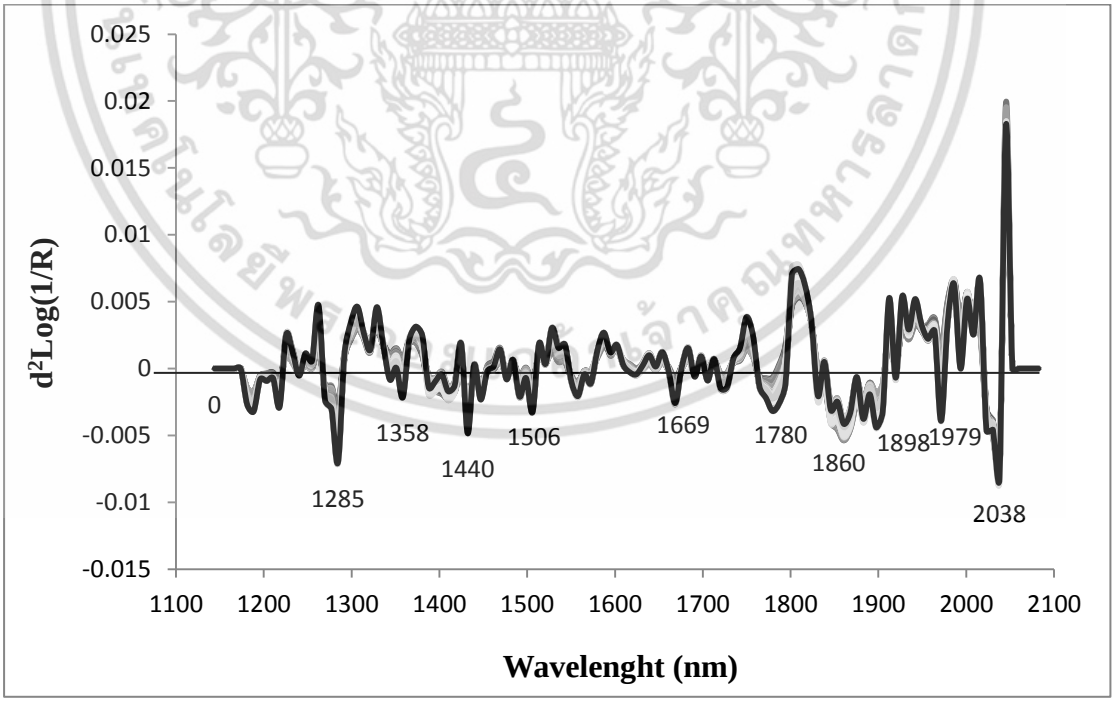

Figure 4.18 Second derivative (second order polynomial with 5 points) of the raw spectra of the grounded bamboo chips scanned by Micro-NIR spectrometer.

The descriptive statistics for the development of various combustion parameters models of NIR-Gun and Micro-NIR are shown in Table 4.8 and 4.9, respectively. The model calibration and predicted statistics of NIR-Gun scanning for combustion performance parameters are shown in Table 4.10-4.12. The models used 13-20 PLS factors for the making various models. The models were unable to predict the values of the test set. The reason may be due to the poor spectra scanning which causes more factors to define the spectra. Another reason may be due to the low variability of the calibration set of samples used for making the model (for combustion index 4.613-2.794E-07, ignition index 11.907-6.994E-03, burnout index 2.040-1.230E-04).

Similarly, the model validation and predicted statistics of Micro-NIR scanning for combustion performance parameters are shown in Table 4.13-4.15. The models used 13-20 PLS factors like NIR-Gun model, and the models were unable to predict the values of the test set. Although the spectra were run in order unlike NIR-Gun scanning spectra and show the similar characteristics, the spectra show lots of noise which causes more factors to define the spectral characteristics and were limited to predict the unknown samples.

Table 4.8 Descriptive statistical for the measurement of combustion performance parameters of grounded bamboo chips for developing NIR-Gun model.

Model	Calibration					Prediction				
	N	Max	Min	Mean	SD	N	Max	Min	Mean	SD
Ignition index	59	11.907E-3	7.07E-03	8.750E-03	1.000E-03	19	11.8E-03	7.140E-03	9.120E-03	1.270E-03
Burnout index	59	2.040E-04	1.220E-04	1.550E-04	1.800E-05	19	2.000E-04	1.250E-04	1.590E-04	1.900E-05
Combustion performance	60	4.613E-07	2.794E-07	3.581E-07	4.059E-08	20	4.569E-07	2.872E-07	3.599E-07	4.465E-08

Table 4.9 Descriptive statistical for the measurement of combustion performance parameters of grounded bamboo chips for developing Micro-NIR model.

Model	Calibration					Prediction				
	N	Max	Min	Mean	SD	N	Max	Min	Mean	SD
Ignition index	60	11.907E-03	6.994E-03	8.853E-03	1.084E-03	20	11.817E-03	7.136E-03	9.775E-03	1.150E-03
Burnout index	60	2.040E-04	1.23E-04	1.550E-04	1.900E-05	20	2.000E-04	1.250E-04	1.580E-04	1.900E-05
Combustion performance	60	4.613E-07	2.794E-07	3.560E-07	4.160E-08	20	4.569E-07	2.934E-07	3.661E-07	4.080E-08

where, N is number of sample, Max is maximum value, Min is minimum value and SD is standard deviation.

Table 4.10 PLS models statistics for the measurement of ignition index of grounded bamboo chips scanned by NIR-Gun spectrometer.

S.No.	Method	Factors	Calibration			Prediction		
			R_c^2	SECV	BIAS	R_p^2	SEP	BIAS
1	Raw	20	0.940	4.609E-04	2.011E-06	NA	1.500E-03	-1.429E-03
2	S-G (5 points)	20	0.837	6.100E-04	2.870E-06	NA	1.592E-03	-1.900E-03
3	1st Derivative (5 points)	19	0.834	6.200E-04	8.622E-07	NA	1.600E-03	-1.800E-03
4	2nd Derivative (5 points)	20	0.950	4.518E-04	1.054E-05	NA	1.600E-03	-1.100E-03
5	Mean normalization	20	0.932	5.000E-04	7.925E-06	NA	1.600E-03	-2.100E-03
6	Maximum normalization	20	0.943	4.790E-04	-4.625E-06	NA	1.300E-03	-1.500E-03
7	Range normalization	18	0.889	4.841E-04	-1.321E-05	NA	1.100E-03	-1.300E-03
8	Baseline offset	20	0.936	4.838E-04	4.544E-06	NA	1.400E-03	-1.600E-03
9	Linear baseline offset	20	0.946	4.767E-04	1.495E-05	NA	1.300E-03	-7.000E-04
10	SNV	20	0.901	4.934E-04	6.103E-06	NA	1.200E-03	-1.300E-03
11	Detrending	20	0.962	4.251E-04	1.234E-05	NA	1.400E-03	-8.000E-04
12	SNV +Detrending	18	0.877	5.176E-04	2.607E-06	NA	1.100E-03	-9.000E-04
13	MSC	20	0.940	4.609E-04	2.011E-06	NA	1.453E-03	-1.429E-03

Table 4.11 PLS models statistics for the measurement of burnout index of grounded bamboo chips scanned by NIR-Gun spectrometer.

S.No.	Method	Factors	Calibration			Prediction		
			R_c^2	SECV	BIAS	R_p^2	SEP	BIAS
1	Raw	20	0.940	8.325E-06	1.704E-07	NA	2.804E-05	-1.949E-05
2	S-G (5 points)	20	0.855	1.051E-05	1.465E-07	NA	3.228E-05	-3.529E-05
3	1st Derivative (5 points)	19	0.821	1.149E-05	1.562E-07	NA	3.083E-05	-3.931E-05
4	2nd Derivative (5 points)	20	0.956	7.788E-06	2.854E-07	NA	3.035E-05	-2.324E-05
5	Mean normalization	20	0.934	9.135E-06	9.486E-06	NA	2.195E-05	-2.423E-05
6	Maximum normalization	20	0.929	8.898E-06	3.850E-07	NA	1.625E-05	-1.737E-05
7	Range normalization	19	0.875	1.039E-05	-6.870E-08	NA	2.159E-05	-1.454E-05
8	Baseline offset	20	0.934	8.864E-07	1.931E-07	NA	2.336E-05	-2.036E-05
9	Linear baseline offset	19	0.934	8.889E-06	1.410E-07	NA	2.299E-05	-1.776E-05
10	SNV	18	0.846	1.090E-05	7.503E-08	NA	2.037E-05	-1.039E-05
11	Detrending	20	0.960	7.503E-06	2.540E-07	NA	2.425E-05	-1.914E-05
12	SNV +Detrending	18	0.851	1.069E-05	8.879E-08	NA	2.037E-05	-1.039E-05
13	MSC	20	0.940	8.254E-06	1.704E-07	NA	2.804E-05	-1.949E-06

Table 4.12 PLS models statistics for the measurement of combustion index of grounded bamboo chips scanned by NIR-Gun spectrometer.

S.No.	Method	Factors	Calibration			Prediction		
			R_c^2	SECV	BIAS	R_p^2	SEP	BIAS
1	Raw	20	0.922	2.048E-08	5.214E-10	NA	1.284E-07	-4.793E-08
2	S-G (5 points)	20	0.836	2.562E-08	5.827E-10	NA	1.602E-07	-5.339E-08
3	1st Derivative (5 points)	16	0.699	2.967E-08	3.715E-10	NA	2.191E-07	-7.498E-08
4	2nd Derivative (5 points)	20	0.943	1.944E-08	6.636E-10	NA	2.191E-12	-7.498E-08
5	Mean normalization	20	0.920	2.083E-08	6.949E-10	NA	1.802E-07	-6.212E-08
6	Maximum normalization	20	0.932	1.844E-08	6.223E-10	NA	4.170E-08	-7.605E-08
7	Range normalization	20	0.896	1.983E-08	1.018E-10	NA	4.393E-08	-7.907E-08
8	Baseline offset	20	0.920	2.133E-08	5.668E-10	NA	4.833E-08	-8.781E-08
9	Linear baseline offset	20	0.947	2.248E-08	8.966E-10	NA	1.768E-07	-2.555E-08
10	SNV	16	0.769	2.943E-08	5.877E-11	NA	5.916E-08	-4.629E-08
11	Detrending	20	0.935	2.076E-08	4.705E-10	NA	1.741E-07	-2.883E-08
12	SNV +Detrending	13	0.716	2.913E-08	4.180E-10	NA	5.267E-08	-3.230E-08
13	MSC	20	0.919	2.103E-08	7.755E-10	NA	9.839E-08	-5.215E-09

Table 4.13 PLS models statistics for the measurement of ignition index of grounded bamboo chips scanned by Micro-NIR spectrometer.

S.No.	Method	Factors	Calibration			Prediction		
			R_c^2	SECV	BIAS	R_p^2	SEP	BIAS
1	Raw	17	0.880	0.001	-3.043E-05	NA	1.600E-03	5.923E-05
2	S-G (5 points)	12	0.610	0.001	5.952E-07	NA	1.500E-03	1.823E-05
3	1st Derivative (5 points)	20	0.833	0.001	1.053E-05	NA	1.600E-03	1.408E-04
4	2nd Derivative (5 points)	19	0.909	0.001	-1.715E-06	NA	1.700E-03	-2.414E-04
5	Mean normalization	17	0.883	0.001	4.424E-07	NA	1.600E-03	6.841E-05
6	Maximum normalization	18	0.888	0.001	2.991E-06	NA	1.600E-03	2.345E-05
7	Range normalization	17	0.882	0.001	2.546E-09	NA	1.600E-03	6.545E-05
8	Baseline offset	19	0.900	0.001	2.152E-06	NA	1.700E-03	-1.173E-05
9	Linear baseline offset	18	0.892	0.001	5.187E-06	NA	1.630E-03	-5.783E-06
10	SNV	18	0.895	0.001	3.376E-06	NA	1.700E-03	1.089E-05
11	Detrending	15	0.870	0.001	-5.558E-06	NA	1.500E-03	4.462E-05
12	SNV +Detrending	17	0.887	0.001	1.278E-06	NA	1.600E-03	1.583E-05
13	MSC	18	0.898	0.001	4.060E-06	NA	1.600E-03	-2.642E-06

Table 4.14 PLS models statistics for the measurement of burnout index of grounded bamboo chips scanned by Micro-NIR spectrometer.

S.No.	Method	Factors	Calibration			Prediction		
			R_c^2	SECV	BIAS	R_p^2	SEP	BIAS
1	Raw	19	0.929	9.618E-06	5.470E-08	NA	3.369E-05	7.500E-06
2	S-G (5 points)	20	0.818	1.157E-05	-1.997E-08	NA	2.796E-05	-6.675E-05
3	1st Derivative (5 points)	19	0.854	1.063E-05	5.849E-08	NA	2.826E-05	1.593E-07
4	2nd Derivative (5 points)	13	0.805	1.168E-05	3.696E-08	NA	2.456E-05	-7.635E-06
5	Mean normalization	19	0.939	9.475E-06	-4.592E-08	NA	3.388E-05	9.259E-06
6	Maximum normalization	14	0.876	1.021E-05	-4.012E-08	NA	2.786E-05	1.884E-06
7	Range normalization	16	0.897	9.981E-06	-1.251E-07	NA	2.975E-05	4.787E-06
8	Baseline offset	16	0.898	9.867E-06	-2.936E-07	NA	3.044E-05	5.798E-06
9	Linear baseline offset	15	0.872	1.055E-05	-2.647E-08	NA	2.750E-05	5.838E-06
10	SNV	18	0.934	9.247E-06	-1.181E-07	NA	2.909E-05	7.304E-06
11	Detrending	15	0.888	1.019E-05	-7.460E-08	NA	2.810E-05	7.293E-06
12	SNV +Detrending	14	0.874	1.042E-05	-6.975E-08	NA	2.909E-05	7.304E-05
13	MSC	15	0.889	1.005E-05	6.229E-08	NA	3.021E-05	6.540E-06

Table 4.15 PLS models statistics for the measurement of combustion index of grounded bamboo chips scanned by Micro-NIR spectrometer.

S.No.	Method	Factors	Calibration			Prediction		
			R_c^2	SECV	BIAS	R_p^2	SEP	BIAS
1	Raw	17	0.908	2.227E-08	3.373E-10	NA	4.921E-08	-5.789E-09
2	S-G (5 points)	16	0.729	2.983E-08	-4.765E-11	NA	5.966E-08	-1.465E-08
3	1st Derivative (5 points)	20	0.862	2.486E-08	-1.618E-10	NA	5.077E-08	-3.601E-09
4	2nd Derivative (5 points)	14	0.824	2.637E-08	3.416E-10	NA	4.774E-08	-6.019E-09
5	Mean normalization	20	0.944	2.056E-08	1.016E-10	NA	4.338E-08	-3.145E-09
6	Maximum normalization	18	0.922	2.163E-08	2.045E-10	NA	4.755E-08	-3.613E-09
7	Range normalization	19	0.938	2.085E-08	6.390E-10	NA	4.691E-08	-2.315E-09
8	Baseline offset	20	0.943	2.071E-08	2.885E-10	NA	4.403E-08	-2.574E-09
9	Linear baseline offset	20	0.941	2.132E-08	2.748E-10	NA	4.077E-08	-4.144E-09
10	SNV	19	0.942	2.135E-08	8.163E-11	NA	4.704E-08	2.743E-09
11	Detrending	18	0.934	2.150E-08	3.392E-10	NA	4.167E-08	-5.311E-09
12	SNV +Detrending	19	0.944	2.232E-08	4.245E-10	NA	4.083E-08	1.265E-09
13	MSC	19	0.944	2.105E-08	1.925E-10	NA	4.476E-08	5.387E-10

The major components of lignocellulosic biomass are cellulose, hemicellulose, and lignin. Cellulose is a polysaccharide molecule having both a well-ordered structure and a randomly ordered structure which consists of hundreds of glucose molecules linked by glucosidic linkage, and the glucan chains are usually connected by hydrogen bonds [119, 120]. While, hemicellulose is another polysaccharide which is more complicated in structure and has higher linkages than cellulose. Hemicellulose, naturally, is connected with cellulose microfibrils by non-covalent linkages [121], and hemicellulose generally consists of more than one type of monosaccharide unit, including both hexose and pentose. Depending on the variety of biomass, hemicellulose may contain xyloglucan, xylan, glucomannans, galactoglucomannans, etc., however, the detailed structure of hemicellulose is still remains unknown [122]. On the other hand, the structure of lignin is very complicated, and it is made of phenolic polymers that consist of three types of phenylpropane untis: p-coumaryl alcohol, coniferyl alcohol, and sinapyl alcohol [123, 124].

Damien Sabatier et al. [23] measure the lignocellulosice compounds of sugarcane biomass by near infrared reflectance spectroscopy (400-2500nm), monochromator spectrometer NIRSystems XDS, inc., using modified PLS regression and obtained the coefficient of determination of prediction of sugarcane hemicellulose, cellulose, lignin 0.45, 0.77, 0.44 and RPD 1.9, 4.2 and 1.9 with factors 14, 13 and 14, respectively, and made a conclusion for the poor prediction of hemicellulose and lignin was that it contain several molecules that causes these parameter to define inadequately. Similarly, carbon and hydrogen were predicted poorly (RPD of internal validation 2.1 and 1.3, respectively) by Jesús Mata Sanchez et al. [125] by using the FT-NIR spectrometer (MPA, Bruker Optics, Ettlingen, Germany). The online prediction of lignocellulose compound of corn stover by Junjie Xue et al. [126] were not found accurate as coefficient of determination of prediction for cellulose, hemicellulose and lignin were 0.77, 0.62 and 0.61 were found by using Matrix-F (Bruker Daltonik GmbH, Bremen German) in diffuse reflection mode. Sanderson et al. [127] were also unable to predicted C, H and O of woody and herbaceous feedstocks with any precision or accuracy by using Pacific Scientific Model 6250 scanning monochromator, near infrared reflectance spectrometer, over the range 1100-2500 nm, and concluded that small population size (SD 0.22, 0.3, 2.08 respectively) may have contributed to some of the inaccuracy and imprecision in NIRS prediction.

4.3.2 Measurement of combustion performance parameters by Fourier transform near infrared instrument (FT-NIR)

The raw spectrum of the grounded bamboo samples scanned by FT-NIR is shown in Figure 4.19. The absorbance shows the wide range of absorbance over the region 8770-8020 cm^{-1} (1140-1247 nm) but with low absorbance intensity which is normally associated with the second overtone of C—H stretch, carbonyl compounds [29]. The important region of absorption are: 7240-6560 cm^{-1}, 4480-4200 cm^{-1} (1381-1524 nm and 2232-2380 nm, respectively, combination region of C—H band) [16]; 5284-5103 cm^{-1} (1893-1960 nm, first overtone O—H band assign as O—H stretch/O—H deformation combination hydroxyl) 29]; 4980-4640 cm^{-1} (2008-2155 nm, first overtone O—H band C—O, O—H stretching combination, primary alcohol) [29]; 4140-3922 cm^{-1} (2415-2550 nm, second overtone of C—H band, C—H bending) [29].

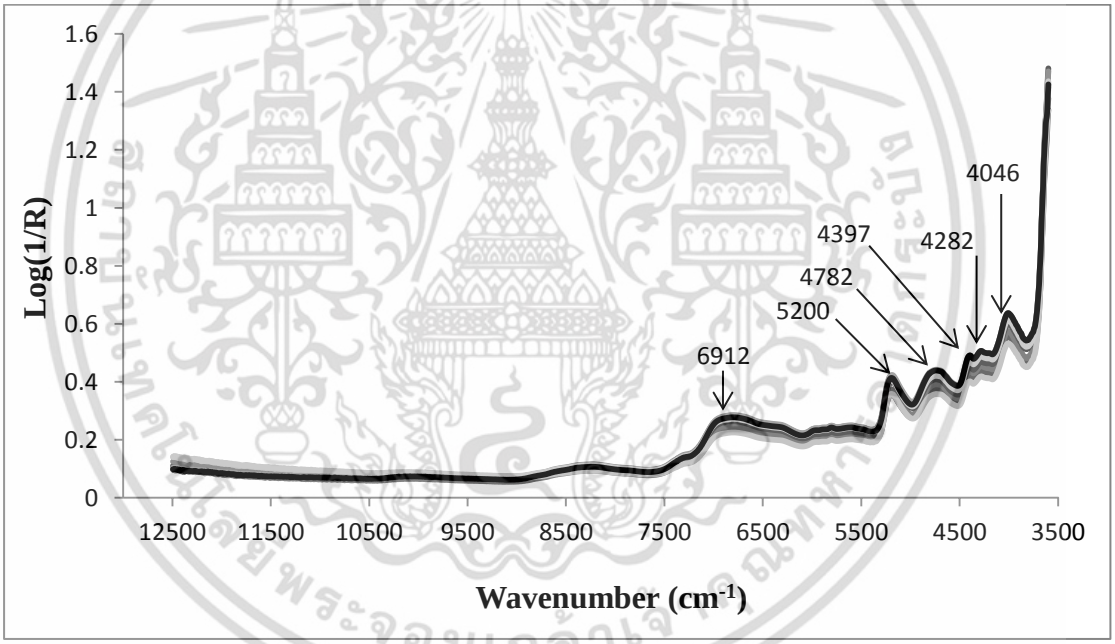

Figure 4.19 Raw spectra of the grounded bamboo chips samples scanned by FT-NIR spectrometer.

The absorbance shows the peaks at around 6912 cm^{-1} (1447 nm, 2×C—H str. + C—H def., aromatic)[28], 5200 cm^{-1} (1923 nm, O—H str. and HOH deformation bending, O—H molecular water)[28], 4782 cm^{-1} (2091 nm, O—H combination, polymeric .OH), 4397 cm^{-1} (2274 nm, O—H str.+C-C str., starch)[28], 4282 cm^{-1} (2335 nm, C—H str.+C—H def., cellulose)[28], 4046 cm^{-1} (2471 nm, C—H combination, lipids, aliphatic compounds) [28]. The absorbance is dominated by the C—H bands.

The scanning of the FT-NIR seems clearly better than diode array spectrometer NIR-instrument. This is, generally, due to the high signal to noise ratio of FT-NIR spectrometer. However, the FT-NIR spectroscopy was also unable to predict the combustion index with any accuracy, but was able to predict the ignition index and burnout index with lower accuracy.

The total number of the sample used for making the model was 80. The descriptive statistics for the development of combustion parameter models are tabulated under Table 4.16. The various combustion parameter models were developed separately using the same spectra. Various pretreatments were performed on the raw spectra. Min-Max normalization was found to be the effective treatment for the calibration of ignition index, whereas multiplicative scattering correction was found effective for calibration of burnout index. The PLS statistics of the ignition index and burnout index are shown in Table 4.17.

Table 4.16 The descriptive statistics for the development of combustion performance parameter for FT-NIR models.

Model	Calibration					Prediction				
	N	Max	Min	Mean	SD	N	Max	Min	Mean	SD
Ignition index	48	11.908E-03	6.994E-03	8.815E-03	1.041E-03	32	11.817E-03	7.073E-03	8.861E-03	1.186E-03
Burnout index	56	2.040E-04	1.220E-04	1.560E-04	1.800E-05	24	2.000E-04	1.230E-04	1.560E-04	1.900E-05
Combustion performance	56	4.613E-07	2.294E-07	3.5991E-07	3.904E-08	32	4.569E-07	2.811E-07	3.564E-07	4.519E-08

where, N is number of sample, Max is maximum value, Min is minimum value and SD is standard deviation.

Table 4.17 PLS statistics of the optimum model of the grounded bamboo chips scanned by FT-NIR spectrometer.

Model	Treatment	Factors	Calibration		Validation			
			R_c^2	RMSEE	R_p^2	RMSEP	Bias	RPD
Ignition index	Min-Max normalization	4	0.297	8.920E-04	0.432	8.870E-3	3.960E-05	1.33
Burnout index	MSC	7	0.683	1.060E-05	0.513	1.380E-05	-2.210E-07	1.43

The R_p^2, bias and RPD of optimum model of ignition index are 0.432, 3.960E-05, and 1.33, with the number of PLS factors of the model 4. The coefficient of determination for prediction set was found higher than calibration set. This may be due to the closeness of the prediction data set to calibration model data set, since the ratio of sample used for prediction and calibration is 1:1.5. The scatter plot of the model is shown in Figure 4.20. The regression coefficient plot and X-loading of first three PLS-factors of ignition index is shown in Figure 4.21 and 4.22, respectively. The most important regions found for the calibration of ignition index were 12007-10036 cm^{-1} (833-996 nm, third overtone of C—H str.) [29], 8706-7876 cm^{-1} (1149-1270 nm, second overtone, C—H str.) [28] and 5404-4575 cm^{-1} (1851-2186 nm, third overtone, C—H bend) [28].

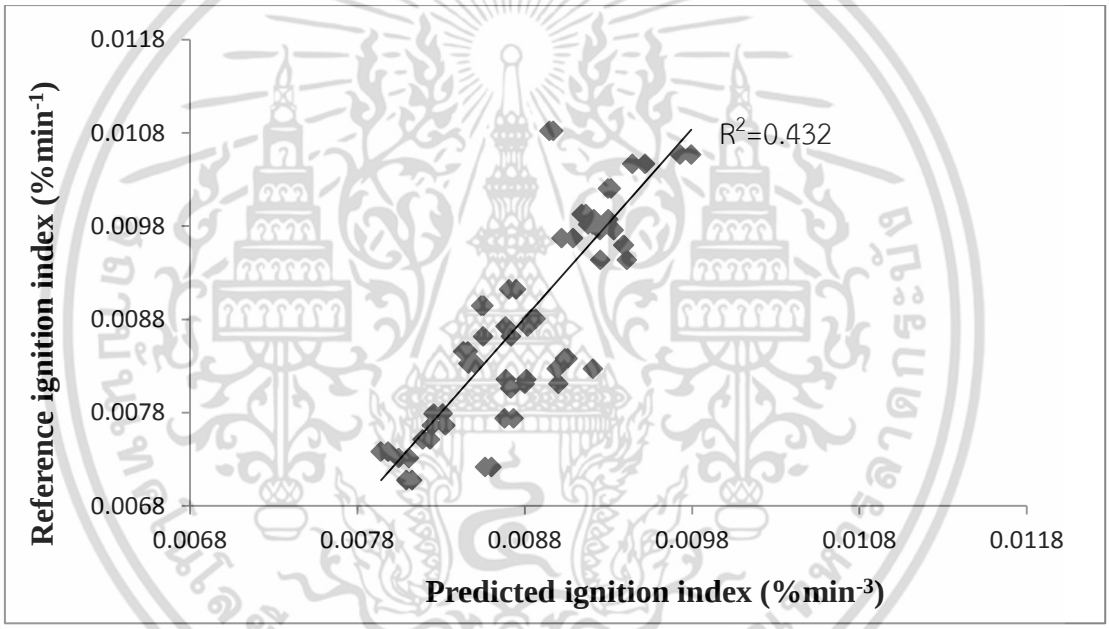

Figure 4.20 Comparison of ignition index of grounded bamboo chips as predicted by FT-NIR spectroscopy and measured by reference test.

In the regression coefficient plot, several minor peaks are observed in the region 12007-10036 cm^{-1} and 8706-7876 cm^{-l}, while clear sharp peaks are seen in the region 5404-4575 cm^{-1} with independent peaks at around 5404 cm^{-1} (1850 nm, 2×O—H def. + C—O def., starch) [28], 5254 cm^{-1} (1903 nm), 5038 cm^{-1} (1985 nm) and 4879 cm^{-1} (2050 nm). Similarly, in X-loading plot, the most influential region 12007-10036 cm^{-1}, 8706-7876 cm^{-1}, and 5404-4575 cm^{-1}. The most important peaks for factor-1 are 5404 cm^{-1} (1850 nm), 5149 cm^{-1} (1942 nm, O—H str.+O—H def., water) [28], 4694 cm^{-1} (2130 nm); factor-2 are 5404 cm^{-1} (1850 nm), 5257 cm^{-1} (1902 nm), 5022 cm^{-1}

(1991 nm), 4732 cm^{-1} (2113 nm); factor-3 are 5404 cm^{-1}(1850 nm), 5350 cm^{-1} (1869 nm), 5254 cm^{-1} (1903 nm), 5072 cm-1, 4856 cm^{-1} (2059 nm), 4674 cm^{-1}(2139 nm). The most important peaks seen in regression coefficient and X-loading and the corresponded vibration bonds are tabulated under Table 4.18.

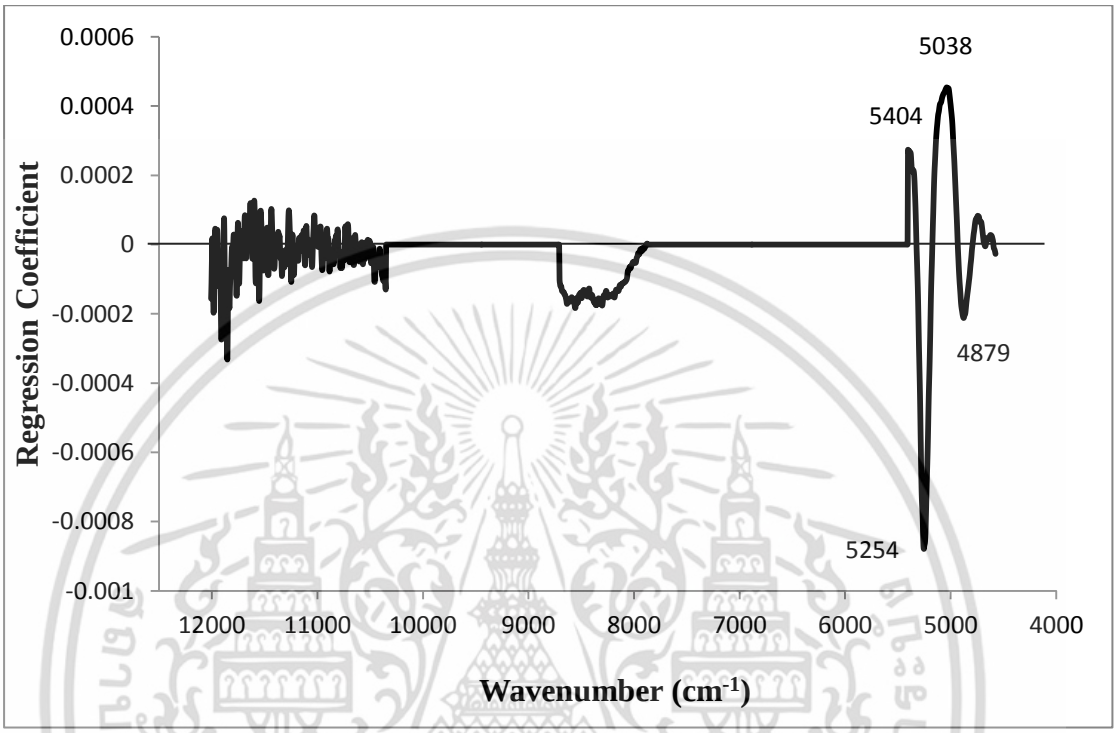

Figure 4.21 Regression coefficient plot of optimum model of ignition index developed from the spectra of grounded bamboo chips scanned by FT-NIR spectrometer.

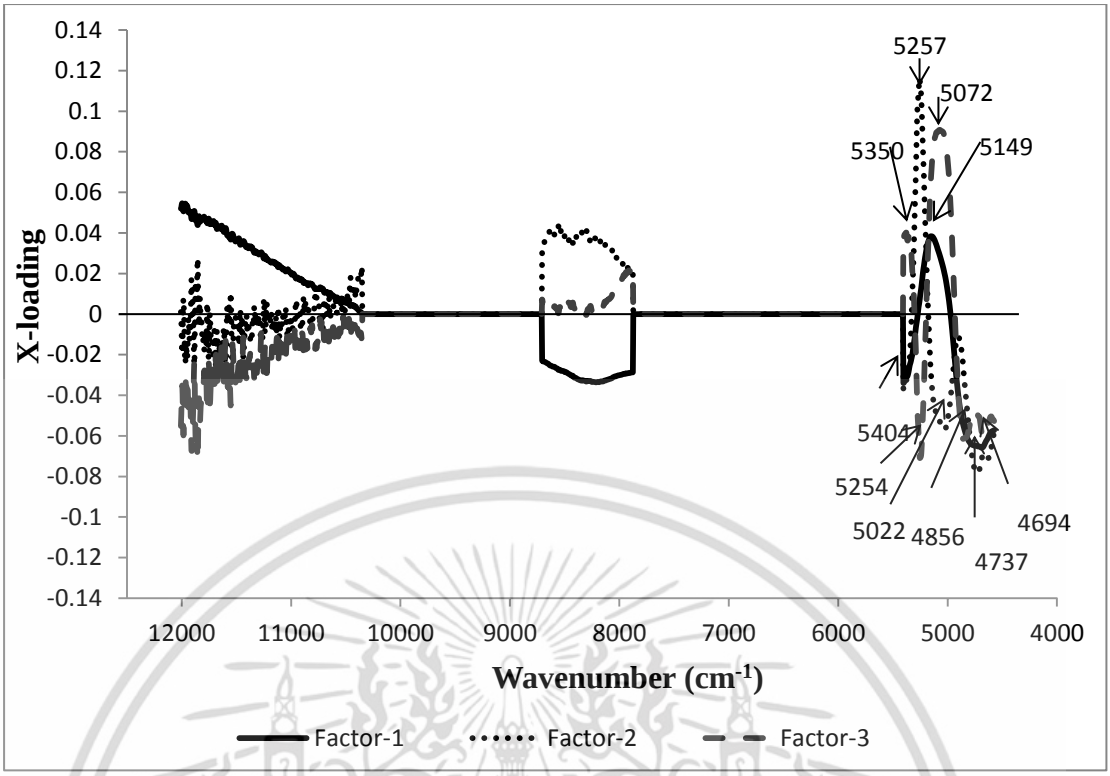

Figure 4.22 First 3 X-loading plot of optimum model of ignition index developed from the spectra of grounded bamboo chips scanned by FT-NIR spectrometer.

The R_p^2, bias and RPD of optimum model of burnout index are 0.513, -2.210E-07, and 1.43, with the number of PLS factors of the model 7. The scatter plot of the model is shown in Figure 4.23. The most important regions found for the calibration of ignition index were 12003-8697cm^{-1} (833-1149 nm) and 7876-4574 cm^{-1}(1270-2186 nm). The region 12003-8697cm^{-1} is normally associated with the second and third overtone of hydrocarbon, and aromatic amines [16].

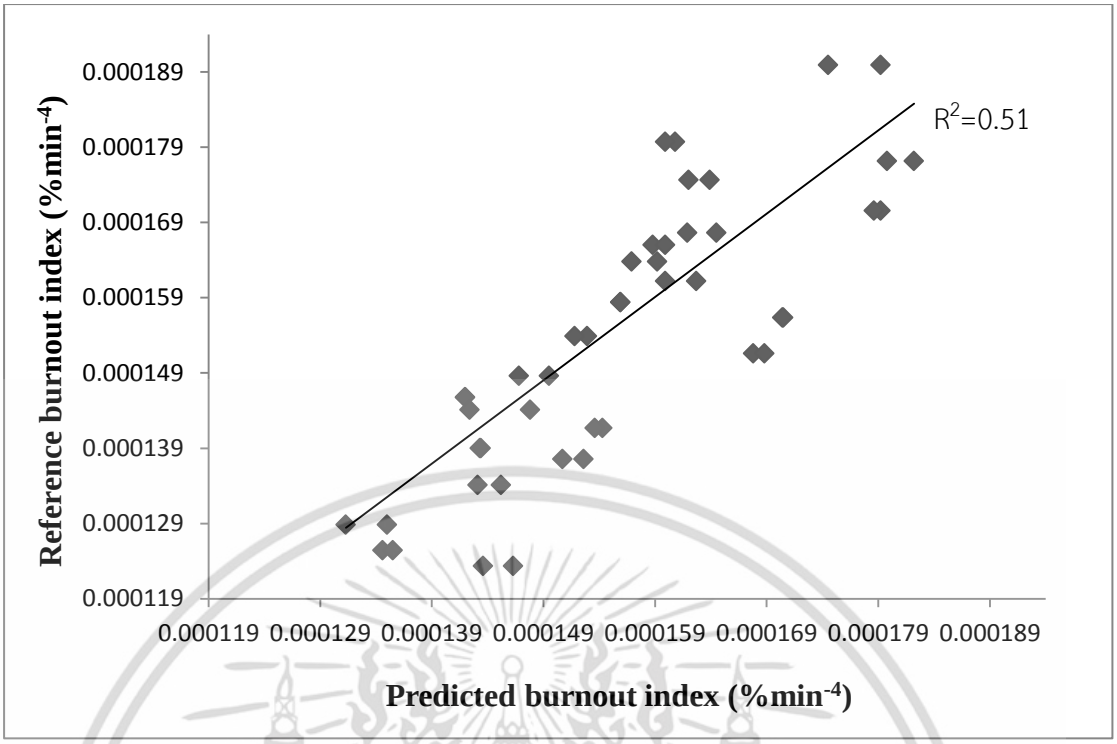

Figure 4.23 Comparison of burnout index of grounded bamboo chips as predicted by FT-NIR spectroscopy and measured by reference test.

The regression coefficient plot and first 3 X-loading of first three PLS-factors of burnout index is shown in Figure 4.24 and 4.25, respectively. In the regression coefficient plot of burnout index, several narrow peaks are observed in the region 12003-8697 cm^{-1} (833-1149 nm), and the peaks in the region 7876-4574 cm^{-1}(1270-2186 nm) are little broad but with the shoulder peaks. The dominating peaks of X-loading of Factor-1 are 10055 cm^{-1} (995 nm), 8697 cm^{-1} (1150 nm); Factor-2 are 5157 cm^{-1}(1939 nm), 4687 cm^{-1} (2134 nm); Factor-3 are 7047 cm^{-1} (1419 nm), 5253 cm^{-1} (1904 nm). Factor-1 shows the effect of 12003-8697cm^{-1} on the model while factor-2 and factor-3 shows the effect of 7876-4574 cm^{-1} (1270-2186 nm). The most important peaks seen in regression coefficient and X-loading and the corresponded vibration bonds are tabulated in Table 4.18. The regression plot and the X-loading plot are affected mainly by the hydrocarbon (10753, 6120, 6110, 5925, 5900, 5675 cm^{-1}) and aromatic amines (6916, 6791, 6656 cm^{-1}).

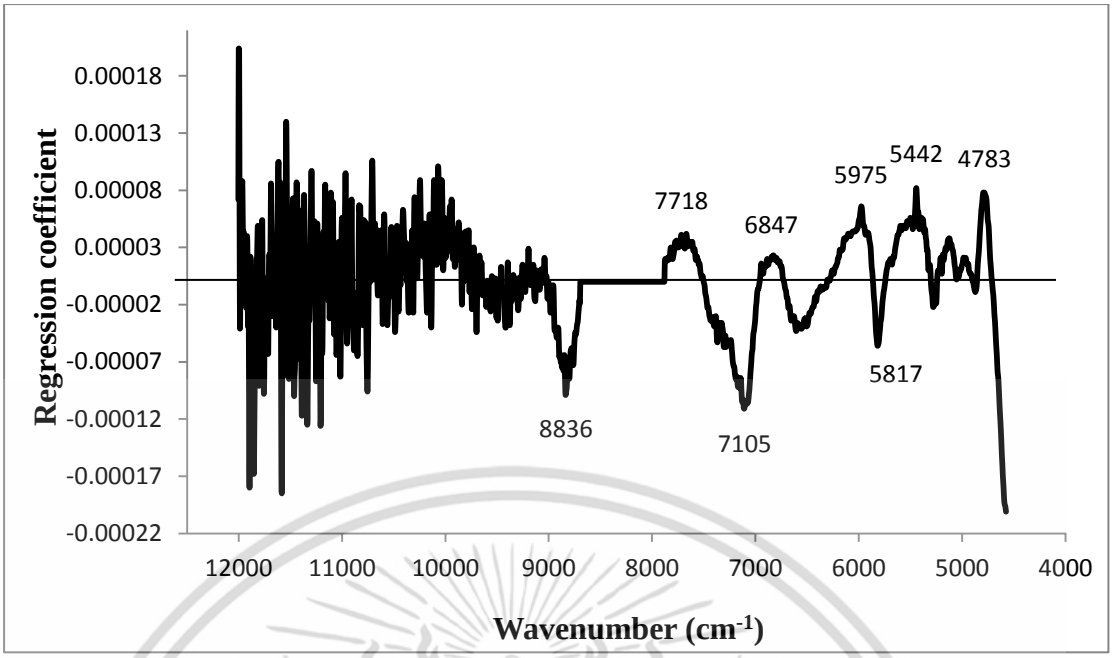

Figure 4.24 Regression coefficient plot of optimum model of burnout index developed from the spectra of grounded bamboo chips scanned by FT-NIR spectrometer.

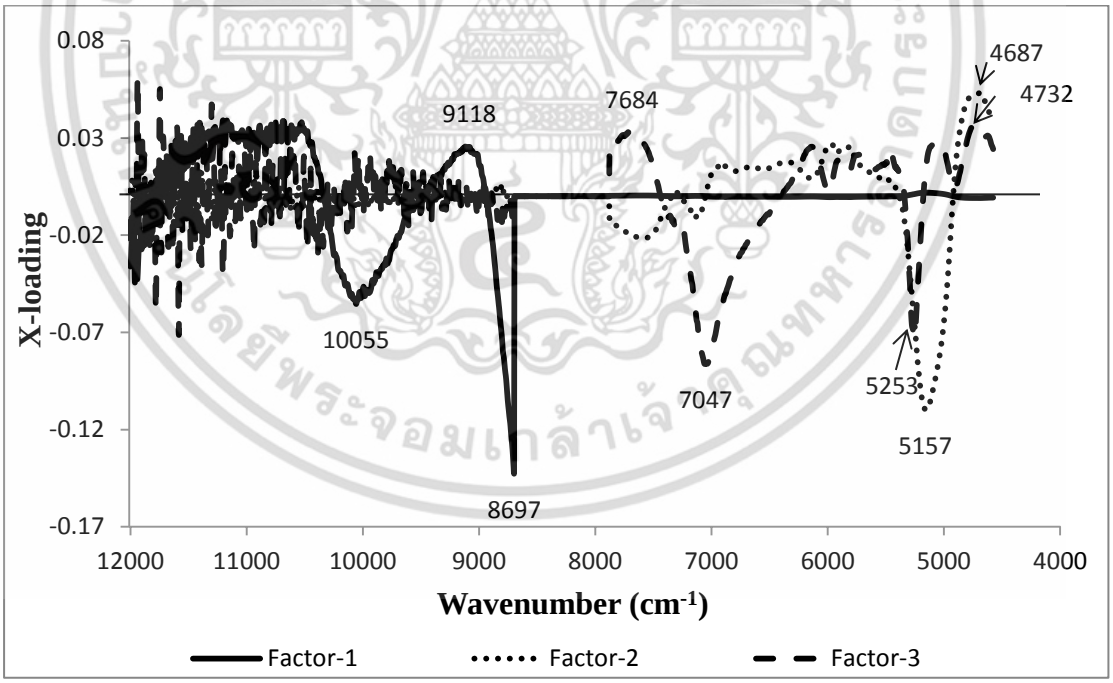

Figure 4.25 First 3 X-loading of optimum model of burnout index developed from the spectra of grounded bamboo chips scanned by FT-NIR spectrometer.

Table 4.18 The dominant peaks on regression coefficient plot and X-loading plot of ignition index and burnout index of FT-NIR model.

PEAK Wavenumber (cm^{-1})	Wavelength (nm)	Nearest wavelength (nm)	Spectral structure	Material type	Source
10055	995	996	O—H(3υ) (—CH_2—OH), primary alcohol	Primary alcohol	[16]
8836	1132				
8697	1150	1152	C—H str. second overtone	CH_3	[28]
7718	1296				
7105	1407	1410	O—H str. first overtone	ROH	[28]
7047	1419	1420	O—H(2υ), .O—H	Hydrocarbon, aromatic	[16]
6847	1460	1460	N—H str. first overtone	$CONH_2$	[28]
5975	1674	1671	CHυ + CHυ (12 + 1), benzene band assignment	C—H aryl	[16]
5817	1719	1725	C—H str. first overtone	CH_2	[28]
5442	1838				
5404	1850	1860	C—CL(7υ), .C—CL	Chlorinated hydrocarbons	[16]
5350	1869				
5257, 5254, 5253	1902, 1903, 1904	1900	O—H str.+ 2×C—H str.	Starch	[28]
5157, 5149	1939, 1942	1940	O—H str.+ O—H def.	Water	[28]
5038	1985	1980	N—H(υN—H and Δ N—H combination), primary aromatic amine in CCL_4 as para-NH_2 grouping	Aromatic amine	[16]
5022	1991	1990	N—H for primary amides	Urea	[16]
4879	2050	2050	N—H asym. str. + amide II	protein	[28]
4856	2059	2060	N—H (3Δ) and N—H	Amides/prote	[16]

			stretching combination	in	
4783	2091	2090	O—H combination	Polymeric .OH	[16]
4732	2113	2110	N—H sym. str. + amide II	$CONH_2$, CONHR	[28]
4694, 4687	2130, 2134	2132	N—H str. + C=O str.	Ammino acid	[28]
4674	2139	2140	=C—H str. + C=C str.	HC=CH	[28]

Chapter 5

Conclusion

From the thermogravimetric analysis, it can be concluded that bamboo chips were easier to burn than the *L. leucocephala* pellet which is verified by the higher value of combustion performance index of bamboo than that of *L. leucocephala* pellet. The higher value of the ignition index of bamboo also implies that the bamboo is easier to ignite as a fuel which is verified by the lower value of ignition temperature. The higher value of ignition temperature and burnout temperature made the *L. leucocephala* pellet to ignite difficult and last longer than bamboo. Consequently, leads to the higher burnout index.

On the other hand, the moisture content models developed from the spectra obtained by scanning from two diode array NIR-instruments (NIR-Gun and Micro-NIR) show the affected of different constituents of bamboo rather than the moisture, and the bands shifting were seen in common. The -OH appear in combination with alkyl group rather than H-atom. Both models are suitable for screening and some approximate calibration. The research shows that the NIR-Gun model can use with caution for the most of applications including research works. This shows that short wavelength was better than long wavelength for the measurement of moisture content in bamboo. Moreover, this research would be helpful for process controlling using the moisture parameter during drying, pelletization and thermochemical conversion.

Furthermore, the diode array NIR-instruments were unable to predict the combustion performance parameter of the grounded bamboo chips with any accuracy. All the models of combustion performance parameter used 13-20 PLS factors for the making the model. The models were unable to predict the values of the test set. The spectra were suffered from the noise, and the variability of the calibration set samples used for making the models (for combustion index 4.613-2.794×10^{-7}, ignition index 0.011907-0.006994, burnout index 2.04-1.23×10^{-4}) were low. This may be the reason why the diode array NIR-instrument failed to predict. On the other hand, the FT-NIR was able to predict the ignition index and burnout index with very low accuracy.

NIR spectroscopy has been successfully used in various field of agriculture. Various authors have been successfully implemented NIR spectroscopy technique for the prediction of not only the moisture content on biomass but also like heating

value of the fuel, ash contain, constituents of biomass and more. However, the model of mine was unable to predict the combustion performance parameter of the bamboo with good accuracy due to low variability of data. So, for the one who want to do research on biomass I would like to suggest to increase the population size of the samples by collecting the different species of same or different biomass, so that the data contains large range and makes the model robust by providing sufficient information while making the model. In addition, I would also like suggest using the whole range of NIR region while making the model.

References

[1] López-González D., Fernandez-Lopez M., Valverde J.L. and Sanchez-Silva L. “Thermogravimetric-mass spectrometric analysis on combustion of lignocellulosic biomass.”, Bioresource Technol., vol. 143, 2013. Pp. 562-574.

[2] Sivasangar S., Taufiq-Yap Y.H., Zainal Z. and Kitagawa K. “Thermal behavior of lignocellulosic materials under aerobic/anaerobic environments.”, Int. J. Hydrogen Energ., vol. 38, 2013. Pp. 16011-16019.

[3] Liu T., McConkey B., Huffman T., Smith S., MacGregor B., Yemshanov D. and Kulshreshtha S. “Potential and impacts of renewable energy production from agricultural biomass in Canada.”, Appl Energ., vol. 130, 2014. Pp. 222-229.

[4] Stern N. 2007. The economics of climate change: the stern review. Cambridge: Cambridge University Press.

[5] Kuttiraja M., Sindhu R., Varghese P. E., Sandhya S. V., Binod P., Vani S., Pandey A., Sukumaran R. K. “Bioethanol production from bamboo (Dendrocalamus sp.) process waste. ”, Biomass Energ., vol. 59, 2013. Pp. 142-150.

[6] Biswas S. “Studies on bamboo distribution in north-eastern region of India.”, Indian Forester, vol. 114, 1988. Pp. 514-531.

[7] Liebman A. and Einav T. Bamboo: an untapped and amazing resource. UNIDO features. http://www.unido.org/index.php? Id= 1000276; 2009.

[8] Chaowana P. “Bamboo: An Alternative Raw Material for Wood and Wood-Based Composites.”, Journal of Materials Science Research, vol. 2, 2013. Pp. 90-102.

[9] Scurlock J.M.O., Dayton D.C. and Hames B. "Bamboo: an overlooked biomass resource?”, Biomass Bioenerg., vol. 19, 2000. Pp 229-244.

[10] Alternative Energy and Efficiency Information Center. “Energy in Thailand: Facts and Figures 2013.”, Department of Alternative Energy Development and Efficiency, Ministry of Energy, Thailand. (2013).

[11] Ramage J, Scurlock J. 1996. Biomass. In: Boyle G, editor. Renewable energy-power for a sustainable future. Oxford: Oxford University Press, pp. 137-182.

[12] Thai Meteorological Department. “Thailand weather, Meteorological knowledge.”, [Online]. Available: http://www.tmd.go.th/info/info.php?FileID=22. 2014.

[13] Demirbas A. “Potential applications of renewable energy sources, biomass combustion problems in boiler power systems and combustion related environmental issues.” Prog. Energ. Combust., vol. 31, 2005. Pp. 171-192.

[14] Hamelinck C.N. and Faaij A.P.C.. “Outlook for advanced biofuels.”,Energ. Policy, vol. 34, 2006. Pp. 3268–3283.

[15] Molino A., Nanna F. and Villone A. “Characterization of biomasses in the

southern Italy regions for their use in thermal processes.", Appl. Energ., vol. 131, 2014. Pp. 180-188.

[16] Workman J. and Weyer L. Jr. (2008). Practical guide to interpretive Near-Infrared Spectroscopy. Boca Raton: CRC press.

[17] Sirisomboon P., Kaewkuptong A. and Williams P. "Feasibility study on the evaluation of the dry rubber content of field and concentrated latex of Para rubber by diffuse reflectance near infrared spectroscopy.", J. Near Infrared Spectros., vol. 21, 2013. Pp. 81–88.

[18] Jin S. and Chen H. "Near-infrared analysis of the chemical composition of rice straw.", Ind. Crop. Prod., vol. 26, 2007. Pp. 207-211.

[19] Peter J. D., Hartmann H., Böhm T., Temmerman M., Rabier F. and Morsing M. "Moisture content determination in solid biofuels by dielectric and NIR reflection methods.", Biomass Bioenerg., vol. 30, 2006. Pp. 935-943.

[20] Posom J. and Sirisimboon P. "Evaluation of the moisture content of Jatropha curcas kernels and the heating value of the oil extracted residue using near-infrared spectroscopy.", Biosyst. Eng., vol. 130, 2015. Pp. 52-59.

[21] Suehara K.-I., Ohta Y., Nakano Y. and Yano T. "Rapid measurement and control of the moisture content of compost using near-infrared spectroscopy.", J. Biosci. Bioeng., vol. 87, 1999. Pp. 769-774.

[22] Fagan C. C., Everard C. D. and McDonnell K. "Prediction of moisture, calorific value, ash and carbon content of two dedicated bioenergy crops using near-infrared spectroscopy.", Bioresource Technol., vol. 102, 2011. Pp. 5200-5206.

[23] Sabatier D., Thuries L., Bastianelli D. and Dardenne P. "Rapid prediction of the lignocellulosic compounds of sugarcane biomass by near infrared reflectance spectroscopy: comparing classical and independent cross-validation.", J. Near Infrared Spec., vol. 20, 2012. Pp. 371-385.

[24] He C., Chen L., Yang Z., Hang G., Liao N. and Han L. "A rapid and accurate method for on-line measurement of straw-coal blends using near infrared spectroscopy.", Bioresource Technol., vol. 110, 2012. Pp. 314-320.

[25] Huang C., Han L., Yang Z., Liu X. "Ultimate analysis and heating value prediction of straw by near infrared spectroscopy.", Waste Manage., vol. 29, 2009. Pp. 1793-1797.

[26] Everard C. D., McDonnell K. P. and Fagan C. C. "Prediction of biomass gross calorific values using visible and near infrared spectroscopy.", Biomass Bioenergy., vol. 45, 2012. Pp. 203-211.

[27] Williams P. 2007. Near-infrared Technology–Getting the best out of light, A Short Course in the Practical Implementation of Near-infrared Spectroscopy for the User. 5th ed. Nanaimo: PDK Grain.

[28] Osborne B.G., Fearn T. and Hindle P.H. 1993. Practical NIR spectroscopy with applications in food and beverage analysis. 2nd ed. UK : Longman Science & Technical.

[29] Murray I. and Williams P. C. 1987. Chemical principles of near-infrared technology. In: William P. and Norris K. eds. Near infrared technology in the agricultural and food industry. Minnesota: American Association of Cereal Chemists, pp. 17-34.

[30] Stuart B. 1996. Modern Infrared Spectroscopy. Chichester: John Wiley & Sons.

[31] Ciurczak E. W. 1992. Principles of near-infrared spectroscopy. In: Burns D. A., Ciurczak E.W. eds. Handbook of Near-Infrared Analysis. 2nd edition, New York: Marcel Dekker, pp. 7 –18.

[32] Günzler H., Gremlich H.-U. 2002. IR Spectroscopy an introduction. Translated by Blumich M.-J. Weinheim: Wiley-VCH.

[33] Birth G. S. and Hecht H. G. 1987. The physics of near-infrared reflectance. In: William P. and Norris K. eds. Near infrared technology in the agricultural and food industry. Minnesota: American Association of Cereal Chemists, pp. 1-15.

[34] Perkins W. D. 1993. Sample handling in infrared spectroscopy—an overview. In: Coleman P. B. ed. Practical sampling techniques for infrared analysis. Boca Raton: CRC press, pp. 11-54.

[35] Culler S. R. 1993. Diffuse reflectance infrared spectroscopy: sampling techniques for qualitative/quantitative analysis of solids. In: Coleman P. B. ed. Practical sampling techniques for infrared analysis. Boca Raton: CRC press, pp. 93-105.

[36] Sablinskas V. 2003. Instrumentation. In: Gauglitz G. and Vo-Dinh T. eds. Hand book of spectroscopy. Weinheim: Wiley-VCH, pp. 48-69.

[37] Lin M., Rasco B. A., Cavinato A. G. and Al-Holy M. 2009. Infrared Spectroscopy—Near Infrared Spectroscopy and Mid-Infrared Spectroscopy. In: Sun D. A. Infrared Spectroscopy for Food Quality Analysis and Control. Amsterdam: Elsevier, pp. 119-143.

[38] Kemeny G. J. 1992. Process analysis. In: Burns D.A., Ciurczak E.W. eds. Handbook of Near-Infrared Analysis. New York: Marcel Dekker, pp. 53-105.

[39] Tran C. D. “Principles and analytical applications of acousto-optic tunable filters, an overview.”, Talanta, vol. 45, 1997. Pp. 237-248.

[40] Tran C. D. “Principles, Instrumentation, and Applications of Infrared Multispectral Imaging, An Overview.”, Anal. Lett., vol. 38, 2005. Pp. 735–752.

[41] Stratis D. N., Eland K. L., Carter J. C., Tomlinson S. J., and Angel S. M. “Comparison of Acousto-optic and Liquid Crystal Tunable Filters for Laser-Induced Breakdown Spectroscopy.”, Appl. Spectrosc., vol. 55, 2001. Pp. 999-1004.

[42] Lajunen L. H.J. 1992. “Spectrochemical analysis by atomic absorption and emission.”, Cambridge: Royal society of chemistry.

[43] Smith B. C. 2011. Fundamentals of fourier transform infrared spectroscopy. 2nd ed. Boca Raton: CRC press.

[44] McClure W. F. 1987. Near-Infrared Instrumentation. In: William P. and Norris K. eds. Near infrared technology in the agricultural and food industry. Minnesota: American Association of Cereal Chemists, Inc. pp. 89-105.

[45] Andrade-Garda J. M., Boque-Marti R., Ferre-Baldrich J. and Carlosena-Zubieta A. 2009. Partial least-squares regression. In: J. M. Andrade-Garda. Basic chemometric techniques in atomic spectroscopy. Cambridge: Royal Society of Chemistry, pp. 181-243.

[46] Geladi P. and Kowalski B. R. “Partial least-square regression: a tutorial.”, Anal. Chim. Acta, vol. 185, 1986. Pp 1-17.

[47] Romia M. B. and Bernàrdez. M. C. 2009. Multivariate calibration for quantitative analysis. In: Sun D. A. Infrared Spectroscopy for Food Quality Analysis and Control. Amsterdam: Elsevier, pp. 51-82.

[48] Rezaa M. T., Beckerb W., Sachsenheimerb K., Mummea J. Hydrothermal carbonization (HTC): Near infrared spectroscopy and partial least-squares regression for determination of selective components in HTC solid and liquid products derived from maize silage. Bioresource Technol., vol. 161, 2014 PP. 91–101.

[49] Rinnan Å., Nørgaard L., Frans van den Berg, Thygesen J. Bro R. and Engelsen S. B. 2009. In: Sun D. A. Infrared Spectroscopy for Food Quality Analysis and Control. Amsterdam: Elsevier, pp.29-50.

[50] Savitzky A. and Golay M. J. E. “Smoothing and differentiation of data by simplified least squares procedures.”, Analytical Chem., vol. 36, 1964, Pp. 1627–1639.

[51] Rinnan Å., van den Berg F., Engelsen S. B.. “Review of the most common pre-processing techniques for near-infrared spectra.”, Trends Anal. Chem., vol. 28, 2009. Pp. 1201-1222.

[52] Hruschka W. R. 1987. Data analysis: Wavelength selection methods. In: William P. and Norris K. eds. Near infrared technology in the agricultural and food industry. Minnesota: American Association of Cereal Chemists, pp. 35-55.

[53] Phetpan K. 2015. “Feasibility for in-line measurement of tapioca starch moisture content using near infrared spectroscopy”. Master dissertation, King Mongkut's Institute of Technology.

[54] CAMO. “The Unscrambler Appendices: Method References.” [Online]. Available : http://www.camo.com/TheUnscrambler/Appendices. Accessed on February

23, 2015.

[55] Wu W., Walczak B., Massart D. L., Prebble K. A. and Last I. R. “Spectral transformation and selection in near infrared spectra classification.”, Anal. Chim. Acta., vol. 315 (1995), pp. 243–255.

[56] Barnes R. J., Dhanoa M. S., and Lister S. J. “Standard Normal Variate Transformation and De-trending of Near-Infrared Diffuse Reflectance Spectra.”, Appl. Spectrosc., vol. 43, 1989. Pp. 772-777.

[57] Conzen J. P. 2006. Multivariate Calibration: A practical guide for developing methods in the quantitative analytical chemistry. 2nd ed. Germany: Bruker Optik GmbH.

[58] Westada F., Afsethb N. K. and Broc R. “Finding relevant spectral regions between spectroscopic techniques by use of cross model validation and partial least squares regression.”, Anal. Chim. Acta, vol. 595, 2007. Pp. 323–327.

[59] Hemminger W. and Sargev S.M. 1998. Definitions, nomenclature, terms and literature. In: Brown M. E. editor. Handbook of thermal analysis and calorimetry (Vol.1, Principles and practice). Amsterdam: Elsevier, pp. 1-74.

[60] Ma B. G., Li X. G., Wang K. and Wang X. G. “Investigation on catalyzed combustion of high ash coal by thermogravimetric analysis.”, Thermochem. Acta., vol. 445, 2006. Pp. 19-22.

[61] Nie Q. H., Sun S. Z. and Li Z. Q. “Thermogravimetric study on the combustion characteristic of brown coal blends.”, J. Combust. Sci. Technol., vol. 7, 2001. Pp. 72-76.

[62] Li X. G., Ma B. G., Xu L., Hu Z. W. and Wang X. G. “Thermogravimetric analysis of the co-combustion of the blends with high ash coal and waste tyres." Thermochim. Acta., vol. 441, 2006. Pp. 79-83.

[63] Idris S. S., Rahman N. A. and Ismail K. “Combustion characteristics of Malaysian oil palm biomass, sub-bituminous coal and their respective blends via thermogravimetric analysis (TGA) .”, Bioresource Technol., vol. 123, 2012. Pp. 581-591.

[64] Xie J.-L. and He F. “Catalyzed combustion study of anthracite in cement kiln.”, J. Chin. Ceram. Soc., vol. 26, 1998. Pp. 792-795.

[65] Qing W., Hao X., Hongpeng L., Chunxia J. and Jingru B. “Thermogravimetric analysis of the combustion characteristics of oil shale semi-coke/biomass blends.”, Oil shale, vol. 28, 2011. Pp. 284-295.

[66] Xu Y., Lin S., Yuan H., Zhu K., He X. and Chen G. “Thermogravimetric Analysis on the Combustion Characteristics for Blended Coals.” Proc. International Conference on Power Engineering-2007, Hangzhou, China, October, 2007. Pp. 153-156.

[67] Xuexin S. 2002. The Experiment Technology and Method of Boiler Combustion [M]. Beijing: Chinese Electrical Power Press.

[68] Fantec Research Institute. FQA-NIR Gun user's manual, Japan.

[69] Viavi Solutions Inc. 2015 MicroNIR™ OnSite. [Online]. Available: http://www.viavisolutions.com/sites/default/files/technical-library-items/microniro
nsite-ds-osp-ae.pdf

[70] Bruker optic GmbH. 2011. MPA user manual. 8th Ed.

[71] Netzsch-Gerätebau GmbH. Thermogravimetric analysis-TGA. [Online}. Available: https://www.netzsch-thermal-analysis.com/us/products-solutions/thermogravimet ric-analysis/tg-209-f3-tarsus/

[72] Panwar N.L., Kaushik S.C. and Kothari S. “Role of renewable energy sources in environmental protection: A review.” Renew. Sust. Energ. Rev., vol. 15, 2011. Pp. 1513-1524.

[73] Demirbas A. “Recent advance in biomass conversion technologies.”, Energy Educ. Sci. Tech., vol. 6, 2000. Pp 19-40.

[74] Rathore N.S. and Panwar N.L. 2007. Renewable energy sources for sustainable development. New Delhi: New India Publishing Agency.

[75] Hein K.R.G., Bemtgen J.M. “EU clean coal technology, co combustion of coal and biomass.”, Fuel Process. Technol., vol. 54, 1998. Pp. 159-169.

[76] Spliethoff H. and Hein K.R.G. “Effect of co-combustion of biomass on emissions in pulverized fuel furnaces.”, Fuel Process. Technol., vol. 54, 1998. Pp. 189-205.

[77] [Online]. Available: http://thai-bamboo.blogspot.com/p/bamboo-species.html

[78] Nehdi I.A., Sbihi H., Tan C.P. and Al-Resayes S.I. “Leucaena leucocephala (Lam.) de Wit seed oil: Characterization and uses.”, Ind. Crop. Prod., vol. 52, 2014. Pp. 582-587.

[79] Pandey V.C. and Kumar A. “Leucaena leucocephala: an underutilized plant for pulp and paper production.”, Genet. Resour. Crop. E., vol. 60, 2013. Pp 1165-1171.

[80] Lim T.K. 2012. Edible Medicinal and Non-Medicinal Plants: Volume 2, Fruits. New York: Springer.

[81] Gutteridge, R.C., 1998. The potential of nitrogen fixing trees in livestock production system. In: Daniel, J.N., Roshetko, J.M. eds. Nitrogen Fixing Trees for Fodder Production: Proceedings of an International Workshop. Forest, Farm, and Community Tree Research Reports (Special Issue, 20–25 March 1995). Winrock International Institute, pp. 1–16.

[82] Prasad J.V.N.S., Korwar G.R., Rao K.V., Mandal U.K., Rao G.R., Srinivas I.,

Venkateswarlu B., Rao S.N. and Kulkarni H.D. “Optimum stand density of *Leucaena leucocephala* for wood production in Andhra Pradesh, Southern India.”, Biomass Bioenerg., vol. 35, 2011. Pp. 227-235.

[83] Meelu O.P. and Morris R.A. “Green manuring research in the Philippines e a review.”, Philipp. J. Crop Sci., vol. 11, 1989. Pp. 153-159.

[84] Savale S.R., Sanglikar R.V., Sthool V.A. and Kadam J.R. “Effect of *Leucaena leucocephala* barriers and bund on erosion losses and yield of pearlmillet + mothbean.”, Asian J. Soil Sci., vol. 2, 2007. Pp. 142-145.

[85] Shelton H.M., Jones R.J. Opportunities and limitations in *Leucaena*. 1995. In: Shelton H. M., Piggin C. M., Brewbaker J. L. eds. Leucaena opportunities and limitations. Proceedings of a workshop held in Bangor, Indonesia. Canberra: ACIAR Proceedings, pp. 16-23.

[86] Rao Y.V. “Leucaena plantations-a-farming experience.”, Leucaena Res. Rep., vol. 5, 1984. Pp. 48-49.

[87] Malik R.S., Dutt D., Tyagi C.H., Jindal A.K. and Lakharia L.K. “Morphological, anatomical and chemical characteristics of Leucaena leucocephala and its impact on pulp and paper making properties.”, J. Sci. Ind. Res., vol. 63, 2004. Pp. 125-133.

[88] Via B.K., Adhakari S. and Taylor S. “Modeling for proximate analysis and heating value of torrefied biomass with vibration spectroscopy.” Bioresource Technol., vol. 133, 2013. Pp. 1-8.

[89] Komilis D., Kissas K. and Symeonidis A. “Effect of organic matter and moisture on the calorific value of solid wastes: An update of the Tanner diagram.”, Waste Manage., vol. 34, 2014. Pp. 249-255.

[90] Li Y. and Liu H. “High-pressure densification of wood residues to form an upgraded fuel. ”, Biomass Bioenerg., vol. 19, 2000. Pp. 177-186.

[91] Luo S. Y., Xiao B., Hu Z. Q., Liu S. M. and Guan Y. W. “Experimental study on oxygen-enriched combustion of biomass micro fuel.”, Energ., vol. 34, 2009. Pp. 1880–1884.

[92] Yang H., Yan R., Chin T., Liang D. T., Chen H., and Zheng C. “Thermogravimetric Analysis-Fourier Transform Infrared Analysis of Palm Oil Waste Pyrolysis.”, Energ. Fuel., Vol. 18, 2004. Pp. 1814-1821.

[93] Barneto A.G., Carmona J.A., Ferrer J.A.C. and Balanco M.J.D. “Kinetic study on the thermal degradation of a biomass and its compost: Composting effect on hydrogen production.”, Fuel, vol. 89, 2010. Pp. 462-473.

[94] Sait H. H., Hussain A., Salema A. A. and Ani F. N. “Pyrolysis and combustion kinetics of date palm biomass using thermogravimetric analysis.”, Bioresource Technol., vol. 118, 2012. Pp. 382-389.

[95] Parthasarathy P., Narayanan K. S. and Arockiam L. “Study on kinetic parameters of different biomass samples using thermo-gravimetric analysis.”, Biomass Bioenerg., vol. 58, 2013. Pp. 58-66.

[96] El-Sayed S.A. and Mostafa M.E. “Pyrolysis characteristics and kinetic parameters determination of biomass fuel powders by differential thermal gravimetric analysis (TGA/DTG).”, Energ. Convers. Manage., vol. 85, 2014. Pp. 165-172.

[97] Liu L. and Chen H. “Prediction of maize stover components with near infrared reflectance spectroscopy (NIRS).”, Spectrosc. Spect. Anal., vol. 27, 2007. Pp. 275-278.

[98] Sirisomboon P. and Chowbankrang R., Williams P. “Evaluation of apparent viscosity of Para rubber latex by diffuse reflection near infrared spectroscopy.”, Appl. Spectrosc., vol. 66, 2012. Pp. 595-599.

[99] Pereira A. F. C., Pontes M. J. C., Neto F. F. G., Santos S. R. B., Galvão R.K.H. and Araújo M.C.U. “NIR spectrometric determination of quality parameters in vegetable oils using iPLS and variable selection.”, Food Res. Internal., vol. 41, 2008. Pp. 341-348.

[100] Riggio M., Sandak J., Sandak A., Pauliny D. and Babiński L. “Analysis and prediction of selected mechanical/dynamic properties of wood after short and long-term waterlogging.”, Construct. Building Mat., vol. 68, 2014. Pp. 444-454.

[101] Gani A. and Naruse I. “Effect of cellulose and lignin content on pyrolysis and combustion characteristics for several types of biomass.”, Renew. Energ., vol. 32, 2007. Pp. 649-661.

[102] Shen D. K., Gu S., Luo K. H., Bridgwater A. V. and Fang M. X. “Kinetic study on thermal decomposition of woods in oxidative environment.”, Fuel, vol. 88, 2009. Pp. 1024-1030.

[103] Liu N. A., Fan W., Dobashi R. and Huang L. “Kinetic modeling of thermal decomposition of natural cellulosic materials in air.”, J. Anal. App. Pyrol., vol. 63, 2002. Pp. 303-325.

[104] Yang H., Yan R., Chen H., Zheng C., Lee D. H. and Liang D. T. “In-depth investigation of biomass pyrolysis based on three major components: hemicellulose, cellulose and lignin.”, Energ. Fuel.., vol. 20, 2006. Pp. 388-393.

[105] Yang H., Yan R., Chen H., Lee D. H. and Zheng C. “Characteristic of hemicelluloses, cellulose and lignin pyrolysis.”, Fuel, vol. 86, 2007. Pp. 1781-1788.

[106] Kastanaki E., Vamvuka D., Grammelis P. and Kakaras E. “Thermogravimetric studies of the behavior of lignite-biomass blends during devolatilization.”, Fuel Process. Technol., vol. 77-78, 2002. Pp. 159-166.

[107] Vamvuka D., Kakaras E., Kastanaki E. and Grammelis P. “Pyrolysis characteristic and kinetics of biomass residuals mixtures with lignite.”, Fuel, vol. 82, 2003. Pp. 1949-1960.

[108] Raveendran K., Ganesh A. and Khilar KC. “Pyrolysis characteristic of biomass and biomass component.”, Fuel, vol. 75, 1996. Pp. 987–998.

[109] Moon C., Sung Y., Ahn S., Kim T., Choi G. and Kim D. “Effect of blending ratio on combustion performance in blends of biomass and coals of different ranks.”, Exp. Therm. Fluid Sci., vol. 47, 2013. Pp. 232–240.

[110] Vamvuka D. and Sfakiotakis S. “Combustion behavior of biomass fuels and their blends with lignite.”, Thermochim. Acta., vol. 26, 2011. Pp. 192–199.

[111] Idris S. S., Rahman N. A., Ismail K., Alias A. B., Rashid Z. A. and Aris M. J. “Investigation on thermochemical behaviour of low rank Malaysian coal, oil palm biomass and their blends during pyrolysis via thermogravimetric analysis (TGA).”, Bioresource Technol., vol. 101, 2010. Pp. 4584–4592.

[112] Vamvuka, D., Kakaras, E., Kastanaki, E. and Grammelis, P. “Pyrolysis characteristics and kinetics of biomass residuals mixtures with lignite.”, Fuel, vol. 82, 2003. Pp. 1949–1960.

[113] Safi M. J., Mishra I. M. and Prasad B. “Global degradation kinetics of pine needles in air.”, Thermochim. Acta, vol. 412, 2004. Pp. 155–162.

[114] Stryer L. 1995. Biochemistry. 4th ed. W.H. New York : Freeman and Company

[115] Othmer K. 2001. Concise Encyclopedia of chemical technology. 4th ed. New York: Wiley Interscience.

[116] Wen J.L., Xiao L.P., Sun Y.C., Sun S.N., Xu F., Sun R.C. and Zhang X.L. “Comparative study of alkali-soluble hemicelluloses isolated from bamboo (Bambusa rigida).”, Carbohydr. Res., vol. 346, 2011. Pp. 111-120.

[117] Cozzolino D., Esler M. B., Dambergs R. G., Cynkar W. U., Boehm D. R., Francis I. L. and Gishen M. “Prediction of colour and pH in grapes using a diode array spectrophotometer (400–1100 nm).”, J. Near Infrared Spectros., vol. 12, 2004. Pp. 105–111.

[118] Murray I. 1986. The NIR spectra of homologous series of organic compounds. In: Hollo J., Kaffa K.L. and Gonczy J.L. eds. NIR/NIT Conference. Budapest, Akademiai Kiado, pp. 13-28.

[119] Gutierrez A., del Rio J. C. and Martinez A. T. “Microbial and enzymatic control of pitch in the pulp and paper industry.”, Appl. Microbiol. Biotechnol., vol. 82, 2009. Pp. 1005–1018.

[120] Kraessig H. A. (1993), Cellulose: Structure, Accessibility and Reactivity, Amsterdam: Gordon & Breach Science Publishers.

[121] Somerville C., Bauer S., Brininstool G., Facette M., Hamann T. and Milne J.

"Toward a systems approach to understanding plant cell walls.", Science, vol. 306, 2004. Pp. 2206–2211.

[122] Kacurakova M., Capek P., Sasinkova V., Wellner N. and Ebringerova A. "FT-IR study of plant cell wall model compounds: pectic polysaccharides and hemicelluloses.", Carbohydr. Polym., vol.43, 2000. Pp. 195–203.

[123] Whetten R, MacKay J, and Sederoff R. "Recent advances in understanding lignin biosynthesis.", Annu. Rev. Plant Biol., vol. 49, 1998. Pp. 585–609.

[124] Eriksson T, Borjesson J, and Tjerneld F. "Mechanism of surfactant effect in enzymatic hydrolysis of lignocellulose.", Enzyme Microb. Technol., vol. 31, 2002. Pp. 353–64.

[125] Sáncheza J. M., Jiménez J. A. P., Villanueva M. J. D., Serrano A., Núñez N. and Giménez J. L. "Assessment of near infrared spectroscopy for energetic characterization of olive by products.", Renew. Energ., vol. 74, 2015. Pp. 599-605.

[126] Xue J., Yang Z., Han L., Liu Y. and Liu Y. and Zhou C. "On-line measurement of proximates and lignocellulose components of corn stover using NIRS.", Appl. Energ., vol. 137, 2015. Pp. 18–25.

[127] Sanderson M. A., Agblevor F., Collins M. and Johnson D. K. "Compositional analysis of biomass feedstocks by near infrared reflectance spectroscopy.", Biomass Bioenerg., vol. 11, 1996. Pp. 365–370.

Appendix

The 16th TSAE National Conference and the 8th TSAE International Conference
การประชุมวิชาการสมาคมวิศวกรรมเกษตรแห่งประเทศไทยระดับชาติ ครั้งที่ 16 ประจำปี 2558 และระดับนานาชาติ ครั้งที่ 8

ET-08

SOME PHYSICAL AND COMBUSTION CHARACTERISTIC OF *LEUCAENA LEUCOCEPHALA* PELLET

*Amrit SHRESTHA[1], Wanphut SAECHUA[1] and Panmanas SIRISOMBOON[1]
[1] *Agricultural Engineering Curriculum, Department of Mechanical Engineering, Faculty of Engineering, King Mongkut's Institute of Techmology Ladkrabang Chalongkrung Road, Ladkrabang, Bangkok, Thailand 10520*

Corresponding author: Amrit SHRESTHA. E-mail: shresthamrit329@gmail.com

ABSTRACT

Leucaena leucocephala pellet can be a superior green fuel for Thailand by taking the advantage of such economic and environmental beneficial plant by establishing good rules and regulations toward afforestation of energy crops without altering the food chain. Before selling the biomass or its pellet, commercially, combustion characteristics must be recognized in advance so that it will get its actual monetary value instead of random cost per unit weight. For this purpose, thermogravimetric analysis (TGA) was performed to determine the ignition temperature, ignition index, burnout index and combustion performance index and found to be 261.7°C, $6.10x10^{-04}$, $8.20x10^{-03}$ and $2.19x10^{-07}$ respectively and higher heating value (HHV) was found to be 18.65 MJ/kg. In addition, bulk density and solid density of pellet was found to be 578.13 kg/m^3 and 1151.10 kg/m^3 respectively.

Keywords: Leucaena leucocephala pellet, Combustion characteristics, Thermogravimetric analysis (TGA)

INTRODUCTION

Current fossil fuel crisis, increasing cost of fuel and rising environmental air pollution concerns has fostered the development of biomass resources as an alternative energy source [1, 2]. Biomasses in term of agricultural resources supply energy in two forms from energy crops and residue of crops [3, 4]. So, a fast growing energy crops are needed which can mitigate the current energy crisis having less impact on environmental pollution. In such case, Leucaena leucocephala can be a crucial plant as it is one of the most fast growing, productive and versatile multipurpose tree which can be grown in wide range of soil and tolerate drought [5-9].

The energy plays a vital role in a country economy [10] and, also, one of the most essential needs for human being. Thailand falls under tropical zone where the average temperature is 27 °C and annual rain fall of 1,200-1,600 mm/year [11]. Leucaena leucocephala is found naturalized in most tropical and subtropical areas of the world [12]. It is advantageous for both energy and environment because biomass is considered as CO2 neutral [13]. In general, pelletization of biomass produce the pellet which has high density and high heating value in compare to raw of same kind [14]. Meanwhile, it easier to store and transport and has greater econo-mic value in the share market [15]. Therefore, Thailand government can take advantage of such economic and environmen-tal benefit energy crops by establishing good rule and regulation toward afforestation of energy crops without altering the food chain. However, the unplanned afforestation and clearance of cultivated land for plantation of energy crops may lead to the food deficiency.

The knowledge of the combustion performance is essential parameters for the design of reactor and optimization of product [16-18]. Lignocellulosic biomass mainly consists of the hemicellulose, cellulose and lignin [19]. Combustion of biomass can be divided into four processes: moisture removal, devolatilization stage, char oxidation, and remaining stage [20]. The decomposition of the biomass begins with the moisture evolution followed by the devolatili-zation. Devolatilization takes place by releasing gaseous and volatile products that leads to the formation of the tar and char [21]. Hemicellulose shows the early decomposition followed by the cellulose and lignin. Hemicellulose has random amorphous structure and rich with the branches while cellulose has long polymer molecules without

branches and orderly crystalline structure which make cellulose more thermally stable than the hemicellulose [22]. In addition, highest thermal stability of the lignin is constantly reported due the strong structure background from the highly branched polysaccharides and the heavy crossed linked aromatic compounds [23].

However, up to date, the study of the Leucaena leucocephala biomass pellet has not yet been reported. Nevertheless, Barneto et al. [24] studied the thermal degradation of a Leucaena leucocephala biomass and its compost, and composting effect on hydrogen production. So, the aim of this work was to perform the primary study on the combustion behavior of ligno-cellulosic biomass pellet by the means of the TGA technique. The combustion characteristics i.e. the ignition temperature (Ti), ignition index (Di), burnout index (Df) and combustion performance index (S) were studied. In addition, some physical and energy properties including higher heating value (HHV), bulk density and solid density of the pellets were investigated.

Material

The Leucaena leucocephala pellet, which was pelletized for commercial purpose were obtained from the factory of Thailand. The pellet, 100 g, was sent to Intertek Testing Service (Thailand) Ltd. for proximate analysis and ultimate analysis which were conducted following the ASTM methods.

Solid density and bulk density measure-ment

Random twenty pieces of pellet was selected. The length and diameter were measured using digital vernier caliper (Digimatic caliper, Mitutoyo, Japan) and weight by electric balance (ARC120, Adventurer, OHAUS, USA. Resolution of 0.01 g) of each pellet was mea-sured. While measuring length and diameter, ten measure-ments were taken on different surface-positions and average was taken.

For the measurement of the bulk density, either volume or weight of pellet was fixed. Firstly, pellet was filled in a cylindrical can of volume 983.69 cm3 and the respective weight was measured using the same electric balance. On the other hand, pellet of 2 kg was weighted and volume was measured. Each process was repeated for ten times and average of the whole process was taken to calculate the bulk density.

Higher heating value deter-mination

The higher heating value was obtained by oxygen bomb calorimeter (C 2000 Basic, IKA, Germany). The sample subjected to the calorimeter was prepared as follows: first, the pellet was undersized into small pieces with mortar and pestle, then was grounded through 2 mm diameter sieve (SM100, Retsch, Germany) and was again grounded using miller (Pulverisette 14, Fritsch, Germany) through 0.2 mm diameter sieve. These samples were kept in zipped plastic bag prior to the testing. The experiment was run for three replications and the average was taken. The sample size was fixed around 0.5 g.

The ground sample left from higher heat-ing value determination was subjected for thermogravimatric analysis. The combustion characteristic of biomass pellet was perfor-med in the thermogravimetric analyzer (TG 209 F3 Tarsus, Netzsch, Germany, 0.1 µg resolution, heating rate ranges from 0.001 to 100 Kmin-1, 6.8 mm diameter aluminum oxide (AL2O3) crucible) in a room tempera-ture of 25°C and the ther-mogravimetric (TG) profile and differential thermogravimetric (DTG) profile were analyzed using Proteus 6.0.0. (Netzsch Software, Germa-ny). At the heating rate of 10°Cmin-1, the temperature of furnace was increased from 30°C to 900°C in an air flux (O2) of 20 mLmin-1. The mass of the sample was monitored continuously as a function of temperature and time. The experiments were performed for two replications to determine their repeatability. The sample size was kept constant at around 6 mg.

The ignition index (Di) is determined by the equation as follows:

$$D_i = \frac{(dw/dt)_{max}}{t_p t_i} \quad \ldots(1)$$

Where (dw/dt)max=maximum combust-ion rate, tp = corresponding time of (dw/dt) max and ti = ignition time.

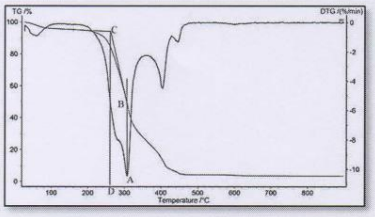

Fig. 1 Ignition temperature determining process

Burnout index (D_f)

Burnout temperature was identified as the corresponding temperature of no further weight loss in TG and DTG curves. Burnout temperature is the temperature on TG and DTG curves that shows the constant mass after the char combustion during the process and the corre-spondent time is known as burning time [25, 28, 29]. The burnout index (D_f) is defined as:

$$D_f = \frac{(dw/dt)_{max}}{\Delta t_{1/2} t_p t_f} \quad \ldots(2)$$

Where $\Delta t_{1/2}$ = time zone of $(dw/dt)/-(dw/dt)_{max} = ½$ and t_f = burnout time.

Combustion performance index (S) A higher combustion index represents better combustion reactivity of the fuel which was calculated as [30-33]:

$$S = \frac{(dw/dt)_{max}(dw/dt)_{mean}}{T_i^2 T_f} \quad \ldots(3)$$

Where, (dw/dt)mean = average combustion rate, Ti = ignition temperature and Tf = burnout temperature.

RESULT AND DISCUSSION

Proximate analysis and the ultimate analy-sis

The proximate analysis and the ultimate analysis results are presented in Table 1. They are the easiest and most widely used method to characterize a biomass fuel. Proximate analysis represents moisture, volatile matter (VM), ash and fixed carbon (FC) on weight percent basis of a biomass whereas ultimate analysis signify weight percentage of carbon(C), hydrogen(H), nitrogen(N), sulfur(S), oxygen(O) that is present on a biomass. In addition, proximate and ultimate analysis correlates the heating value of fuel. Heating value of the fuel highly depends upon FC, VM, C, and H whereas heating value decrease with higher content of ash and oxygen [45]. Nitrogen and sulfur leads to the formation of harmful emission. Fixed carbon is responsible for the formation of char [14].

Proximate analysis	Method	Result (wt %)
Moisture	ASTM E 871-82 (R06)	7.59
Volatile matter	ASTM E 871-82 (R06)	72.91
Ash	ASTM D 1102-84 R07)	1.96
Fixed carbon	Calculation	17.55
Ultimate analysis		
Carbon	CHN Analyzer	44.98
Hydrogen	CHN Analyzer	6.20
Nitrogen	CHN Analyzer	0.52
Sulfur	ASTM E 775-87 (R086), B-IPC	0.04
Oxygen	Calculation	46.31
Chloride	ASTM E 776-87 (R09)	Less than 0.01

Solid density and bulk density measurement

Bulk density and solid density of pellet was found to be 578.13 kg/m3 and 1151.10 kg/m3 respectively. The solid density was found almost double the bulk density. This may be due to the void spaces between the pellets as the orientation, shape and size of the pellet effect on the bulk density.

Higher heating value

The experimental higher heating value (HHVe) was found to be 17.23 kJ/kg. This exper-imental higher heating value includes heat of condensation released from the water vapor during the combustion process. So, this value was converted into anhydrous higher heating value as [45, 46]:

$$HHV = \frac{HHV_e}{1-MC} \quad \ldots(4)$$

Where, HHV = higher heating value, HHVe = experimental higher heating value and MC = moisture content in decimal.

The anhydrous higher heating value (HHV) was found to be 18.65 kJ/kg. This value was in range of higher heating value for hard wood [45].

Combustion performance

The ignition temperature, ignition index, burnout index and combustion index with the peak temperature and respective mass loss are listed in Table 2. Ignition temperature

determines the easiness to ignite the fuel. A fuel with high ignition temperature is more difficult to ignite and vice versa [34]. The higher value of combustion performance of fuel is desired for better combus-tibility, whereas higher burnout temperature defines the difficulty to burn and thus requires longer time while lower value indicates the reduced presence of unburnt [30]. The value of Df was found higher and Di lower than that of coal [25], while the S was found higher than coal [32]. The higher value of Df and S and lower value of Di signify that L. leucephalla pellet is easier to burn than coal, which connotes the possibility for the future fuel.

Table 2 Combustion characteristics of L. leucocephala

Parameter	value
$(dw/dt)_{max}$ (%min^{-1})	10.45
$(dw/dt)_{mean}$ (%min^{-1})	1.11
T_{max} (°C)	307.5
t_{max} (min)	28.0
T_i (°C)	261.7
t_i (min)	23.6
T_f (°C)	776.25
t_f (min)	74.95
$\Delta t_{1/2}$ (min)	23.42
D_f (10^{-03})	8.20
D_i (10^{-04})	6.10
S (10^{-07})	2.19

Thermogravimetric analysis of Leucaena leu- cocephala pellet

The combustion profile of wood pellet, Leucaena leucocephala, is shown in the Figure 2. The combustion profile can be categorized into four stages: moisture removal (<110 °C); devolatilization (197-350 °C); char combustion (360-600 °C) and residue decomposition (>600 °C). The peak temperature associates with different stages with peak mass loss are shown in Table 3. L. leucocephala consist mainly holocellulose (hemicellusose, cellulose) and lignin [24]. When the moisture is removed from the sample, the pellet started to degrade slowly. After 195 °C, volatilization of volatile soared up, which leads to formation of char [16, 21].

The combustion begins with the volatilization of hemicellulose and cellulose and partial decomposition of lignin [35, 36]. Hemicellulose shows the early decomposition [2, 23] followed by cellulose [2, 22] and lignin, which showed the wide range of decomposi-tion [2, 23]. The sharp peak at 308.1°C in the temperature range of 200°C to 355°C was associated with cellulose and a very small shoulder peak at 284.6°C to the left was of hemicellulose [37, 38].

The third stage was associated with the char oxidation which depicted two separate peaks. The first char oxidation peak (stage H), which elevated at 405.6°C with higher decomposition rate 4.57 %min-1, was associated with the oxidation of holocellulose [24]. However, cellulose contributes less to the char formation as most of it mass loss during the volatilization [39-44]. Therefore, this peak is mainly associated with the hemicellulose. In addition, a second separate peak (stage L) which rose at 443.7 °C is mainly associated with the lignin oxidation [16, 24]. Similar lignin curve was evolved during combustion of lignocellulosic biomass, pine bark, at lower heating rate [1]. The profile above 600 °C was defines as the remaining char residue and inorganic compound decomposition. A very insignificant peak was observed above the temperature of 605 °C which was mainly associated with the combustion of inorganic matter [16, 24].

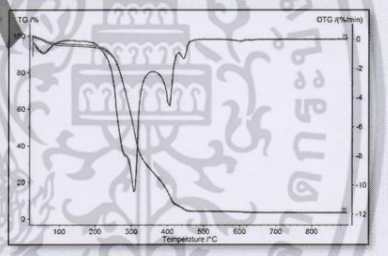

Fig. 2 TG and DTG profile of L. leucocephala

Table 3 Combustion performance

Parameters			Value
Devolatilization	T_{peak} °C		308.1
	$(dw/dt)_{max}$ (%min^{-1})		10.44
Char oxidation	Stage H	T_{peak} (°C)	405.6
		$(dw/dt)_{max}$ (%min^{-1})	4.57
	Stage L	$(dw/dt)_{max}$ (%min^{-1})	443.7
		$(dw/dt)_{max}$ (%min^{-1})	1.34
Residue (%)			3.37

CONCLUSION

The combustion characteristic of L. Leucocephala pellet was analyzed by the means of TGA. The main combustion profile depicted two different stages. Firstly, the combustion of volatile matter takes place from 197°C to

350°C. The second stage was related with char combustion which depicted two separate peaks mainly associated with hemicellulose and lignin. As L. Leucocephala pellet has higher combustion index compared to coal, it can be a good source of fuel which might help to mitigate the energy crisis and lessen the air pollution. In future, biomass can be a good source of fuel for combustion.

ACKNOWLEDGEMENTS

The authors would like to thank the King Mongkut's Institute of Technology Ladkrabang Faculty of Engineering, Department of Mechanical Engineering, Agricultural Engineering Curriculum and Near Infrared Spectroscopy, Research Center for Agricultural Product and Food for their instrument and financial support.

REFERENCES

[1] López-González, D., Fernandez-Lopez, M., Valverde, J.L. and Sanchez-Silva L. Thermogravimetric-mass spectrometric analysis on combustion of lignocellulosic biomass. Bioresource Technol. 143: 562-574 (2013)

[2] Sivasangar, S., Taufiq-Yap, Y.H., Zainal, Z. and Kitagawa, K. Thermal behavior of lignocellulosic materials under aerobic/anaerobic environments. Int. J. Hydrogen Energ. 38: 16011-16019 (2013)

[3] Liu, T., McConkey B., Huffman T., Smith S., MacGregor B., Yemshanov, D. and Kulshreshtha S. "Potential and impacts of renewable energy production from agricultural biomass in Canada. Appl Energ. 130: 222-229 (2014)

[4] Stern N. The economics of climate change: the stern review, Cambridge University press, Cambridge, (2007)

[5] Prasad, J. V. N. S., Korwar, G.R.,Rao,K.V., Mandal,U.K.,Rao,G.R.,Srinivas,I., Venkateswarlu, B., Rao, S.N. and Kulkarni H.D. Optimum stand density of Leucaena leucocephala for wood production in Andhra Pradesh, Southern India. Biomass Bioenerg. 35: 227-235 (2011)

[6] Meelu, O.P. and Morris R.A. Green manuring research in the Philippines e a review. Philipp. J. Crop Sci. 11:153-159 (1989)

[7] Savale, S.R., Sanglikar, R.V., Sthool, V.A. and Kadam, J.R. Effect of Leucaena leucocephala barriers and bund on erosion losses and yield of pearlmillet + mothbean. Asian J. Soil Sci. 2: 142-145 (2007)

[8] Shelton, H.M. and Jones, R.J. Opportunities and limitations in Leucaena, pp. 16-23, in H.M. Shelton, C.M. Piggin and J.L. Brewbaker (Eds.) Leucaena opportunities and limitations: proceedings of a workshop held in Bangor, Indonesia, ACIAR Proceedings, Canberra (1995)

[9] Gutteridge, R.C. The potential of nitrogen fixing trees in livestock production system, pp. 1–16, in J.N. Daniel and J.M. Roshetko (Eds.) Nitrogen Fixing Trees for Fodder Production: Proceedings of an International Workshop. Forest, Farm, and Community Tree Research Reports, Winrock International Institute, Morrilton (1998).

[10] Ramage J. and Scurlock J. Biomass, in G. Boyle (Ed.) Renewable energy-power for a sustainable future, Oxford University Press, Oxford, (1996)

[11] Thai Meteorological Department. Thailand weather, Meteorological knowledge. [Online]. Available: http://www.tmd.go.th/info/info.php?-FileID=22. 2014

[12] Lim, T.K. Edible Medicinal and Non-Medicinal Plants: Volume 2, Fruits. Springer, New York (2012)

[13] Demirbas, A. Potential applications of renewable energy sources, biomass combustion problems in boiler power systems and combustion related environmental issues. Prog. Energ. Combust. 31: 171-192 (2005)

[14] Poddar, S., Kamruzzaman, M., Sujan, S.M.A., Hossain, M., Jamal, M.S., Gafur, M.A. and Khanam, M. Effect of compression pressure on lignocellulosic biomass pellet to improve fuel properties: Higher heating value. Fuel 131:43-48 (2014)

[15] Vinterback, J. Pellets 2002: the first world conference on pellets. Biomass and Bioenergy 27: 513–520 (2004)

[16] López-González, D., Fernandez-Lopez, M., Valverde, J. L. and Sanchez-Silva, L. Thermogravimetric-mass spectrometric analysis on combustion of lignocellulosic biomass. Bioresource Technol. 143:562–574 (2013)

[17] Yorulmax, S. Y. and Atimaya, A. T. Investigation of combustion kinetics of treated and untreated waste wood samples with thermogravimetric analysis. Fuel Process. Technol. 90: 939-946 (2009)

[18] Cordero, T., Rodriguez-Maroto, J. M., Rodriguez-Mirasol, J. and Rodriguez, J. J. On the kinetics of thermal decomposition of wood and wood components. Thermochim. Acta 164: 135-144 (1990)

[19] El-Sayed, S. A. and Mostafa, M. E. Pyrolysis characteristics and kinetic parameters determination of biomass fuel powders by differential thermal gravimetric analysis (TGA/DTG). Energ. Convers. Manage. 85: 165-172 (2014)

[20] Qing, W., Hao, X., Hongpeng, L., Chunxia, J. and Jingru, B. Thermogravimetric analysis of the combustion characteristic of oil shale semi-coke/biomass blends. Oil Shale 28: 284-295 (2011)

[21] Gani, A. and Naruse, I. Effect of cellulose and lignin content on pyrolysis and combustion characteristics for several types of biomass. Renew. Energ. 32: 649-661 (2007)
[22] Yang, H., Yan, R., Chen, H., Lee, D. H. and Zheng, C. Characteristic of hemicelluloses, cell-ulose and lignin pyrolysis. Fuel 86: 1781-1788 (2007)
[23] Yang, H., Yan, R., Chen, H., Zheng, C., Lee, D. H. and Liang, D. T. In-depth investigation of biomass pyrolysis based on three major components: hemicellulose, cellulose and lignin. Energ. Fuel. 20: 388-393 (2006)
[24] Barneto, A. G., Carmona, J. A., Ferrer, J. A. C. and Balanco, M. J. D. Kinetic study on the thermal degradation of a biomass and its compost: Composting effect on hydrogen production. Fuel 89: 462-473 (2010)
[25] Ma, B.-G., Li, X.-G., Wang, K. and Wang, X.-G. Investigation on catalyzed combustion of high ash coal by thermogravimetric analysis. Thermochem. Acta, 445: 19-22 (2006)
[26] Nie, Q.-H., Sun, S.-Z. and Li, Z.-Q. Thermogravimetric study on the combustion characteristic of brown coal blends. J. Combust. Sci. Technol. 7: 72-76 (2001)
[27] Li, X.-G., Ma, B.-G., Xu, L., Hu, Z.-W. and Wang, X.-G. Thermogravimetric analysis of the co-combustion of the blends with high ash coal and waste tyres. Thermochim. Acta 441 79-83 (2006)
[28] Idris, S. S., Rahman, N. A. and Ismail, K. Combustion characteristics of Malaysian oil palm biomass, sub-bituminous coal and their respective blends via thermogravimetric analysis (TGA). Bioresource Technol. 123: 581-591 (2012)
[29] Xie, J.-L. and He, F. Catalyzed combustion study of anthracite in cement kiln. J. Chin. Ceram. Soc. 26: 792-795 (1998)
[30] Qing, W., Hao, X., Hongpeng, L., Chunxia, J. and Jingru, B. Thermogravimetric analysis of the combustion characteristics of oil shale semi-coke/biomass blends. Oil shale 28: 284-295 (2011)
[31] Nie, Q. H., Sun, S. Z. and Li, Z. Q. Thermogravimetric analysis on the combustion characeristics of browncoal blends. Combust. Sci. Technol. 7: 71-76 (2001)
[32] Xu, Y., Lin, S., Yuan, H., Zhu, K., He, X. and Chen, G. Thermogravimetric Analysis on the Combustion Characteristics for Blended Coals. International Conference on Power Engineering-2007, Hangzhou, pp. 153-156 (2007)
[33] Xuexin, S. The Experiment Technology and Method of Boiler Combustion [M]. Chinese Electrical Power Press,2002. Beijing, China
[34] Idris, S. S., Rahman, N.A. and Ismail, K. Combustion characteristics of Malaysian oil palm biomass, sub-bituminous coal and their respective blends via thermogravimetric analysis (TGA). Bioresource Technol. 123: 581–591 (2012)
[35] Shen, D. K., Gu, S., Luo, K. H., Bridgwater, A. V. and Fang, M. X. Kinetic study on thermal decomposition of woods in oxidative environment. Fuel 88: 1024-1030 (2009)
[36] Liu, N. A., Fan, W., Dobashi, R. and Huang, L. Kinetic modeling of thermal decomposition of natural cellulosic materials in air. J. Anal. App. Pyrol. 63:303-325 (2002)
[37] Kastanaki, E., Vamvuka, D., Grammelis, P. and Kakaras, E. Thermogravimetric studies of the behavior of lignite-biomass blends during devolatilization. Fuel Process. Technol. 77-78: 159-166 (2002)
[38] Vamvuka, D., Kakaras, E., Kastanaki, E. and Grammelis, P. "Pyrolysis characteristic and kinetics of biomass residuals mixtures with lignite. Fuel 82: 1949-1960 (2003)
[39] Raveendran, K., Ganesh, A. and Khilar, KC. Pyrolysis characteristic of biomass and biomass components. Fuel 75: 987–998 (1996)
[40] Moon, C., Sung, Y., Ahn, S., Kim, T., Choi, G. and Kim, D. Effect of blending ratio on combustion performance in blends of biomass and coals of different ranks. Exp. Therm. Fluid Sci. 47: 232–240 (2013)
[41] Vamvuka, D. and Sfakiotakis, S. Combustion behavior of biomass fuels and their blends with lignite. Thermochim. Acta 26: 192–199 (2011)
[42] Idris, S. S., Rahman, N. A., Ismail, K., Alias, A. B., Rashid, Z. A. and Aris, M. J. Investigation on thermochemical behaviour of low rank Malaysian coal, oil palm biomass and their blends during pyrolysis via thermogravimetric analysis (TGA). Bioresource Technol.101: 4584–4592 (2010)
[43] Vamvuka, D., Kakaras, E., Kastanaki, E. and Grammelis, P. Pyrolysis characteristics and kinetics of biomass residuals mixtures with lignite. Fuel 82: 1949–1960 (2003)
[44] Safi, M. J., Mishra, I. M. and Prasad, B. Global degradation kinetics of pine needles in air. Thermochim. Acta 412: 155–162 (2004)
[45] Telmo, C. and Lousada, J. Heating values of wood pellets from different species. Biomass Bioenerg. 35: 2634–2639 (2011)
[46] DD CEN/TS 14918. Solid bio fuels – method for the determination of calorific value. British Standards Institution, London (2005)

Author biography

Name-Surname	Amrit Shreshta
Date of birth	19 January 1989
Current address	419/1-2 M3 Chaiyapon, Kakeingam soi 1 Khunhyingliam Rd. Ladkrabang, Bangkok, 10520
Permanent address	Dhading Bensi, Neelkantha-5, Nepal
Email address	shresthamrit329@gmail.com
Contact number	0941850865
Education background	Master of Engineering (Agricultural Engineering), 2016 King Mongkut's Institute of Technology Ladkrabang Ladkrabang, Bangkok, Thailand Bachelor in Mechanical Engineering, 2011 Kathmandu University Kavre, Dhulikhel, Nepal
Conferences	Shrestha A., Saechua W. and Sirisomboon P. "Some physical and combustion characteristic of *Leucaena leucocephala* pellet.", The 16th Thai Society of Agricultural Engineering International Conference and 8th Thai Society of Agricultural Engineering International Conference (TSAE2015), Thailand (2015), Pp. 127-132.